type of step(S-2) consists of insertion of CH_x species in a metal-carbon bond to give higher carbon containing partially hydrogenated species. e.g., A_2, A_3... etc. The third type of steps(S-3) hydrogenate the surface species A_i in the main chain to produce olefins and hydrocarbons. The three steps, S-1 to S-3, are present in FTS reaction network. Oxygenate synthesis reaction network consist of the above three steps and step 4(S-4), which consists of inserting a CO ligand in a metal-carbon bond to produce a oxygen containing surface species. This oxygen containing species then give rise to oxygenates.

Very little is known about the slow steps in the reaction networks under synthesis conditions[24]. The delplot method provides a new and easy tool to find, first the number of slow steps and second the location of slow steps. Assume that all the steps 2 through 4 are effective-first order with rate constants k_1. As shown earlier, here the effective rank of a product P is same as the network rank of the product P. The effective rank of the product P can be found by using basic and extended delplot analysis. Let us first consider the FTS network only. The number of slow steps depend on whether steps 2 and 3 are fast or slow on the process time scale.

Thus from table 3.3, in many cases there is a one-to-one correspondence between the combination of the nature of steps(e.g., S,S,F), and the network rank of the products. Thus by applying delplot analysis to the hydrocarbon products, the network rank can be found and then the combination of nature of steps can be found from table 3.3. Scheme B and F give the same effective rank of hydrocarbon products, i.e., 1.2.3.4 for different combinations of slow and fast steps. Also, schemes C and H give the same effective rank of the hydrocarbons. The two-indistinguishable schemes in FTS reaction can be discerned by applying this method to oxygenates reaction network.

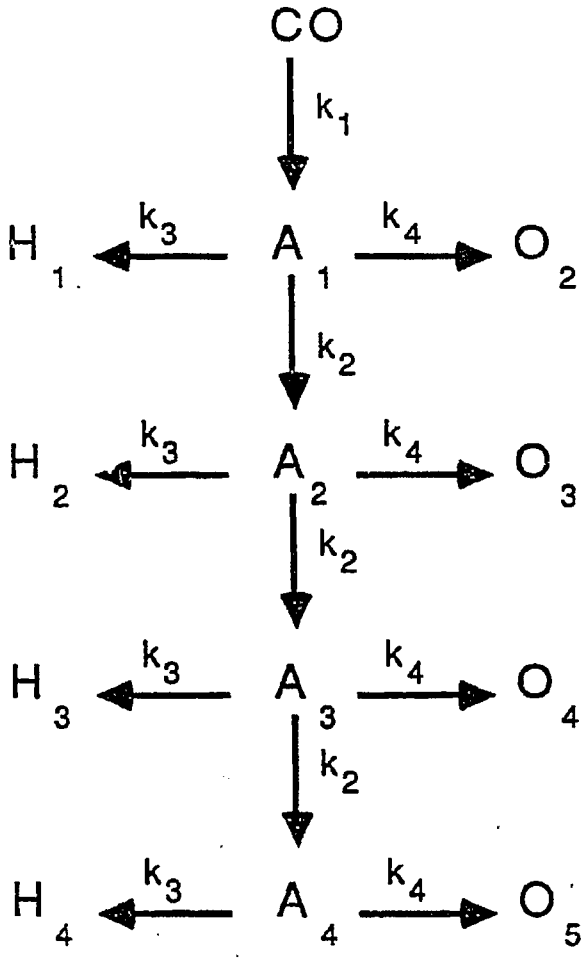

Figure 3.2: Fisher-Tropsch synthesis and oxygenate synthesis network[23]

Table 3.3: Effective rank of Fisher-Tropsch products with different combination of slow and fast steps

Scheme	S-1	S-2	S-3	$\hat{N}(H_1)$	$\hat{N}(H_2)$	$\hat{N}(H_3)$	$\hat{N}(H_4)$
A	S	S	S	2	3	4	5
B	F	S	S	1	2	3	4
C	F	F	S	1	1	1	1
D	F	F	F	0	0	0	0
E	S	F	S	2	2	2	2
F	S	S	F	1	2	3	4
G	F	S	F	0	1	2	3
H	S	F	F	1	1	1	1

F-fast, S-slow

When this method is applied to oxygenate synthesis, there is one more step. Thus each scheme can be labelled as A1 or A2, depending on whether step 4 is slow or fast on the process time scale.

Here again there is one-to-one correspondence between the combination of nature of steps and the network rank of products except for scheme (B1, F2) and (C1, H2). Thus from table 3.4 it is possible to find the number and position of the slow steps in the Fisher-Tropsch synthesis and oxygenate synthesis reaction network.

3.5 Miscellaneous Delplots

3.5.1 Non-Integer Rank Delplot

A non-integer rank delplot (y/x^r versus x, $r \notin N$) is used to find bounds on the order of the reaction. This method illustrates the coupling between the rank of the product and the order of the reaction. The fractional rank delplot is illustrated using equation (3.30). An analysis similar to equation (3.43) for non-integer r yields

$$ {}^{r}C_A = \frac{k_2' \times A_0^{r-1}}{(A')^r_{\tau=0}} \times nB_0^{n-1} \times \lim_{\tau \to 0} \frac{(\frac{d(B)}{d\tau})_{\tau=0}}{\tau^{r-2}} \qquad (3.70) $$

As a special case, when , $n = 1$ and $r = 2$, equation (3.70) reduces to equation (3.33). The characteristics of ${}^{r}C_A$ for all r and n are summarized in table 3.5 on page 132.

$$ A \xrightarrow{k_1} B \xrightarrow{k_2} C \qquad (3.71) $$

The first reaction is first order with respect to A, while the second reaction is nth order with respect to B. The fractional-rank delplot intercept for a rank, $r \leq 2$ is zero when the order of the second reaction is greater than one. Thus

Table 3.4: Effective rank of Fisher-Tropsch products and oxygenate products with different combination of slow and fast steps

Scheme	S-4	$\hat{N}(H_1)$	$\hat{N}(H_2)$	$\hat{N}(H_3)$	$\hat{N}(O_2)$	$\hat{N}(O_3)$	$\hat{N}(O_4)$
A1	S	2	3	4	2	3	4
A2	F	2	3	4	1	2	3
B1	S	1	2	3	1	2	3
B2	F	1	2	3	0	1	2
C1	S	1	1	1	1	1	1
C2	F	1	1	1	0	0	0
D1	S	0	0	0	1	1	1
D2	F	0	0	0	0	0	0
E1	S	2	2	2	2	2	2
E2	F	2	2	2	1	1	1
F1	S	1	2	3	2	3	4
F2	F	1	2	3	1	2	3
G1	S	0	1	2	1	2	3
G2	F	0	1	2	0	1	2
H1	S	1	1	1	2	2	2
H2	F	1	1	1	1	1	1

F-fast. S-slow

there is coupling between the rank of the product and the order of the reaction in fractional-rank delplots.

${}^{r}C_A$ is zero when $r \leq 2$ and $n > 1$. In contrast ${}^{r}C_A \longrightarrow \infty$, when $r \geq 2$ and $n < 1$. Also ${}^{r}C_A$ is indeterminate, if $r > 2$ and $n > 1$ and if $r < 1$ and $n < 1$.

3.5.2 Product-Based Delplot

The basic, the extended and the non-integer rank delplots are reactant-based because the basis set in the plot of y/x^r versus x is the conversion of the reactant, x. Different types of delplots can be defined by changing the basis set. The conversion can be based on any reactant. However, this concept cannot be simply extended to products because there is no easy way of defining conversion of the product in terms of observable quantities. The only condition for the ordinate in the delplot is that it should be of the $\frac{0}{0}$ form, so that in the limit, the intercept is determined by the rate of approach to zero instead of its value at zero conversion. A $\frac{0}{0}$ form can be defined for a product-based delplot as follows. For example, for a reaction scheme given by equation (3.72)

$$A \xrightarrow{k_1} B \xrightarrow{k_2} C \xrightarrow{k_3} D \tag{3.72}$$

the product based delplot for a basis B is given by

$${}^{1}P_B = \lim_{t \to 0} \frac{P/A_0}{B/A_0} \tag{3.73}$$

Here, instead of using conversion of a reactant as basis, the molar yield of the product B($y_B = B/A_0$) is used as a basis. Thus in general the product-based delplot consists of plotting y/y_B^r versus y_B. A Taylor series expansion of equation (3.73) for product C and D yields

$${}^{1}C_B = \lim_{t \to 0} \frac{(C')_{t=0}}{(B')_{t=0}} \tag{3.74}$$

Table 3.5: Results from non-integer rank delplots

r	n	${}^{r}C_{A}$
≤ 2	> 1	0
≥ 2	< 1	∞
> 2	> 1	indeterminate
< 2	< 1	indeterminate
2	1	finite

Equation (3.74) yields

$$^{1}C'_{B} = 0$$

Similarly

$$^{1}D_{B} = 0$$

Obviously here $^{1}B_{B} = 1$. Thus the first rank product-based delplots for primary products is finite but the first rank product-based delplot for non-primary products are zero.

Continued expansions of numerator similar to analysis of equations (3.28) and (3.29) gives:

$$^{2}C_{B} \sim \frac{k_2}{k_1}$$

$$^{3}D_{B} \sim \frac{k_2 k_3}{k_1^2}$$

Thus for a series of first order reactions, the rth rank primary product-based delplot intercept is finite for product of rank r and zero for all products of rank greater than r. Incorporation of parallel paths in the networks also gives similar results to the reactant-based delplots, although the numerical value of the intercepts differs from the reactant-based delplot intercepts. In principle, product-based delplots can be also defined for non-primary products but the analysis becomes extremely complicated. This is because if the basis set is a non-primary product, then the denominator of equation (3.74) needs more than one Taylor series expansion. This repeated expansion of the denominator introduces time "τ" in the denominator at each stage of Taylor series expansion, which complicates the process of evaluating limits.

3.6 Identification of Reaction Steps

3.6.1 Introduction

This section deals with synthesis of reaction network. The delplot method can be used to simplify the problem of synthesis of reaction network, even though it cannot solve the problem completely. There are two methods for synthesis of reaction network. In the first method that is the general method, the rate constants for each possible reaction is calculated. At present this method can be applied only to first order reactions. The method of Wei and Prater[9] is the only method in this category. In the second method a reaction network is proposed based on the chemical knowledge of the system, then a functionality for the rate expression is assumed. This method becomes extremely complicated for multi-products systems even when the rate expressions are linear. For example, for a set of first order reversible reactions between 8 species, there are 56 reaction steps. In the third method, the product rank is first found, then the connecting steps between product are identified based on certain rules. Lee and Akella[12] have proposed a method in this category, that is based on successive laplace transformation of the data. This method applies only to irreversible first order reaction. The successive laplace transformation of the data makes this method cumbersome and difficult to apply to realistic systems. Based on the method proposed in the earlier section, the delplot method can be used to simplify the problem of synthesis of reaction network. The delplot method for reaction network synthesis can be applied in two stages. In the first stage the products are separated according to their rank. At the end of the first stage products are grouped as primary, secondary, tertiary and so on. In the second stage, the reaction steps from a product of lower rank to a product of next higher rank are identified. For example, for the network given in figure 3.1 on page 100 with species A as the reactant, steps 1, 2, 3, 4, 5, 6, 7 and 9 can be identified. The delplot method cannot identify reaction steps between products

of same rank and from products of higher rank to products of lower rank. Using the same example, steps 8, 10 and 11 fall into this category and hence cannot be identified using delplot analysis and A as an reactant. Step 8 can be identified if D is used as a reactant and step 10 can be identified if C is used as a reactant. By definition of the rank of the product, there cannot be any reaction steps from products of lower rank to products of rank higher than one more than the reactant in that step.

3.6.2 Example

An illustrative example is shown in figure 3.3 on page 136. In this example, there are two reactants A and B and five products C, D, E, F and G. The feed consists of A and B only. Assume that the result of the first stage, after applying basic and extended delplot, is as shown in figure 3.3. Thus C and D are primary products. E and F are secondary products and G is a tertiary product. Since this is a two reactant system there are three different ways of finding intercepts. The mixed basis set is not considered here, for example, ${}^{2}C_{AB}$. The intercepts at different ratio of initial concentration(ϵ) of reactants is found. Then, the reaction steps between the reactants and primary products are found.

Four first rank intercepts, ${}^{1}C_{A}$, ${}^{1}D_{A}$, ${}^{1}C_{B}$ and ${}^{1}D_{B}$ can be defined. Assume that the stoichiometric coefficients are unity and the reactions are first order. Table 3.6 on page 137 list various reaction schemes between reactants A and B, and primary products C and D, with its intercepts.

Results of scheme 1 and 2 of table 3.6 show that the intercepts corresponding to the reactant not being consumed in the reactions leading to primary product diverges. If any two intercepts are unity, then there are no cross steps as shown in scheme 3 and 4 of table 3.6. In scheme 5-8 of table 3.6, there is only one distinct intercept independent of ϵ. In contrast, in scheme 9, all intercepts are

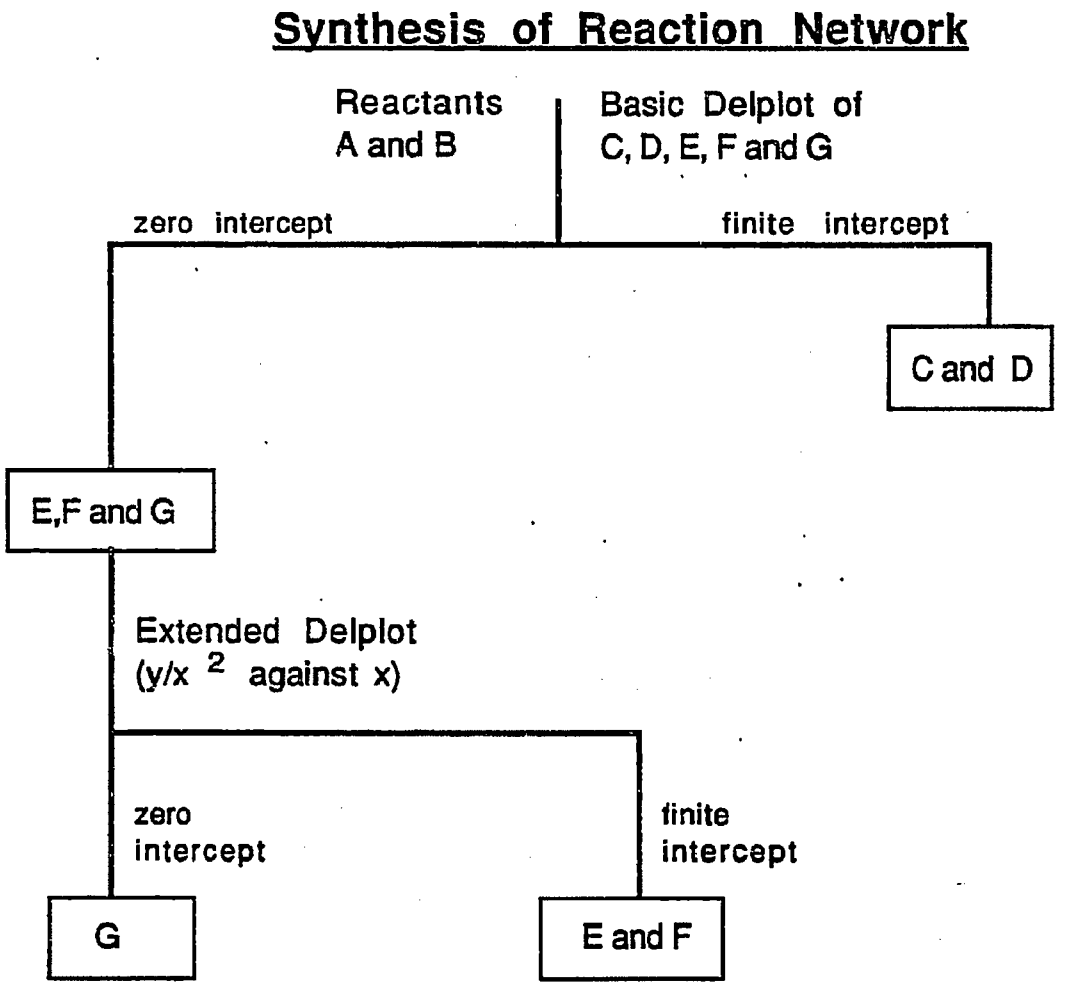

Figure 3.3: Strategy for use of delplot analysis in the identification of reaction steps in networks.

Table 3.6: Identification of reaction steps from reactants to primary products

#	Scheme	^1C_A	^1D_A	^1C_B	^1D_B
1	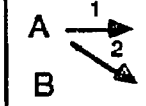	$\frac{k_1}{k_1+k_2}$	$\frac{k_2}{k_1+k_2}$	diverges	diverges
2	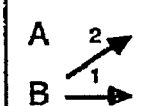	diverges	diverges	$\frac{k_2}{k_1+k_2}$	$\frac{k_1}{k_1+k_2}$
3	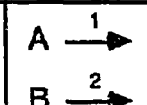	1	$\frac{k_2}{k_1\varepsilon}$	$\frac{k_1\varepsilon}{k_2}$	1
4	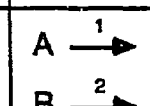	$\frac{k_2}{k_1\varepsilon}$	1	1	$\frac{k_1\varepsilon}{k_2}$
5	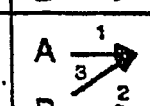	$1+\frac{k_3\varepsilon}{k_1}$	$\frac{k_2}{k_1\varepsilon}$	$\frac{k_3+k_1\varepsilon}{(k_2+k_3)}$	$\frac{k_2}{k_2+k_3}$
6	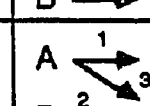	$\frac{k_1}{k_1+k_3}$	$\frac{k_2+k_3\varepsilon}{(k_1+k_3)\varepsilon}$	$\frac{k_1\varepsilon}{k_2}$	$1+\frac{k_3\varepsilon}{k_1}$
7	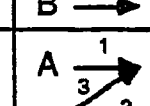	$\frac{k_2}{k_1\varepsilon}$	$1+\frac{k_3}{k_1\varepsilon}$	$\frac{k_2}{k_2+k_3}$	$\frac{k_3+k_1\varepsilon}{(k_2+k_3)}$
8	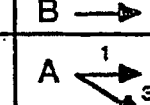	$\frac{k_2+k_3\varepsilon}{(k_1+k_3)\varepsilon}$	$\frac{k_1}{k_1+k_3}$	$1+\frac{k_3}{k_2\varepsilon}$	$\frac{k_1\varepsilon}{k_2}$
9	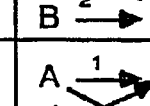	$\frac{k_1+k_4\varepsilon}{(k_1+k_3)\varepsilon}$	$\frac{k_2+k_3\varepsilon}{(k_1+k_3)\varepsilon}$	$\frac{k_4+k_1\varepsilon}{(k_2+k_4)}$	$\frac{k_2+k_3\varepsilon}{(k_2+k_4)}$

functions of ϵ. Thus, the value of the intercept and its variation with ϵ can be used to discriminate between rival reaction networks. An algorithm based on the characteristics of the intercepts in table 3.6 is shown in figure 3.4.

Network-independent and kinetics-independent guidelines can be formulated from results of table 3.6. For example, if the first rank intercept (after correcting for stoichiometric coefficient) is,

$$^1C_A = 1$$

then, C is formed only from A and A is consumed only in the reactions where C is formed. This is observed in scheme 3 and 4 of table 4. For first order reactions, if the intercept of a primary product C

$$^1C_A \neq f(\epsilon_j)$$

for all j where ϵ_j is the ratio of initial concentration of reactant j to a standard reactant, then C is formed only from A. This is observed in schemes 5-8 of table 3.6.

After identifying the reaction steps between reactants and products, a similar procedure is used to identify reaction steps between primary products and secondary products. Assume that the results of algorithm in figure 3.4 on page 139 yield scheme 3 of table 3.6.

Table 3.7 shows the intercepts for various reaction schemes between primary products and secondary products. Here again, the variation of second rank intercepts with ϵ is used to discriminate between rival reaction networks. Schemes 1-4 of table 3.7 on page 141 each have two distinct second rank intercepts independent of ϵ. In contrast, schemes 5-8, have one distinct second rank intercept independent of ϵ. Scheme 9 has no intercepts independent of ϵ. Thus the intercepts can be used to identify reaction steps from products of rank (r-1) to products of

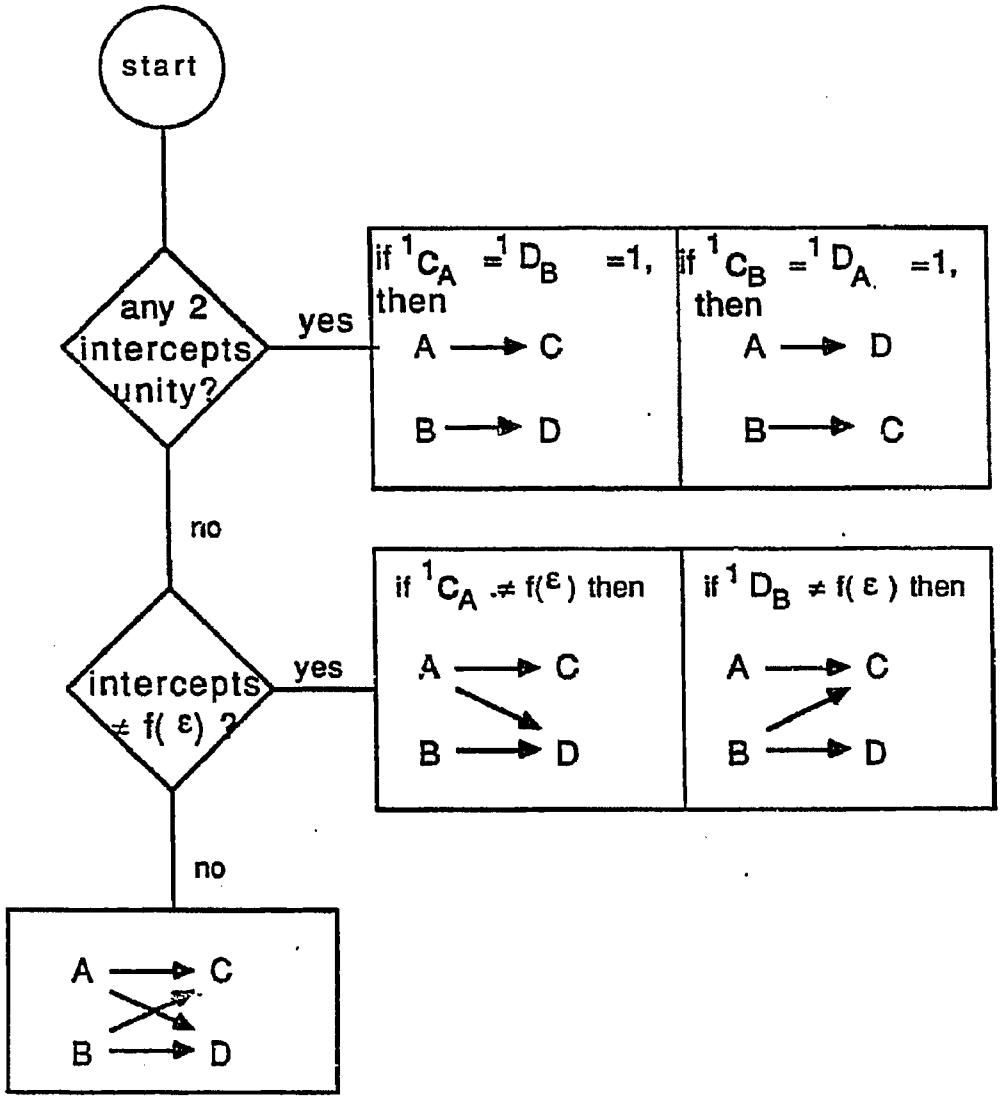

Figure 3.4: Identification of steps from reactants to primary products.

rank r. Figure 3.5 on page 142 shows an algorithm used to discriminate between rival reaction networks.

3.6.3 Overall Scheme

At this point the overall scheme will be summarized. Figure 3.6 summarizes the overall scheme of delplot analysis. Typical kinetic data consists of mole fractions of various components as a function of process time(batch time or space time). This is shown in the upper left corner of figure 3.6. Then, delplot analysis is performed on this data as shown in earlier sections of this chapter. The delplot analysis yield, delplot intercepts and effective rank of the product. The next stage is to find network rank of the product from the effective rank. Here, prior knowledge of the system is needed for higher rank products. For primary products, the effective rank of the product is always same as the network rank. This is illustrated by the straight line going from the box symbolizing effective rank to the box symbolizing network rank, marked with $r \leq 1$. For higher rank products, prior knowledge of order of reaction is needed. However in many systems we know that the reactions are first order or second order. After the network rank is obtained, additional network information can be obtained by monitoring the variations in the delplot intercepts. Particularly, as explained in this section, reaction steps can be identified.

3.7 Separation of Regimes

3.7.1 Order of Magnitude Analysis

A primary product is a product that has one slow step between the reactant and itself on the time scale of "process time". The process time is the contact time. If the process time scale varies over a large range, a reaction can be slow or fast in two different regions of process time(or GHSV or conversion). Thus

Table 3.7: Identification of reaction steps from primary products to secondary products

#	Scheme	^2E_A	^2F_A	^2E_B	^2F_B
1	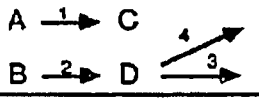	$\frac{k_4\,k_2}{k_1^2\varepsilon}$	$\frac{k_3\,k_2}{k_1^2\varepsilon}$	$\frac{k_4}{k_2}$	$\frac{k_3}{k_2}$
2	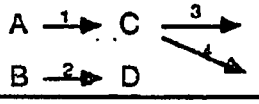	$\frac{k_3}{k_1}$	$\frac{k_4}{k_1}$	$\frac{k_1\,k_3\,\varepsilon}{k_2^2}$	$\frac{k_1\,k_4\,\varepsilon}{k_2^2}$
3	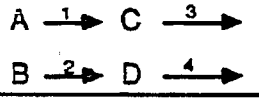	$\frac{k_3}{k_1}$	$\frac{k_4\,k_2}{k_1^2\varepsilon}$	$\frac{k_1\,k_3\,\varepsilon}{k_2^2}$	$\frac{k_4}{k_2}$
4	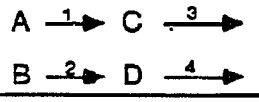	$\frac{k_4\,k_2}{k_1^2\varepsilon}$	$\frac{k_3}{k_1}$	$\frac{k_4}{k_2}$	$\frac{k_1\,k_3\,\varepsilon}{k_2^2}$
5	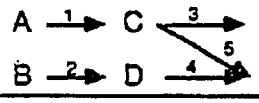	$\frac{k_3}{k_1}$	$\frac{k_5}{k_1}+\frac{k_4\,k_2}{k_1^2\varepsilon}$	$\frac{k_1\,k_3\,\varepsilon}{k_2^2}$	$\frac{k_4}{k_2}+\frac{k_5 k_1\varepsilon}{k_2^2}$
6	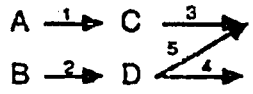	$\frac{k_3}{k_1}+\frac{k_5\,k_2}{k_1^2\varepsilon}$	$\frac{k_2 k_4\varepsilon}{k_1^2}$	$\frac{k_5}{k_2}+\frac{k_3 k_1\varepsilon}{k_2^2}$	$\frac{k_4}{k_2}$
7	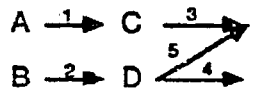	$\frac{k_4\,k_2}{k_1^2\varepsilon}$	$\frac{k_3}{k_1}+\frac{k_5\,k_2}{k_1^2\varepsilon}$	$\frac{k_4}{k_2}$	$\frac{k_5}{k_2}+\frac{k_3 k_1\varepsilon}{k_2^2}$
8	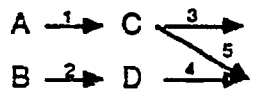	$\frac{k_5}{k_1}+\frac{k_4\,k_2}{k_1^2\varepsilon}$	$\frac{k_3}{k_1}$	$\frac{k_4}{k_2}+\frac{k_5 k_1\varepsilon}{k_2^2}$	$\frac{k_1\,k_3\,\varepsilon}{k_2^2}$
9	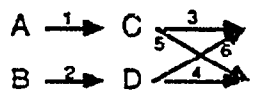	$\frac{k_3}{k_1}+\frac{k_6\,k_2}{k_1^2\varepsilon}$	$\frac{k_5}{k_1}+\frac{k_3\,k_2}{k_1^2\varepsilon}$	$\frac{k_6}{k_2}+\frac{k_3 k_1\varepsilon}{k_2^2}$	$\frac{k_3}{k_2}+\frac{k_5 k_1\varepsilon}{k_2^2}$

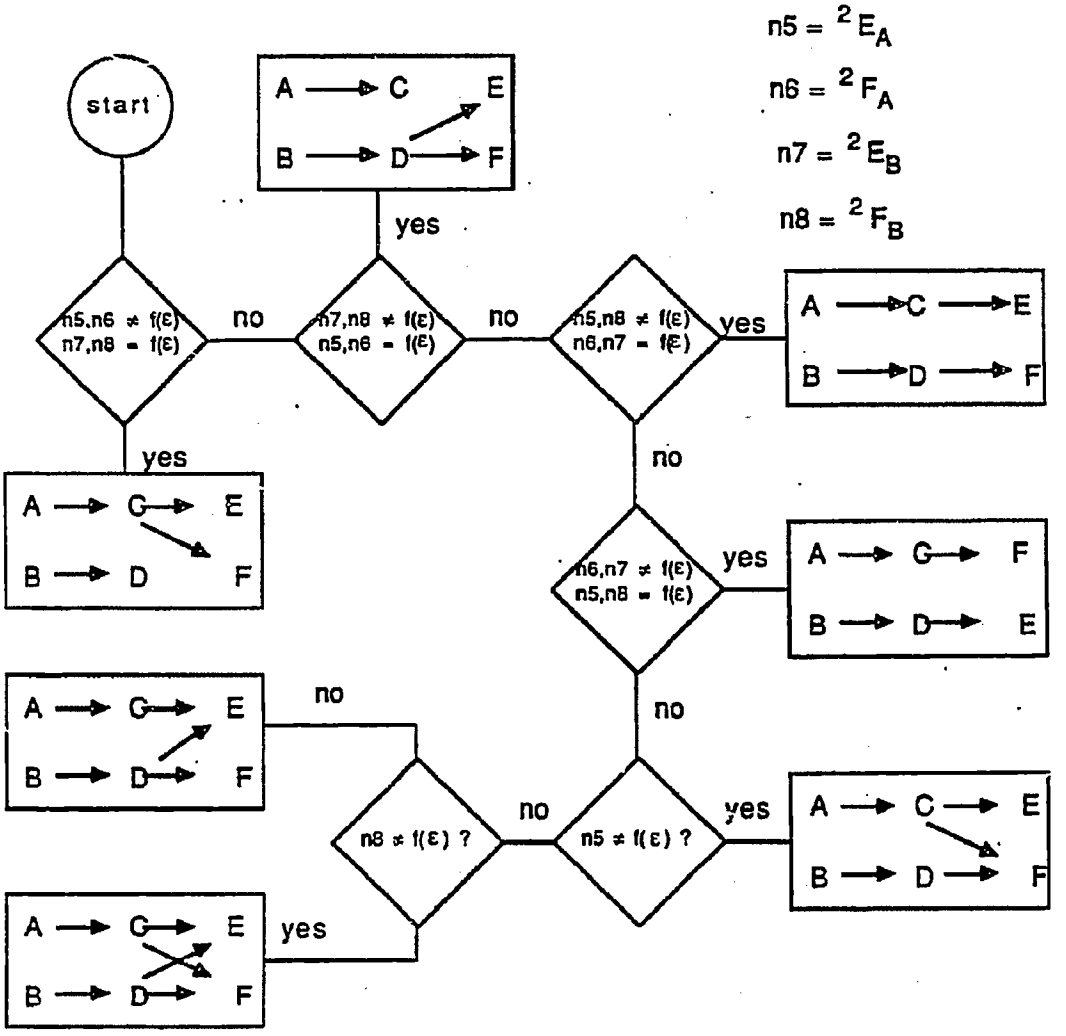

Figure 3.5: Identification of the steps from primary products to secondary products.

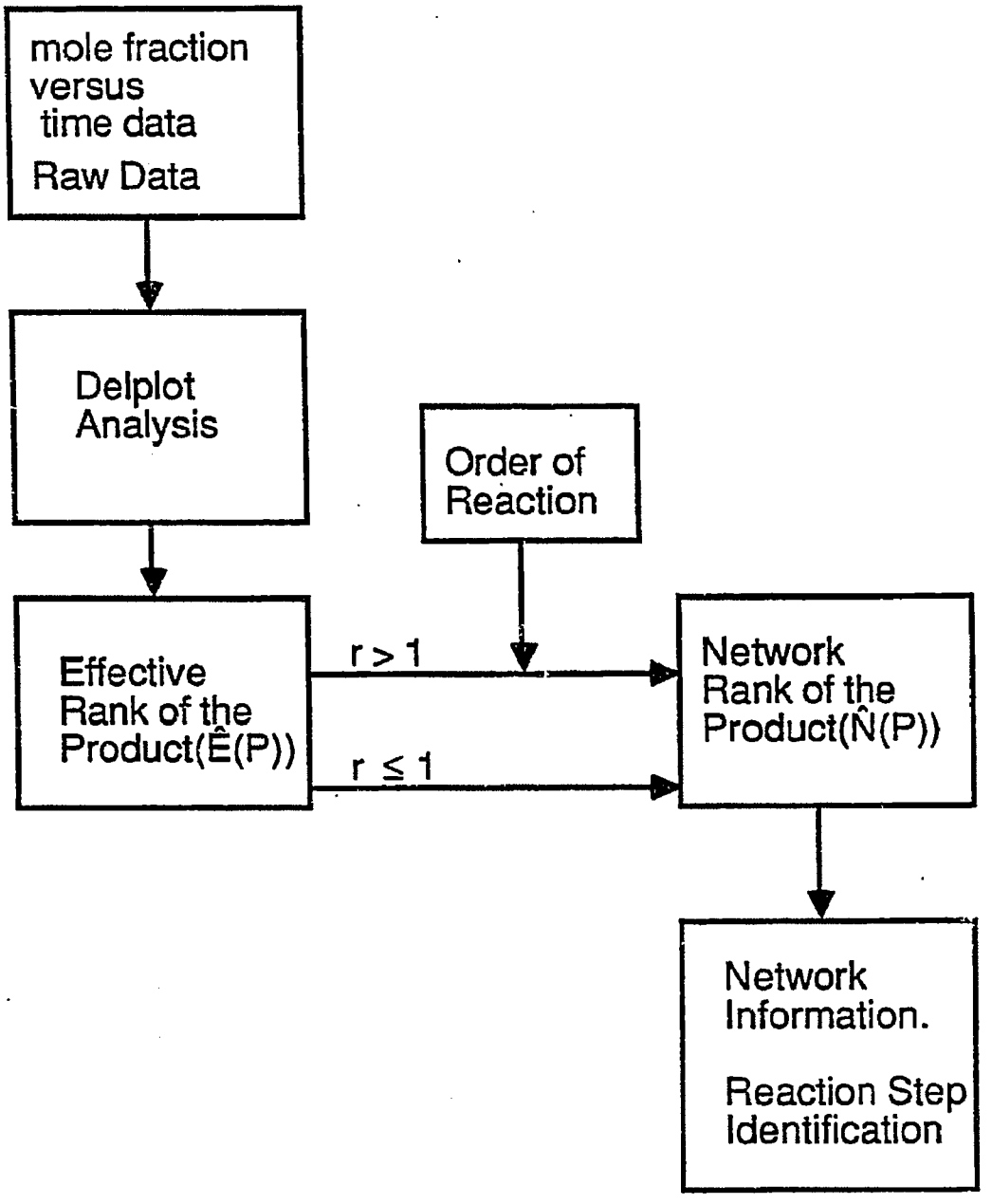

Figure 3.6: Overall scheme of delplot analysis

a product can be primary or secondary in different ranges of process time. The delplot method can be used to identify these regimes of time scale.

A simple reaction scheme

$$A \xrightarrow{k_1} B \xrightarrow{k_2} C \tag{3.75}$$

will il' .strate the separation of regimes.

The exact solution to the above scheme when the only starting material is A is

$$A = A_0 e^{-k_1 t}$$

$$B = \frac{A_0 \times k_1}{k_2 - k_1} \times (e^{-k_1 t} - e^{-k_2 t})$$

$$C = A_0 - A - B$$

If there are no limitations on process time that can be measured, that is we can get data at small process time scales then

$${}^1C_A = 1 - \lim_{t \to 0} \frac{-k_1}{k_2 - k_1} \times \frac{e^{-k_1 t} - e^{-k_2 t}}{1 - e^{-k_1 t}}$$

Expanding the exponential terms and taking the limits

$${}^1C_A = 0$$

This is also true for $k_2 \gg k_1$. This implies that C is a secondary product on a small process time scale. However if we limit the process time scale τ such that

$$\frac{1}{k_2} \ll t \ll \frac{1}{k_1} \tag{3.76}$$

The above inequality holds when one cannot obtain data over the time scale of $\frac{1}{k_2}$. Often one of reactions in the pathway is fast and this fast step does not affect

the rank of the product as long as it is fast over the entire range of process time investigated.

The delplot intercept calculated from the rigorous solution under the following conditions

$k_1 t \ll 1$ and $k_2 t \gg 1$ is

$$ {}^1C_A = 1 - \lim_{\substack{k_1 t \to 0 \\ k_2 t \to \infty}} \frac{k_1}{k_2(1 - e^{-k_1 t})} $$

$$ {}^1C_A = 1 - \lim_{\substack{k_1 t \to 0 \\ k_2 t \to \infty}} \frac{1}{k_2 t + \frac{(k_2 t)(k_1 t)}{2} - \cdots} \tag{3.77} $$

$$ {}^1C_A = 1 - \lim_{k_2 t \to \infty} \frac{1}{k_2 t} $$

$$ {}^1C_A = 1 \tag{3.78} $$

Hence C is primary product when $k_1 t \ll 1$ and $k_2 t \gg 1$. Thus if $k_2 \gg k_1$, C is a secondary product when the process time scale(τ) is much less than $\frac{1}{k_2}$ and C is primary product when the process time scale is much greater than $\frac{1}{k_2}$.

3.7.2 Singular Perturbation Analysis

A more rigorous proof for the above concept is shown below using singular perturbation theory [25, 26]. Here again, the reaction scheme of equation (3.75) is considered. The regime where product C is primary, corresponds to the case where the Bodenstein approximation holds for B. This is the outer solution in singular perturbation theory. In the outer solution regime, the highest order derivative and the initial condition for B is neglected. In the regime where C is a secondary product, the Bodenstein approximation is no longer valid and the outer solution

has to be used. In the outer solution the highest order derivative and the initial boundary condition for B is to considered.

Bowen et al.[27] have investigated the applicability of the Bodenstein approximation using singular perturbation theory. For the example illustrated above, the inner solution and the outer solution is derived using the singular perturbation theory.

At large times, the steady state approximation holds reasonably well. The outer solution is applicable only after a certain critical time when the derivative term of equation (3.80) becomes negligible.

First, the equations are to be non-dimensionalized.

Let

$$\alpha = \frac{A}{A_0}$$

$$\lambda = \frac{k_2}{k_1}$$

$$\beta = \frac{B\lambda}{A_0}$$

and

$$\xi = k_1 \tau$$

Thus the mass balances of A and B can be written as

$$\frac{d\alpha}{d\xi} = -\alpha \tag{3.79}$$

and

$$\frac{1}{\lambda}\frac{d\beta}{d\xi} = \alpha - \beta \tag{3.80}$$

The boundary conditions are

$$\alpha(0) = 1$$

$$\beta(0) = 0$$

The solution for A is always the same and is

$$A^o = A_0 e^{-\xi}$$

The variation of B in the outer solution region can be found by expanding β in terms of $\frac{1}{\lambda^n}$.

$$\beta^o = \sum_{n=0}^{\infty} \frac{\beta_n}{\lambda^n} \tag{3.81}$$

Substituting the above expression for β in equation (3.80), and then collecting coefficients of term of different powers of λ we get

$$\beta_0 = e^{-\xi}$$

and

$$\beta_n = e^{-\xi}$$

thus

$$\beta^o = e^{-\xi}\left[1 + \frac{1}{\lambda} + \frac{1}{\lambda^2} + \cdots\right]$$

$$\beta^o = \frac{e^{-\xi}}{1 - \frac{1}{\lambda}}$$

$$B^o = \frac{A_0 e^{-\xi}}{\lambda - 1} \tag{3.82}$$

where $\xi = k_1 \tau$, $\lambda = \frac{k_2}{k_1}$, and $\lambda \to \infty$.

The outer solution does not satisfy the initial boundary condition for B. Near the initial condition, that is within the boundary layer, the outer solution is not valid. Hence the inner solution has to be found.

For the inner solution we have to define an expanded time scale $\omega = \lambda\xi$. In the inner solution region, the derivative term for B cannot be neglected and all

the terms are of the same order of magnitude. The inner solution can be derived as follows

The solution for A will not change

$$A^i = A_0 e^{-\frac{\omega}{\lambda}}$$

For B , the balance equation is

$$\frac{d\beta}{d\omega} = e^{\frac{-\omega}{\lambda}} - \beta \tag{3.83}$$

β can again be expressed as a perturbation expansion with respect to $\frac{1}{\lambda}$

$$\beta^i = \sum_{n=0}^{\infty} \frac{\beta_n^i}{\lambda^n} \tag{3.84}$$

Substituting the above expansion (3.84) in the equation (3.83) and equating the coefficients of $\frac{1}{\lambda^n}$, we get

$$\frac{d\beta_n^i}{d\omega} = \frac{(-1)^n \omega^n}{n!} - \beta_n^i \tag{3.85}$$

The boundary conditions for each function is

$$\beta_n^i(0) = 0 \tag{3.86}$$

Solving equations (3.85) with boundary conditions (3.86), we get

$$\beta_0^i = 1 - e^{-\omega}$$

$$\beta_1^i = 1 - \omega - e^{-\omega}$$

$$\beta_2^i = \frac{\omega^2 - 2\omega - 1}{2} - e^{-\omega}$$

Thus we have

$$B^i = \frac{A_0}{\lambda}\Big[1 - e^{-\omega} - \frac{1}{\lambda}(\omega - 1 + e^{-\omega}) + \frac{1}{2\lambda^2}(\omega^2 - 2\omega + 2 - 2e^{-\omega}) + O(\frac{1}{\lambda^3})\Big] \tag{3.87}$$

The delplot intercept from the outer regime can be found by taking the limit of the outer solution as $\xi \to 0$. But the inner solution as $\omega \to \infty$ should be same as the outer solution as $\xi \to 0$. Here we have to take the double limit of the outer solution as $\xi \to 0$and $\omega \to \infty$. Hence the delplot intercept from the outer solution is

$${}^1C_A = 1 - \lim_{\substack{\xi \to 0 \\ \omega \to \infty}} \frac{B^o}{A_0 - A^o}$$

$${}^1C_A = 1 - \lim_{\substack{\xi \to 0 \\ \omega \to \infty}} \frac{e^{-\xi}}{(\lambda - 1)(1 - e^{-\xi})} \tag{3.88}$$

which can be simplified to

$${}^1C_A = 1 - \lim_{\substack{\xi \to 0 \\ \omega \to \infty}} \frac{1}{(\lambda\xi - \frac{\lambda\xi^2}{2} + \cdots)}$$

but $\omega = \lambda\xi$,

$${}^1C_A = 1 - \lim_{\substack{\xi \to 0 \\ \omega \to \infty}} \frac{1}{(\omega - \frac{\omega\xi}{2} + \cdots)}$$

thus

$${}^1C_A = 1$$

Hence C is primary product in the space time region where the outer solution is valid.

If we take the inner solution equations

$${}^1C_A = 1 - \lim_{\omega \to 0} \frac{B^i}{A_0 - A^i}$$

$$ {}^{1}C_A = 1 - \lim_{\omega \to 0} \frac{1 - \frac{\omega}{2} - \frac{\omega}{2\lambda} - \cdots}{1 + \frac{\omega}{2\lambda} + \cdots} \qquad (3.89) $$

$$ {}^{1}C_A = 0 $$

Thus singular perturbation theory shows that the delplot of product C has a finite intercept and hence product C is a primary product in the outer solution regime. Similarly a delplot of product C has a zero intercept in the inner solution regime and hence is a secondary product. Thus the delplot method can be used to separate regimes of space time where a given product can be primary or secondary. An example of a product that changes rank in two different space time regimes will be discussed in chapter 8.

3.8 Conclusions

In this chapter, a new method for analysis of reaction network was developed. This method can

sort products according to their rank

find the reaction rate function in simple systems

identify reaction steps in a complex reaction network

separate regimes of time where product rank changes.

The advantages of this method are in its simplicity, the ease of application and the better precision of this method. Also, this method often decouples the rank of the product from the order of the reaction so as to serially determine the rank of the species, next the kinetic rate equation and third the parameter values. The concept of effective order and effective rank is also developed and used. Effective rank of the product is used to find the applicability of delplot analysis. Furthermore, a

simple algebraic recursive equation(EPRE) shows the coupling between effective rank of the product and the order of the reaction for integral order reactions.

The disadvantages of this method are:-

1. Often it is difficult to differentiate between small and finite intercept and zero intercept. Hence some times an effective product rank cannot be assigned.

2. For higher rank product, prior knowledge of the order of the reactions is needed.

3. The method becomes cumbersome for non-integer orders for higher rank products.

4. This method is not a total solution to the problem of reaction network and reaction rate function identification, however, it is a partial solution to an otherwise insolvable problem.

REFERENCES

1. G.F. Froment and K.B. Bischoff, "Chemical Reactor Analysis and Design", John Wiley, New York, 1979.

2. J.B. Butt, "Reaction Kinetics and Reactor Design", Prentice-Hall, Englewood-Cliffs, New Jersey, 1980.

3. J.M. Smith, "Chemical Engineering Kinetics", McGraw-Hill, New York, 1981.

4. J.C. Jungers, J.C. Balaceanu, F. Coussemant, F. Eschard, A. Giraud, M. Hellin, P. LePrince and G.E. Limido, "Cinetique Chimique Applique", Technip, Paris, 1958.

5. L.K. Doraiswamy and M.M. Sharma, "Heterogeneous Reactions: Analysis, Examples and Reactor Design", John Wiley, New York, 1984.

6. J.J. Carberry, "Chemical and Catalytic Reaction Engineering", McGraw-Hill, New York, 1976.

7. M. Boudart, "Kinetics of Chemical Processes", Prentice-Hall, Englewood CLiffs, New Jersey, 1968.

8. G.P. Mathur and G. Thodos, Chem. Eng. Sci. 1966, 21, 1191.

9. M. Boudart, Chem. Eng. Sci. 1967, 22, 1387.

10. E.E. Peterson, Chem. Eng. Sci. 1965, 20, 587.

11. J. Wei and C.D. Prater, Advances in Catalysis, 13, Academic Press, New York(1962).

12. M.T. Klein and P.S. Virk, I.E.C. Fund.1983, 22, 35.

13. H. Hofmann, Appl. Catal. 1985, 15, 79.

14. I.M. Akella and H.H. Lee, Chem. Eng. Journal, 1981, 22, 25.

15. H.H. Lee, "Heterogeneous Reactor Design", Butterworth. Boston. 1985.

16. H.H. Lee. AIChE J. 1978, 24, 116.

17. H.H. Lee, AIChE J. 1977, 23, 116.

18. K.J. Laidler, J. Chem. Educ. 1988, 65. 250.

19. V. Gold, Pur. Appl. Chem. 1983. 55, 1281.

20. J.R. Murdoch, J. Chem. Educ. 1981, 58, 32.

21. D. Kost and A. Pross, Educ. in Chem. 1977, 14, 87.

22. W.J. Ray. J. Biochemistry.1983, 22, 4625.

23. W.M.H. Sachtler, Proc. 8th Intl. Congr. Catal. 1984, Vol. I, p151. Dechema. Berlin.

24. P. Bileon and W.M.H. Sachtler, Adv. Catal.1981, Academic Press. New York.1981.

25. M.D. Greenberg, "Foundations of Applied Mathematics", Prentice-Hall, Englewood Cliff, New Jersey, 1978.

26. A.K. Kapila, "Asymptotic Treatment of Chemically Reacting Systems", Pitman, Boston, 1983.

27. J.R. Bowen, A. Acrivos and A.K. Oppenheim. Chem. Eng. Sci. 1963. 18. 177.

CHAPTER 4
EQUIPMENT AND EXPERIMENTAL METHODS

4.1 Flow Microreactor

Figures 4.1 and 4.2 shows the flow diagram of the reactor. The details of the all pieces of equipment used in this reactor assembly are given in table 4.1. There were four feed gases, three of them were high pressure lines while the fourth was a low pressure gas feed for test reactions at low pressure. The design pressure was 1000psia. The gases have flow limit valves to shut off the gases if the instantaneous flow rate exceeds above a set limit. The hydrogen gas was passed through a filter, a line regulator and a catalytic oxygen remover followed by a molecular sieve trap for removing water. Hydrogen was then passed through a filter, digital mass flow controller and a check valve before feeding it to the mixing manifold. The line filter before the mass flow controller prevents fine dust from entering the mass flow controller and the check flow valve prevents back flow from the manifold.

The connection between the hydrogen line and manifold was controlled by a diaphragm valve, which give good service for repeated use at high pressures. The helium line was similar to the hydrogen line except that the oxygen and the water was simultaneously removed in a water trap. The CO manifold has a carbonyl trap that cracks the Fe and Ni carbonyls formed in the cylinder. Initially a heated charcoal trap was used, however it formed lot of carbon dioxide. Then a heated alkalized alumina trap was successfully used. This was followed by a water removal trap. The carbon monoxide line after the trap was Teflon coated

to prevent formation of carbonyls in the line. The gas manifold has ten openings. The pressure transducer and the rupture disc were located on the manifold. The low pressure gas line was also hooked up to the manifold. The entire reactor assembly and the analytical system is placed within a hood.

Table 4.1: Equipment details of the components of the high pressure reactor

Equipment	Model	Purchased from
Pressure transducer	PLC, 0-1000psia	Test Equipment
Back Pres. Regulator	Mity-Mite, SD-91W	Test Equipment
Mass Flow Controller	High Pres.-5850	Brooks
Line filters	6184-p4FF	Matheson
Flow limit valves	Model LV	Veriflo
Hydrogen purifier	Model B8087	Engelhard
Oxygen/Water remover	Model 98	AIRCO
Rupture Disc	Model 10-61AF4	High Pres. Equip.
Diaphragm Valves	SS-4D4S	Swagelok
Check valves	SS-2C-10	Swagelok
Water remover	SG-6140-2	Linde
aluminized reactors	custom-made	Alloy Surfaces

The reactor was connected to the manifold through a Teflon coated stainless steel line. The reactor consists of two sections (figure 4.3). The top section has an internal diameter of 1/4 inch, while the internal diameter of the bottom section was 1/8 inch. The glass wool was seated at the cone shape section connecting the top and the bottom section. Typically the height of the glass wool would range from 1 4-1 2 inch. The catalyst was then seated over the glass wool. Typical

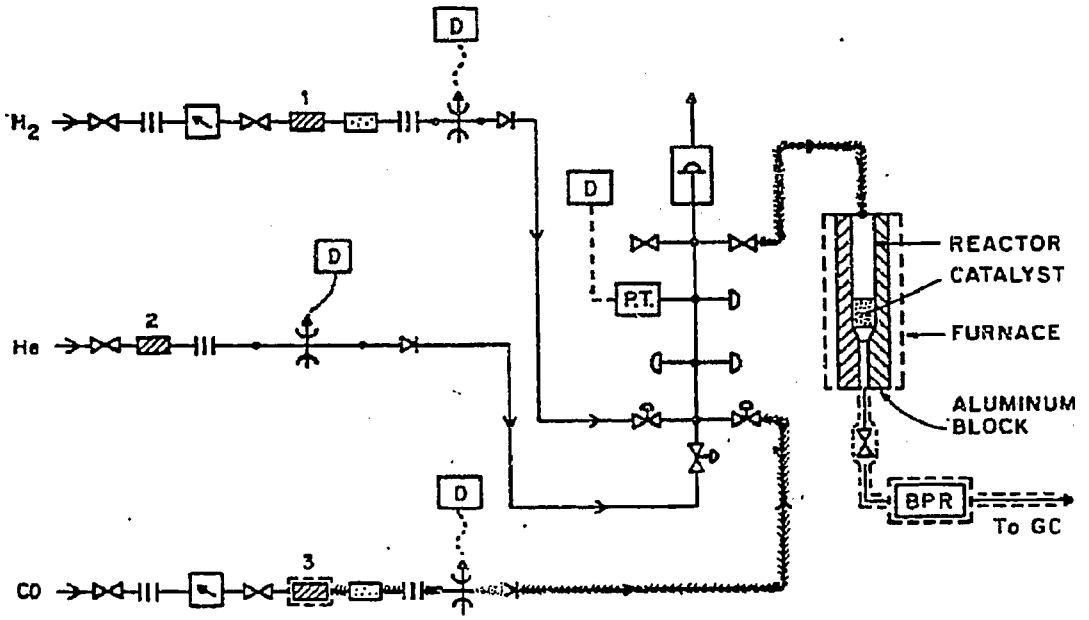

Figure 4.1: Flow diagram of the high pressure reactor

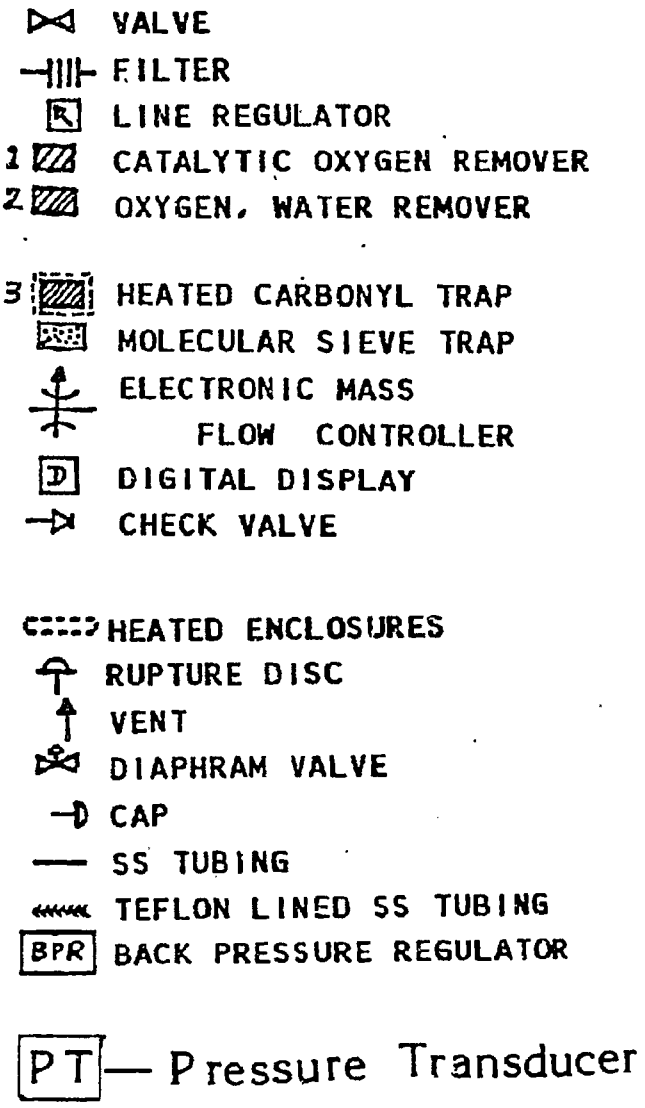

Figure 4.2: Key to the flow diagram of the high pressure reactor given in figure 3.1

catalyst loading was 0.5-1.0gm and typical height of the catalysts bed was 1-2cm. The reactor was made of internally aluminized stainless steel. The details are given in table 4.1. Empty reactor runs under similar conditions did not show any reaction of carbon monoxide and hydrogen under typical reaction conditions. However the presence of secondary reactions cannot be ruled out. The reactor was periodically checked for disruption of the aluminized layer, and replaced whenever necessary. The reactor effluent was then passed through a high temperature valve and the back pressure regulator. All the reactor effluent lines were heated to 120C to prevent condensation of products. A simple vapor pressure calculations of expected product distribution suggested that under the low conversions used there was no substantial condensation. The pressure of the gas manifold was controlled by the pressure on the nitrogen on the other side of the diaphragm. The exit of the diaphragm back pressure regulator was fed to the air actuated sampling valve in the analytical system. Again the interconnecting lines were heated.

4.2 Test Reactions

Ethylene hydrogenation was performed to test the hydrogenation activity of the catalyst. Ethylene hydrogenation was performed on calcined and reduced Rh/Al_2O_3, Mo/Al_2O_3, Al_2O_3 and $Rh\text{-}Mo/Al_2O_3$. But more importantly the effect of gas phase CO on the hydrogenation activity of these catalysts was studied. Ethylene was fed through the fourth line in the gas purification system and was purified by passing it through a CuO trap and a Zeolite trap to remove oxygen and water respectively. The flow rate was monitored with a mass flow controller. A glass reactor was used to avoid base hydrogenation activity of aluminized stainless steel (used in high pressure reaction runs). The catalyst was reduced under 25scc/min of hydrogen at 200C for 1 2hr, 350C for 1/2 hr and at 500C for 1hr. The catalyst was then cooled under hydrogen to 30C. The catalyst was contacted with ethylene only in the presence of hydrogen and helium to avoid poisoning of

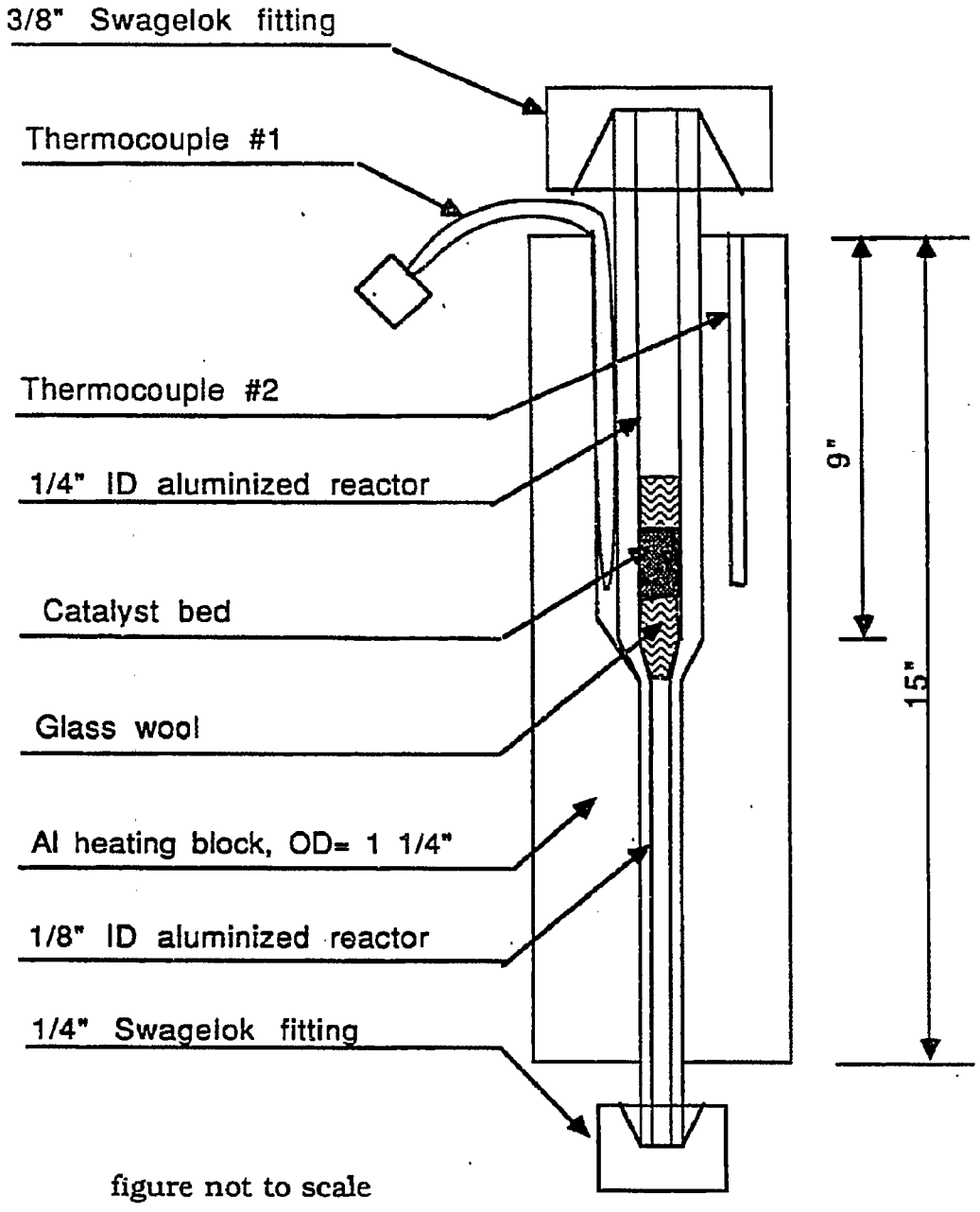

Figure 4.3: Cross-sectional view of the high pressure reactor assembly

the catalyst. The initial transient of ethylene was suppressed by flowing a large excess of helium with ethylene. The flowrate of helium was then decreased to the required value. The same procedure was used to avoid poisoning due to an initial surge of carbon monoxide.

4.3 Analytical System

The analytical system for most reactor runs consisted of a Valco air actuated six port injection valve heated at 130C, a Valco digital valve sequencer, a HP 5700A gas chromatograph equipped with a thermal conductivity detector and a HP 3390A integrator. A 12 feet Porapack QS column was used. For separation of acetic acid and methanol, Porapack T was used. The carrier gas was purified helium, at a flow rate of 25cc/min. The thermal conductivity detector was operated at 250C and 200mA. The reported response factors[1,2] were used to calculate the water-free, hydrogen-free mole fractions. An alumina column was used to separate ethylene, CO and ethane to analysze the reactor effluent during ethylene hydrogenation.

4.4 Static Chemisorption

A Micromeritics 2100D surface area analyzer was connected to a gas purification and gas feed system. Hydrogen and helium were connected to the manifold. A flow through cell was used to treat the sample. The catalysts was reduced under flowing hydrogen at 200C for 1 2 hour, at 350C for 1/2 hour and at 500C for 1 hour. After reduction, the catalysts was outgassed for 1 hour. Then the sample was cooled to room temperature and the amount of total chemisorption and reversible chemisorption was measured. An ASTM 3908 0.5%Pt/Al_2O_3 catalysts gave consistent results on this apparatus.

4.5 Flow Chemisorption

The flow chemisorption apparatus, shown in figure 4.4 consists of a glass reactor in a furnace, gas purification manifold, pulse injections system and a thermal conductivity detector. The catalyst was reduced under the same schedule as in reactor runs. The catalyst was then cooled to room temperature under helium. Then $5\mu l$ of CO was pulsed, the inlet CO pulse was monitored as a negative signal on the output of the thermal conductivity detector. The CO in the exit stream from the reactor was monitored to check adsorption. The CO breakthrough through the catalyst bed was used to suggest complete chemisorption. Thus the number of CO pulses needed to get a CO signal in the outlet stream gave a rough estimate of the CO chemisorption. The peak areas were then integrated to give an accurate estimate of the amount of CO chemisorbed.

4.6 X-Ray Diffraction

A Phillips 3500 automated powder diffractometer with diffracted beam monochromator and nickel filtered Cu radiation at 45kV and 40mA was used. The wavelength of the copper radiation was 1.5418Å. The sample was pressed onto an aluminum sample holder. Typical survey scans were from $2\theta = 10 - 80$ and $\Delta 2\theta = 0.05$ with count time of 1-10sec.

4.7 X-Ray Fluorescence Spectroscopy

A Phillips automated x-ray fluorescence spectrometer PW1410 30 operating in quantitative mode was used to obtain elemental analysis of rhodium and molybdenum.

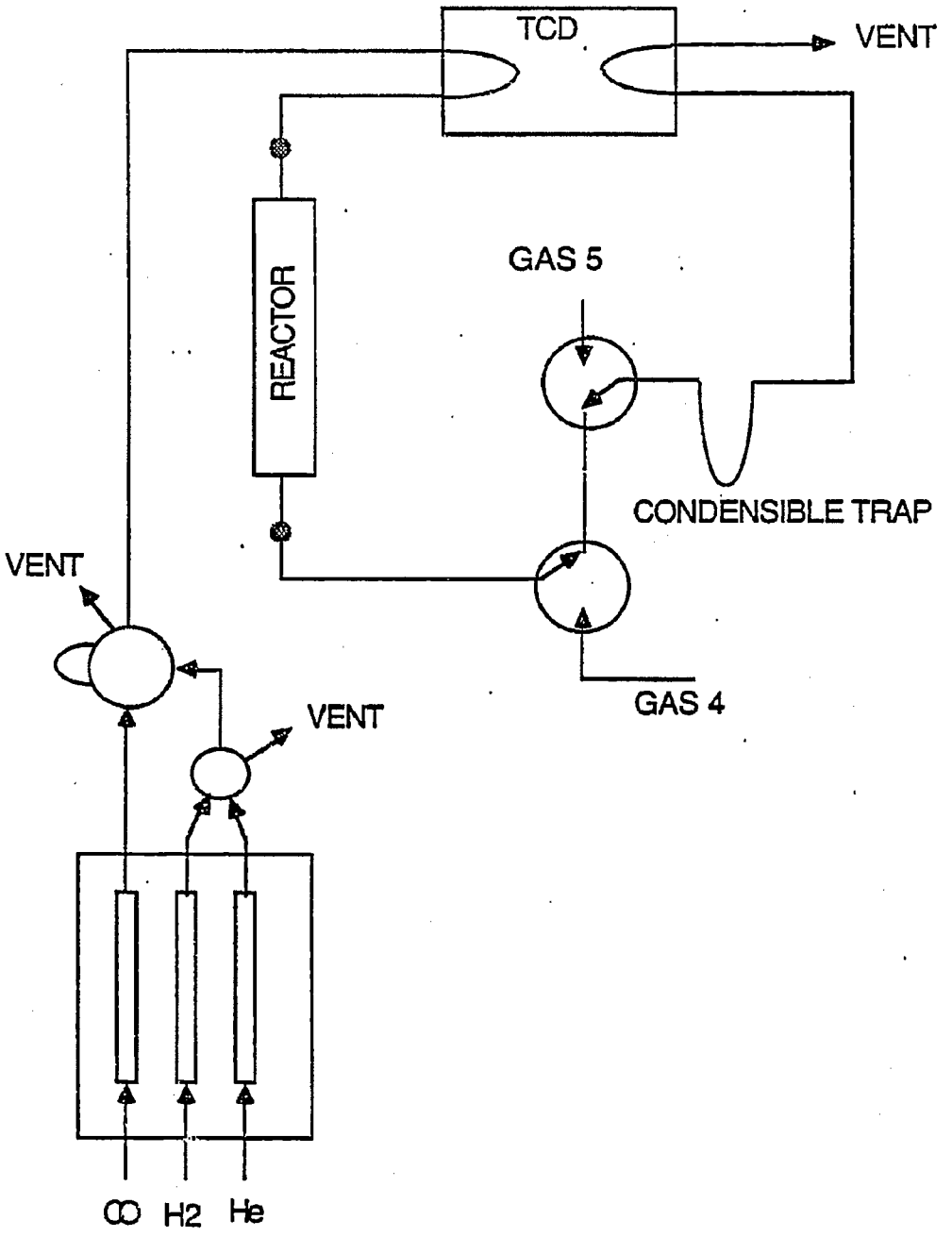

Figure 4.4: Set-up for flow chemisorption apparatus

4.7.1 Calibration

Mo and Rh loadings were checked with XRF. A Phillips PW1410 80 X-Ray Spectrometer was used. Samples were mixed in an appropriate amount with orthoboric acid. The samples were ground and mixed in a ball mill for an hour. Cu K X-Rays and LiF(200) crystal was used. The Mo K_β and Rh K_α lines overlap. Instead of deconvoluting the overlapped peaks, the weak Rh K_β lines were monitored. $Rh(NO_3)_3 3H_2O$ was tried as a standard. Owing to the hygroscopic nature of the above salt , the results were not repeatable. Then $RhCl_3$ salt was used as a standard; this salt was from an old batch and the exact amount of hygroscopic water in it may not be accurate. Also, MoO_3 was used as a standard for solid samples. There may be interference between the Rh and Mo apparent cross-sections . This is due to the higher absorption cross-section of Mo for X-rays emitted by Rh than the absorption cross-section of Rh for X-rays emitted by Mo.

4.7.2 Effect of Particle Size on the Selection of Standards

This section discusses the selection of standards. The role of particle size in solid standards is often not appreciated. Solid standards have micron size particles. The average distance between the two particles is of the same order of magnitude as the length scale of absorption of X-rays emitted by Rh and Mo, e.g., for $60\mu m$ particles, separation between particles is $\approx 0.12cm$ while the length scale for absorption of X-rays in the sample is $\approx 0.2cm$. Thus a substantial amount of X-rays are absorbed before it reached the other element. This is not true with the catalysts sample because Mo and Rh are dispersed on the atomic scale. Hence non-interference of Rh and Mo peaks in solid standards did not imply non-interference in the catalyst samples. In a liquid phase solution the Mo and Rh atoms were well dispersed on the atomic level. Hence non-interference of peaks should be checked in the liquid phase. Liquid samples were prepared by dissolving

Rh nitrate and ammonium molybdate (molybdenum trioxide is sparingly soluble in water). Liquid samples did not show any interference between Rh and Mo peaks.

4.8 X-Ray Photoelectron Spectroscopy

A PHI model 550 spectrometer equipped with an aluminum anode and a double pass cylindrical mirror analyzer was used. The aluminum anode was operated at 10kV and 40mA. The double pass cylindrical mirror analyzer was operated at a pass energy of 50eV and 100eV for detailed scans and survey scans respectively.

Survey scans were taken for each sample and after each treatment to check for extraneous impurities in the chamber and in the sample. Magnesium was present in the XPS survey scans as an impurity from the previous experiments in the chamber. Periodic washing of the sample probe with dilute nitric acid kept the magnesium impurity at low level. This was necessary because the Mg Auger lines were close to the $Rh(3d_{5/2})$ lines for the Al x-rays.

The catalysts samples were ground between glass slides. The ground sample was then pressed into an aluminum die using a hammer. The sample was pressed such that it does not fall off on its own weight. Figure 4.5 on page 166 shows the gas treatment unit for XPS studies. Helium(UHP grade) and hydrogen(UHP grade) were further purified by removing oxygen by passing them through a regenerated copper oxide trap and by removing water by passing them through a regenerated zeolite trap. Carbon monoxide was passed through a zeolite trap only. All the flowrates were controlled by downstream mass flow controllers. The temperature of the sample was heated at a rate not greater than 8C/min. The fresh catalysts were first reduced at 250C and 350C for 1/2 hour each under flowing

hydrogen. Then the temperature was increased to 400C and the catalyst reduced under flowing hydrogen for one hour.

Carbon monoxide adsorption was done by flowing CO at room temperature. Reactions were carried out on these catalysts by flowing a mixture of hydrogen/carbon monoxide =2, total flowrate of 50scc/min at 200C for 2 hours. Various loadings of Na/Al_2O_3 samples were also run for comparison. To see the effect of reaction, some of the used catalysts from the reaction studies were also investigated. Finally, the effect of sodium addition on the surface -OH groups and the role of silanes was investigated. Two samples, Al_2O_3 and 2% Na/Al_2O_3 were silanized. A solution of $\approx$ 5 volume % of hexamethyl disilazane(HMDS) in spectroscopic grade n-hexane was prepared. Then the samples were mixed with the solution. The samples were then equilibrated in the solution for six hours. The mixture was then heated to 70C and later evacuated for 12 hours.

The XPS investigation was carried out to investigate the chemical state of rhodium after various treatments on the catalysts. These treatments included, reduction, carbon monoxide adsorption and carbon monoxide hydrogenation reactions. The effect of the amount of sodium added on the chemical state of rhodium was also investigated. Using the peak areas of the various elements, the physical state, i.e., the state of aggregation of various components, was probed. Finally, XPS was used to elaborate silanization reaction on sodium modified rhodium/alumina.

Also, for the silanization studies additional data was collected for Si(2p) and N(1s) regions. The intensity of the peaks in the carbon and rhodium region was low in spite of the many scans collected. Hence there was a large error($\pm$0.3eV) in the binding energies of the peaks in the carbon and the rhodium region. The signal/noise in the XPS peak areas was large, and hence quantitative XPS has substantial errors, i.e., noise and drift, up to 30%. A survey scan over 0-1000eV

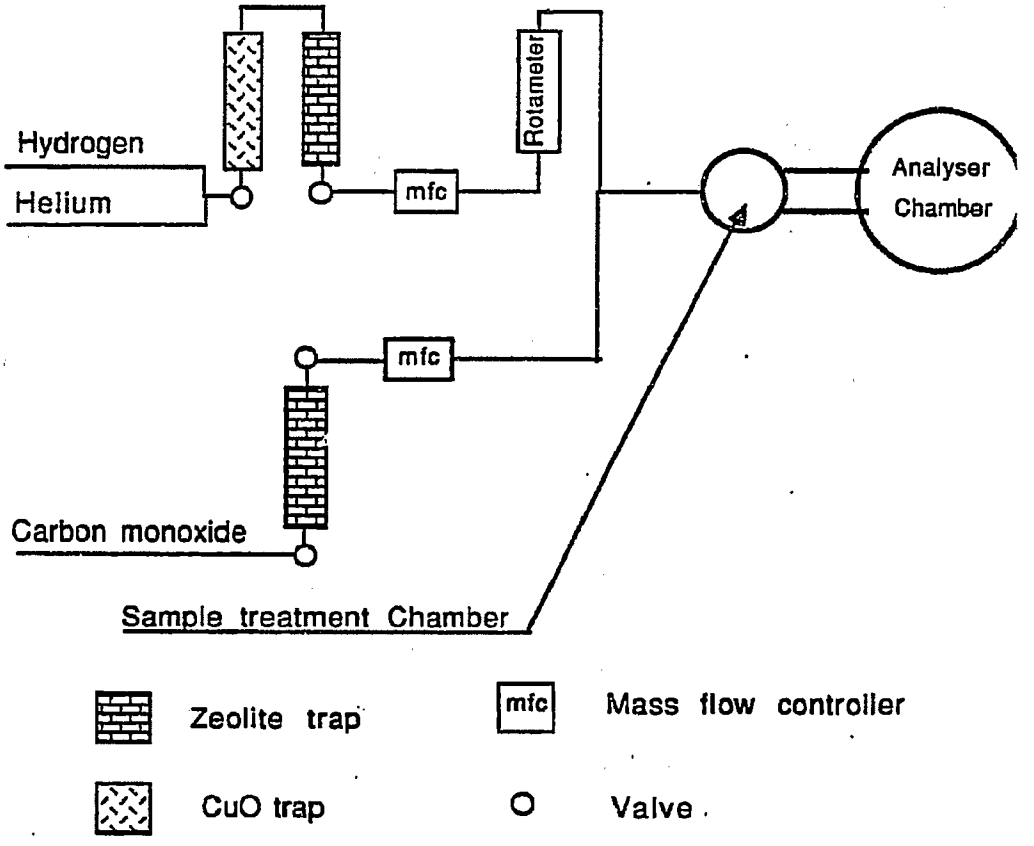

Figure 4.5: Flow diagram for gas feed system for X-Ray photoelectron spectroscopy

was taken before each run. All the data was collected at 30C under a pressure less than 5×10^{-8} torr. The sample holder was positioned to get the maximum signal intensity. The correct alignment of the sample was checked by confirming the absence of two aluminum peaks; one from the catalyst support and the other from the aluminum sample holder.

4.9 Temperature Programmed Methods

Temperature programmed reduction(TPR) and temperature programmed desorption(TPD) was performed on various sodium modified rhodium/alumina catalysts. The reducibility of rhodium, the adsorption states of hydrogen, and the effect of sintering was investigated. Figure 4.6 on page 168 shows the flow diagram of the apparatus used for TPD/TPR studies. The sample was heated at a linear rate in flowing gas with the inlet and outlet gas composition compared in two sides of a thermal conductivity detector. The outlet gas was dried in a dry ice/acetone cold trap before it was analyszed. The difference signal from the detector was stored on a time-sharing computer as a function of time. The output of the furnace thermocouple was also recorded to insure that a linear heating rate was maintained. Hydrogen consumption was quantified by calibration from the area, in millivolt-minutes, under the trace of the thermal conductivity detector output.

A typical run consists of loading approximately 75mg of catalysts and heating it at 40 degrees C/min in 60 cc/min of 5% H_2 in N_2 from room temperature to about 660C. The sample was then cooled within 5 minutes to about -40C in the same gaseous stream. The flow was switched to pure nitrogen at this stage to do temperature programmed desorption. The TPD data was collected at the same heating rate. The peak areas, representing hydrogen uptake were within 5-7%. It was observed that at higher programming rates the peaks were sharper and the

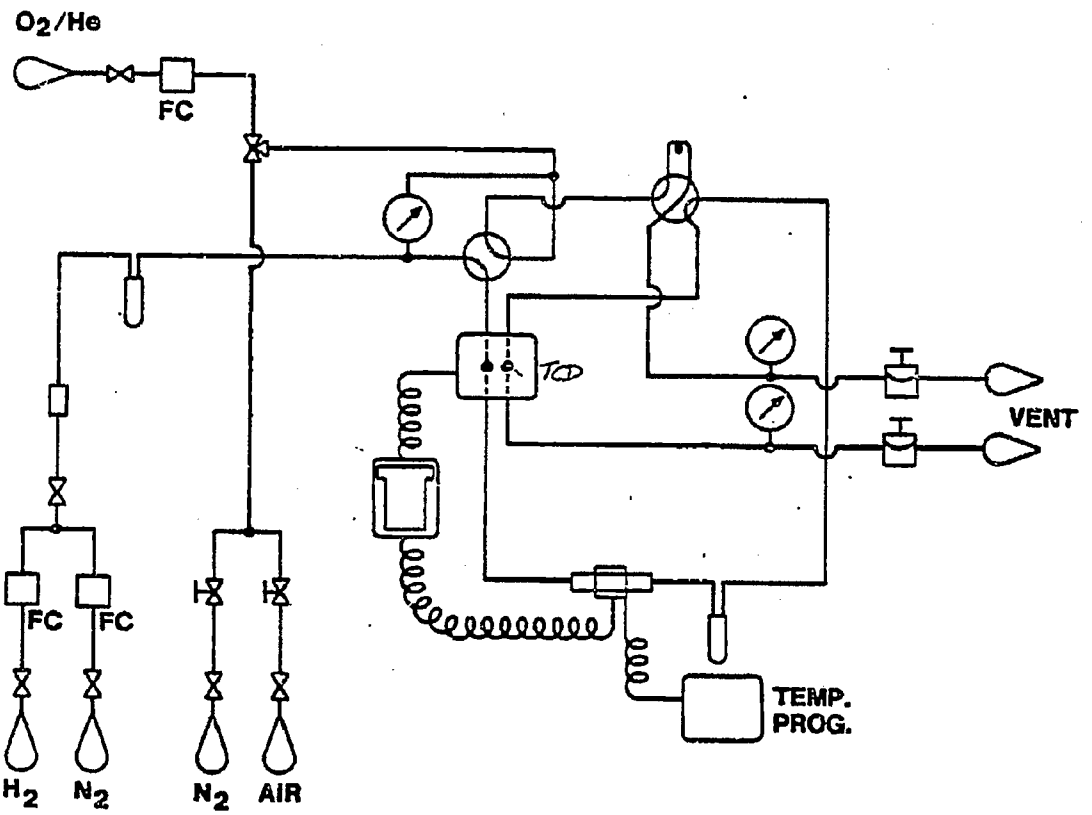

Figure 4.6: Flow diagram of TPR/TPD apparatus

maximum temperature was slightly shifted. For oxidation runs, the catalyst after TPD was cooled to room temperature in the nitrogen stream and the flow was switched to 2% O_2 in He.

4.10 Electron Spin Resonance Spectroscopy

Electron spin resonance spectra were collected on Varian E-109 spectrometer operating at 9.05 GHz. DPPH was used as an external standard. ESR spectra were recorded at room temperature and at liquid nitrogen temperature. Two sets of samples were used. The first set consisted of calcined Al_2O_3 , Mo/Al_2O_3 , Rh/Al_2O_3 and $Rh\text{-}Mo/Al_2O_3$ catalysts. The second set consisted of the above catalysts after reduction under reduction at 200C(1/2hr), 350C(1/2hr) and at 500C(1hr) in a flow-through cell. CO was then chemisorbed at room temperature on the above catalysts. The experimental set-up for the sample preparation was same as the one used in chemisorption described earlier. The sample cell was then isolated from the vacuum manifold and the sample cell was then transferred to the glove box. The samples were then transferred to a quartz sample tube and sealed with stopper and parafilm. ESR spectra on these samples were collected at room temperature and at liquid nitrogen temperature. The typical parameters used in the runs were given in table 4.2.

Table 4.2: Parameters for ESR runs

Scan range = 5.0kG	Field set = 3500G
Scan time = 8-16 min	Time constant =0.128
Modulation amplitude = 2.0G	Modulation frequency = 100kHz
Receiver gain = 4000	Microwave power = 5.0 mW
Microwave frequency = 9.05 GHz	

4.11 Ion-Scattering Spectroscopy

A modified 3M Model 525B spectrometer interfaced with a minicomputer was used. The nominal beam diameter was 150μm. Typically the ion beam was rastered over 2.5mm x 2.5mm. Data was collected from 3mm^2 area from the center. The ion beam was operated at 80nA. Helium ions were used to find elemental compositions, while Neon ions were used for sputtering The sample was ground and pressed onto an indium foil, which was put in the spectrometer. The sample was heated to 100C to accelerate the outgassing. Since the sample cannot be treated, ISS spectra were collected only for calcined samples.

4.12 Transmission Electron Microscopy and EDX

A Phillips EM400T electron microscope with a maximum accelerating voltage of 120kV was used. A STEM unit and a EDAX PV9100 unit was also connected to the electron microscope. The catalysts sample was first ground using glass slides. The copper grid, was then brushed over the sample. The sample holder was then inspected under an optical microscope to check for entrained particles on the grid. The copper grid was then mounted on the sample holder.

4.13 Solid-State NMR Spectroscopy

Two approaches were undertaken. In the first approach, a chemisorption flow through cell was used. The catalysts was reduced under hydrogen, evacuated and cooled. The sample was then dosed with ^{13}CO , the sample valve was closed and the cell was then transferred to a glove box maintained under nitrogen. The sample was later transferred to NMR sample tube which was then sealed with epoxy(Devon 2-Ton Epoxy).

The second sample preparation method consists of attaching a NMR sample tube to the sample preparation cell. The sample was treated under flowing gases in a manifold shown in figure 4.7. After dosing, the sample valve was closed and the sample preparation cell was disconnected from the manifold. The entire assembly shown in figure 4.8 was rotated by 90 degrees so that the NMR sample tube was vertical and the sample fell into the tube. The tube was flame sealed away from the constriction. It was later sealed at the constriction by a professional glass blower who wrapped the sample with wet asbestos so that it was not heated during sealing. Care was taken to keep the seal symmetrical. The samples were run on a Chemmagnetics M100S spectrometer with magic angle spinning and cross-polarization. Single pulse and 90-τ-180-τ pulse experiments were also done. Typical pulse widths were 5.5μsec, spectral width of 14kHz and contact time of 8ms. The details of the spectrometer are given elsewhere[3.4].

4.14 Low Pressure IR

A Nicolet 7199 dual beam FT-IR was used. A low pressure transmission IR cell with water cooled NaCl windows and self supporting catalysts wafer was used. The details of the cell and the gas manifold are given in detail elsewhere[5.6]. The catalysts was reduced in flowing hydrogen at 200C for 1/2 hr, 300C for 1/2hr and at 400C for 3hr. Because of the temperature limitations on the cell, the catalysts could not be heated above 400C. The instrument resolution was 2cm^{-1}.

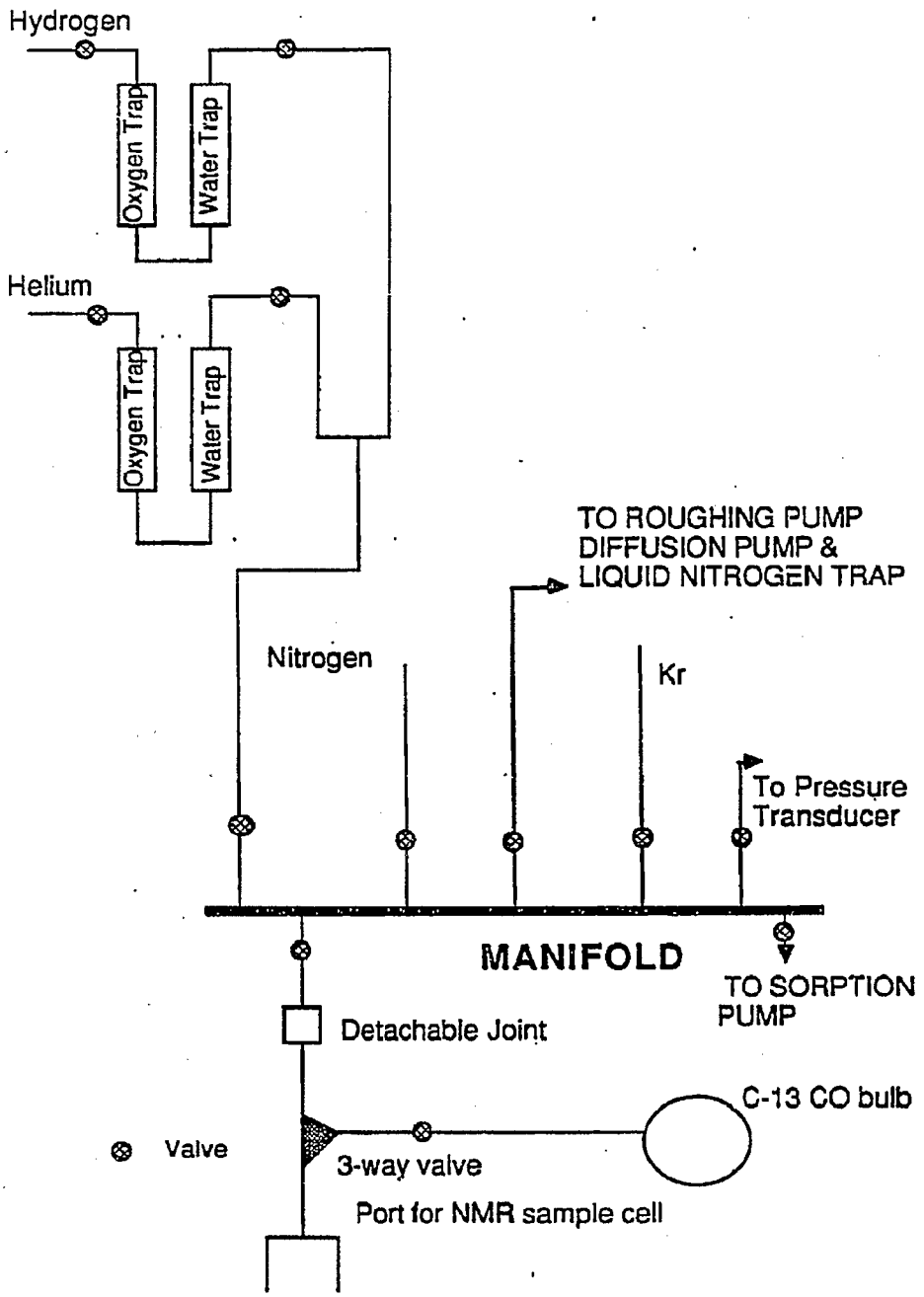

Figure 4.7: Set-up for NMR sample preparation

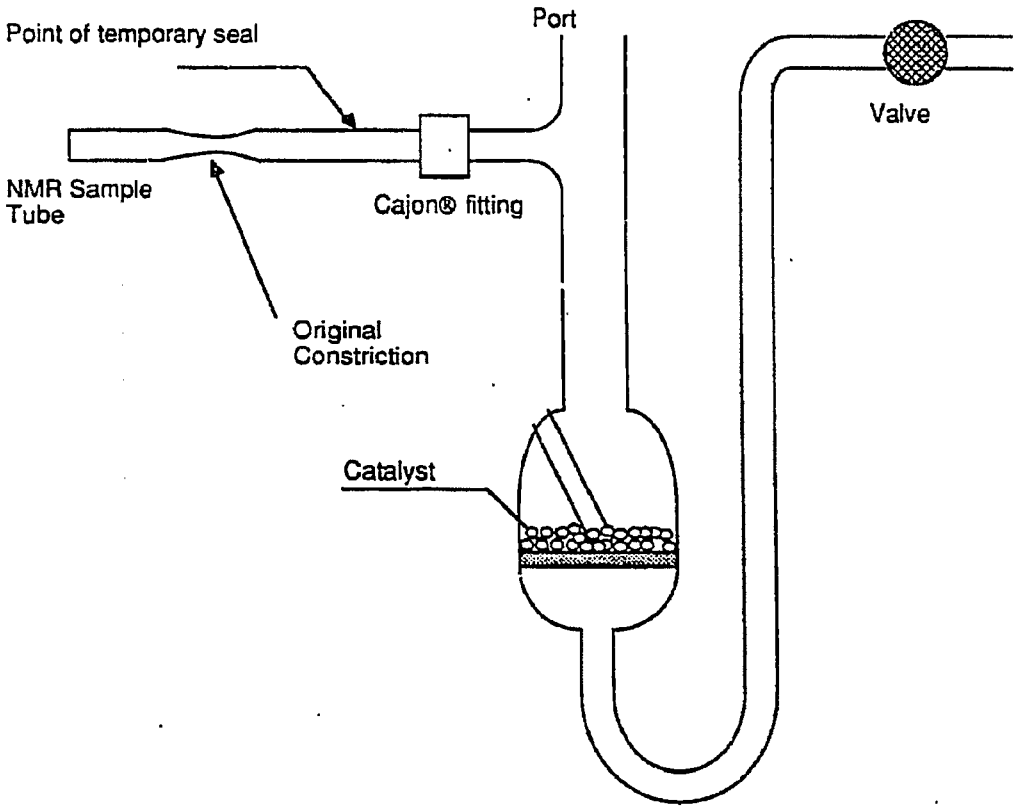

Figure 4.8: Sample preparation cell for NMR runs

REFERENCES

1. W.A. Dietz, J. Gas Chromatog. 1967, 5, 68.

2. D.M. Rosie and E.F. Barry, J. Gas Chromatog. 1973, 11, 249.

3. L.C. Hasselbring, Ph.D. Dissertation, University of Delaware, 1987.

4. D.J. Barabino, Ph.D. Dissertation, University of Delaware, 1988.

5. T.R. Krause, Ph.D. Dissertation, University of Delaware, 1987.

6. R. Barth, B.C. Gates, Y. Zhao, H. Knozinger and J. Hulse, J. Catal.1983, 82, 147.

CHAPTER 5
THE EFFECT OF SUPPORT, MODIFIERS AND CATALYST PRECURSOR IN CO HYDROGENATION

5.1 Introduction

This chapter discusses the results of testing various modified rhodium catalysts for CO hydrogenation. Specifically, the effect of metal salt precursor, the support and the modifier has been studied. The aim of this exploratory research phase described in this chapter was to identify many interesting systems for further detailed kinetic and characterization studies. The effect of many catalyst preparation variables can be great and is not well-understood.

Recall that as discussed in chapter 2, most of the reported investigations of the effect of modifiers on CO hydrogenation have been on Rh/SiO_2 . Because of the good mechanical and crystal framework strength of alumina and because of the wide range of surface properties of alumina, supported alumina catalysts are generally preferred. Hence supported alumina catalysts will be the primary focus of this thesis. However, the effect of modifiers on other supports such as MgO, La_2O_3 , SiO_2 , TiO_2 and Florisil was also investigated.

5.2 Catalyst Preparation

Extrudate CATAPAL γ-Al_2O_3 obtained from Air Products was first ground to 60-100 mesh size. The CATAPAL Al_2O_3 is made from aluminum isopropoxide and is one of the purest industrial alumina available. The Al_2O_3 was then air

calcined at 500C. The surface area of the alumina is $\approx 200 m^2$ gm. Rh was impregnated from an acidic rhodium nitrate solution obtained from Engelhard. Unless otherwise specified, rhodium was impregnated using Rh-nitrate solution and a coimpregnation technique was used. The catalyst was then air calcined at 500C. Again, unless otherwise specified, the catalyst was reduced under hydrogen at 200C for 1/2 hour, at 350C at 1/2 hour and at 500C at 1 hour. Most of the catalysts preparation was done by Dr. Chakka Sudhakar.

Rh(II) acetate/Al_2O_3 catalyst was prepared by multiple impregnation of Rh(II) acetate dimer in MeOH. The multiple impregnations were needed because of the limited solubility of Rh(II) acetate dimer in MeOH. The catalysts was dried at 80C for 12 hours. The dried catalyst is bluish green in color. Rh/Al_2O_3 catalysts were also prepared from $RhCl_3\ 3H_2O$, to investigate the effect of chloride precursor on the reactivity. Here excess of HCl is used similar to the method reported by DaCruz et al.[1]. The dried catalyst is brick red in color.

Na_3RhCl_6/Al_2O_3 catalyst was prepared by aqueous impregnation of Na_3RhCl_6/Al_2O_3 , similar to the method of Tamaru et al.[2]. Also, a $Rh\text{-}Na/Al_2O_3$ catalyst was prepared from coimpregnation of Rh and Na using rhodium nitrate and sodium nitrate. This catalyst is golden yellow in color. $Rh\text{-}K/Al_2O_3$ catalyst was prepared by coimpregnating potassium nitrate and rhodium nitrate salts. 1%Na reduced-$5\%Rh/Al_2O_3$ catalyst was prepared by impregnating sodium from aqueous solution of sodium nitrate onto reduced $5\%Rh/Al_2O_3$. Later the catalyst was dried at 110C for 20 hours. This catalyst was not recalcined.

Rh Florisil catalysts were prepared by impregnating rhodium nitrate solution on florisil. Florisil is a synthetic silica-magnesia gel of 60-100mesh size. The florisil support is first air calcined. The silicated Al_2O_3 used, was air calcined at 500C for 2 hours. Silicated alumina is 6% SiO_2 and the rest is γ-Al_2O_3 . MgO, MCB reagent ACS grade was air calcined before impregnating it with a

no-excess aqueous solution of rhodium to make Rh/MgO catalysts. The calcined catalyst was light brown in color. Rh/La_2O_3 catalyst was prepared by impregnating rhodium from a rhodium nitrate solution in ethanol, similar to the method of Ponec et al. [3]. The catalyst was air calcined at 500C for 2 hours.

Degussa P-25 TiO_2 was air calcined at 500C for 2 hours. $La(NO_3)_3$ was used to impregnated lanthanum in titania and alumina supported catalyst. The calcined La/TiO_2 catalyst was white in color. TiO_2/Al_2O_3 was prepared impregnating titanium from a solution of Ti isopropoxide in isopropyl alcohol. This catalyst was not calcined because the titanium propoxide is volatile. Rh-Ti Al_2O_3 is prepared by impregnating rhodium from rhodium nitrate solution on the TiO_2/Al_2O_3 produced by the above method.

Pd/SiO_2 is prepared by impregnating Pd from an aqueous solution of palladium nitrate on silica. The dried catalyst was dark brown in color. An attempt at coimpregnating Rh and Pd failed since it yielded a dark turbid solution. Adding nitric acid did not dissolve the particles. Hence Rh-Pd/SiO_2 catalyst was prepared by sequential impregnation method.

Rh-Mn-Mo catalyst was prepared by impregnating Mn and Mo from manganese nitrate and ammonium heptamolybdate. The calcined catalyst was light yellow in color.

Rh-Ce/Al_2O_3 catalyst was prepared by coimpregnation from an aqueous solution of ammonium cerium nitrate and rhodium nitrate. A multi-component catalyst containing Rh and Mo on titania coated florisil was prepared. The titania coating on florisil was given by filling up the pores of florisil with titanium isopropoxide, similar to the incipient wetness method. The catalyst composition corresponds to the 16%Ti/Florisil. The catalyst was then kept in moist atmosphere for 12 hours to hydrolyze the isopropoxide. The material was then wetted with

water and dried at 110C for 12 hours. The catalyst was then air calcined at 500C for 2 hours. Then Mo and Rh were impregnated on this mixed oxide by a coimpregnation technique. The impregnated was then dried at 110C for 12 hours. and air calcined at 500C for 2 hours. Another set of Rh-Mo/TiO_2 /Florisil was prepared by sequential impregnation technique.

Rh-Sn/Al_2O_3 catalyst was prepared by coimpregnating a no-excess aqueous solution of rhodium chloride and stannous chloride. The dried catalyst is purple in color. Rh/Co-Mo/Al_2O_3 was prepared by impregnating a no-excess aqueous solution of rhodium nitrate on Co/Mo/Al_2O_3 catalyst obtained from American Cynamid(HDS-16A). The catalyst was then dried at 110C for 12 hours and air calcined at 500C for 2 hours. The calcined catalyst was black in color. Rh-Mo/TiO_2 catalyst was prepared by sequential impregnation of rhodium and molybdenum. First a no-excess aqueous impregnation of molybdenum from a solution of pH=1 was done. Then the catalyst was dried at 110C and air calcined at 500C. This was followed by aqueous impregnation of rhodium from rhodium nitrate solution, drying and air calcination. The color of the catalyst after rhodium impregnation was light orange and after calcination was dark brown.

5.3 Results and Discussions

5.3.1 Rhodium Precursor

Table 5.1 shows the performance of Rh/Al_2O_3 catalysts prepared from different precursors. The reactor was operated in a differential mode. Appendix 1 shows that there are no significant transport limitations. The overall carbon monoxide conversion includes the water gas shift reaction. The selectivity to oxygenates is on a carbon dioxide free basis. Thus the % total oxygenates given in the table 5.1 show the percentage of carbon converted to oxygenates based on the total carbon converted to all products excluding carbon dioxide. The %C2+

oxygenate selectivity is the fraction of the carbon in oxygenates as C2 or higher oxygenates. The secondary products such as ethers and esters are counted in terms of their parent molecule, e.g., dimethyl ether is counted twice as C1 oxygenates, 1/3 of the carbon in MeOEt is counted as C1 oxygenates and 2/3 of the carbon in MeOEt is counted as C2 oxygenates.

First, the catalyst prepared from nitrate salts are compared with the catalyst prepared from chloride salts. The activity of the catalyst prepared from nitrate salts(nitrate) is slightly higher than the overall activity for CO hydrogenation of catalyst prepared from Chloride salts(Cl). Also the selectivity to total oxygenates is higher on the Cl-catalyst than with the nitrate-catalyst. Furthermore, as seen from table 5.1. the %C2+ oxygenates is slightly higher on the Cl-catalyst as compared to nitrate-catalyst. There are some subtle changes in the product distribution, not listed in table 5.1. For example, the higher amount of acetaldehyde is formed on Cl-catalyst as compared to nitrate-catalyst, and less methane and higher hydrocarbons are formed on Cl-catalyst as compared to nitrate-catalyst.

Then a series of experiments with Rh/Al_2O_3 catalysts prepared from Rh(II) acetate were conducted. Rh(II) acetate is an unusual Rh(II) dimer compound that has a strong Rh-Rh bond. It was previously found that Rh(II) acetate is an active catalysts for CO insertion[4]. The catalytic properties of Rh(II) acetate/Al_2O_3 was first tested at 150C because Worley et al.[5] have found from IR spectroscopy that Rh(II) acetate when deposited on Al_2O_3 still retains the dimer structure at 150C. However, the catalysts prepared from the dimer was not active until about 225C. The dimer also decomposes at around 225C. These catalysts are labelled as Ac. After a series of test runs, these catalysts were reduced under hydrogen at 500C. and this set of catalysts are labelled as AcH. There is no difference in the reactivity of the Ac and AcH catalysts at a reaction temperature of 250-275C. These set of catalysts, both Ac and AcH are less active than the Cl-catalyst. For example, as shown in table 5.1. at 450psi, CO/hydrogen=0.5 and at 250C, the

%CO conversion for Cl-catalyst is 9.1 at 1500GHSV and is 3.3% at 1500GHSV for AcH catalyst and is 2.5% at 1500GHSV. The total oxygenate selectivity is low, for example, 28-35% for Cl-catalyst and nitrate-catalyst but is 14-25% for the AcH and Ac catalyst. This difference in the overall selectivity may be because of the increase in the operating temperature. The %C2+ oxygenates fraction of the total oxygenates is same in AcH, Ac , nitrate and Cl-catalyst.

For comparison, the data using Johnson Mathey, and Engelhard catalyst are also listed. The JM catalyst is more active but has twice the rhodium loading of the U Del prepared catalyst. The JM catalyst also has higher overall selectivity to oxygenates. In contrast, the Engelhard (EN) catalyst is much less active than both JM and Cl catalyst, but the loading of Rh is 5-times lower than Cl catalyst. Also, catalyst prepared from Rh nitrate crystals obtained from Johnson Mathey, were less active than the catalyst prepared from the Rh nitrate solution from Engelhard.

These results show interesting trends when compared to the results reported by Jackson et al.[6]. The catalysts reported by Jackson were silica supported and were not calcined. The activity trend for silica supported catalysts was, $Cl > Nit > acet > Nit - calcined$. In contrast the trend for alumina supported catalysts, reported in table 5.1 is $nitrate - calcined > Cl - calcined > Acetate \sim Acet - reduced$. The reasons for this drastic changes in the trend of activity is not clear. Changing rhodium precursor caused a two order of magnitude change in the activity for CO hydrogenation on Rh/SiO_2 catalysts[4]. In comparison, the changes on Rh/Al_2O_3 are much smaller. This may be because, Al_2O_3 unlike SiO_2 has a substantial portion of the co-ion sitting on the support which may be far away from the metal crystallite.

The total selectivity to oxygenates depends on the overall conversion. Ideally, the catalyst should be tested and compared at the same temperature, partial

Table 5.1: The effect of rhodium precursor on the performance of supported rhodium/alumina catalysts

cat-lysts	temp C	pres psi	$CO:H_2$	GHSV	%CO conv	% TOT oxyg	%C2– oxyg	C% to CO_2
Nitrate	250	450	0.5	3000	5.7	28.9	82.4	0.9
Nitrate (3% Rh)	250	450	0.5	1500	9.1	27.5	87.9	1.4
Chloride	250	450	0.5	3600	6.1	31.3	89.4	0.6
Chloride	250	450	0.5	3600	4.8	32.1	89.7	0.5
Chloride	250	450	0.5	1800	9.2	30.0	92.2	0.9
Chloride (3% Rh)	250	750	0.5	3600	5.2	33.4	88.6	0.7
Acetate	250	450	0.5	1500	3.2	14.7	50.0	5.4
Acetate	250	450	0.5	1500	2.5	14.7	66.9	3.1
Acetate	275	450	0.5	1500	8.5	12.0	60.3	1.4
Acetate	275	750	0.5	1500	10.6	13.2	69.0	1.7
Acetate (3% Rh)	250	750	0.5	1500	3.2	14.6	67.0	1.8
Acet-H	250	450	0.5	1500	3.3	20.7	75.5	2.7
Acet-H	275	450	0.5	1500	10.1	14.4	86.7	1.7
Acet-H	250	750	0.5	1500	4.0	26.6	87.8	1.6
Acet-H (3% Rh)	250	450	0.5	1500	2.9	25.0	89.3	2.0
JM (5%)	250	450	0.5	3333	7.6	28.9	92.5	1.8
EN (0.5% Rh)	275	450	0.5	720	5.8	26.3	80.5	11.9

pressure of CO and hydrogen, and the space rate adjusted to get the same conversion. However, because of the limitations in the space rate, the above conditions cannot be used for all catalysts. Hence whenever possible, the catalysts are compared at the same temperature, and partial pressure of carbon monoxide and hydrogen. The effect of conversion on the selectivity to oxygenates is then found from the selectivity versus conversion plots. The activity is found by the space required at the same temperature to get the same conversion.

The effect of metal salt precursor on the performance of the catalysts is shown in figure 5.1. As seen from figure 5.1, the selectivity versus conversion plot for the catalysts derived from nitrate salts and from chloride salts is similar to the selectivity versus conversion plot of the JM catalyst. Hence very little difference in the selectivity was observed on these catalysts. In contrast the selectivity-conversion plot, shown as open symbols, for Ac and AcH catalysts lie below the selectivity-conversion plot for JM, Nitrate and Cl catalysts. This suggest that the Ac and the AcH catalysts are less selective than the Nitrate, JM and Cl catalysts.

5.3.2 Support

In this subsection the effect of support on the performance of supported rhodium catalysts is discussed. The catalysts were compared at 30atm and hydrogen/CO=2. The activity of the catalysts varied as

$$TiO_2\text{-}500 > TiO_2\text{-}300 > Al_2O_3 > La_2O_3 > MgO > SiO_2$$

The TiO_2 -500 and TiO_2 -300 are reduced at 500C and 300C respectively. Thus the Rh/TiO_2 catalysts were the most active of all the catalysts. The selectivity to oxygenates varied as

$$MgO > La_2O_3 > SiO_2 > Al_2O_3 = TiO_2$$

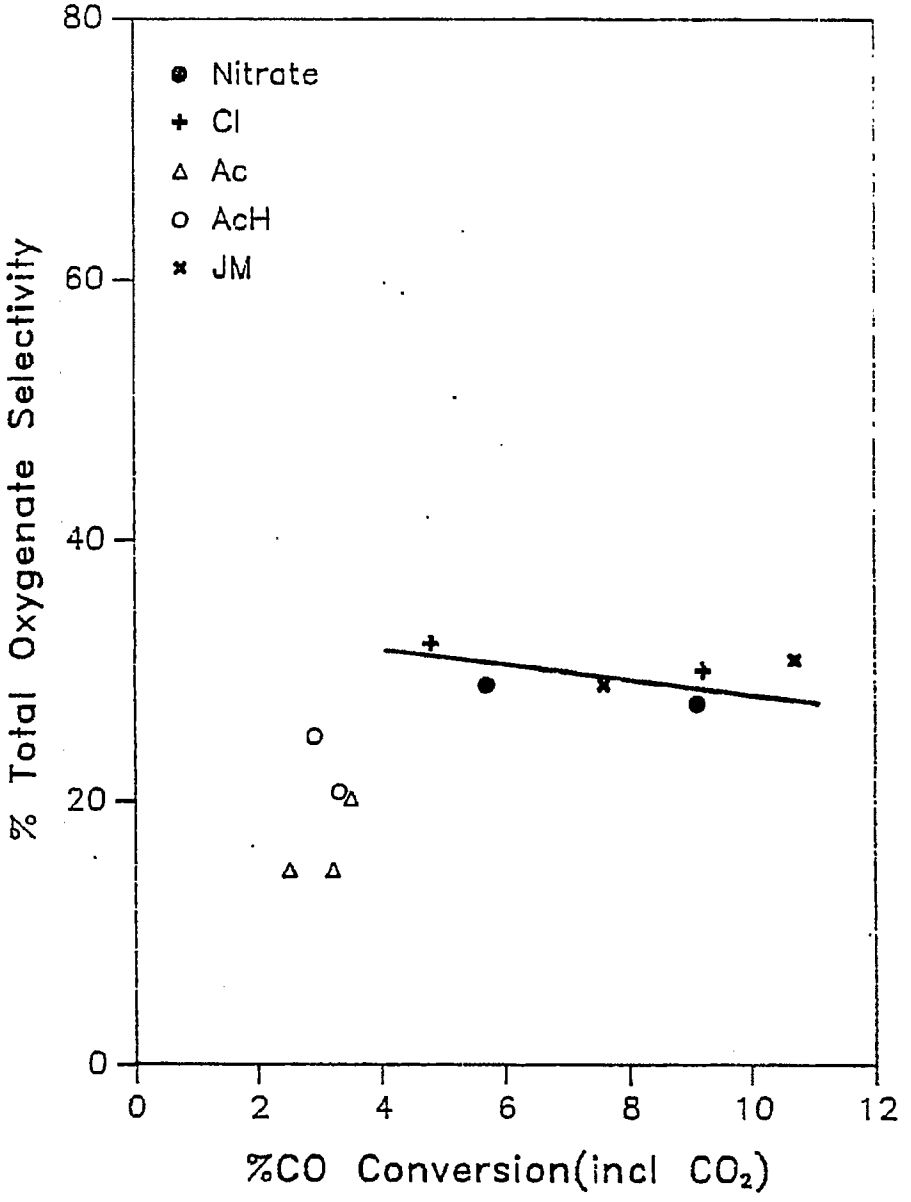

Figure 5.1: Selectivity-Conversion plot for Rh/Al_2O_3 derived from different metal salt precursor, at 250C, CO/hydrogen=2, and 30atm.

These conclusions can be reached from the data given in tables 5.2 and 5.3. In comparison, Florisil supported rhodium catalysts listed in table 5.8 have low activity and form only methanol. There is no MeOMe formed on any supports except Al_2O_3 . Small amount of MeCHO is formed on La_2O_3 supported catalysts and very little EtCHO is formed on any support except SiO_2 . These activity results agree with other investigations[7,8]. The high selectivity at low conversions is puzzling.

Here again, the selectivity versus conversion plot shown in figure 5.2 illustrates the differences in the selectivities of various supported catalysts. Rh/La_2O_3 and Rh/MgO have higher selectivity to oxygenates than Rh/SiO_2 . Also Rh/Al_2O_3 has much lower selectivity to oxygenates than Rh/SiO_2 . The Rh/TiO_2 catalyst are very active as seen by the lower temperature used, i.e., 225C instead of 250C. The Rh/TiO_2 catalysts has a higher selectivity to oxygenates than Rh/Al_2O_3 .

5.3.3 Modifiers

5.3.3.1 Rh/Al_2O_3

Table 5.4 shows the effect of addition of modifiers on the performance of alumina supported rhodium catalysts. Specifically Mn, Mo, Ce, Sn and Ti modifiers were used. Table 5.5 shows the summary of the results given in table 5.4. Addition of Mn decreases the activity of Rh/Al_2O_3 slightly. The selectivity to oxygenates and the selectivity to C2+ oxygenates is not dramatically affected. In contrast, Wilson et al.[9] have reported that addition of Mn to Rh/SiO_2 increased the activity for CO hydrogenation.

Also, the titanium modified catalysts, reduced at 300C(Ti-300) showed same activity as Rh/Al_2O_3 . The selectivity to oxygenates was slightly lower and the selectivity to C2+ oxygenates is not affected. The titania modified catalysts were

Table 5.2: Effect of support on the performance of supported rhodium catalysts

catalyst	temp C	pres psi	$CO:H_2$	GHSV	%CO conv	% TOT oxyg	%C2– oxyg	C% to CO_2
Al_2O_3	250	450	0.5	3000	5.7	28.9	82.4	0.9
Al_2O_3	250	450	0.5	1500	9.1	27.5	87.9	1.4
SiO_2	275	450	0.5	1500	2.9	63.4	94.8	0.4
SiO_2	250	450	0.5	1500	0.6	75.2	95.2	0.0
SiO_2	275	750	0.5	1500	3.1	68.7	88.8	1.8
TiO_2 -300	235	450	0.5	4500	7.6	26.2	89.4	2.8
TiO_2 -300	235	750	0.5	4500	9.2	27.0	86.0	2.9
TiO_2 -300	225	750	0.5	2250	12.0	30.9	87.3	3.5
TiO_2 -500	235	450	0.5	4500	8.1	26.7	89.2	2.1
TiO_2 -500	225	450	0.5	2250	10.3	29.7	90.2	2.7
TiO_2 -500	225	750	0.5	2250	11.4	31.1	90.6	2.1
MgO-400	250	450	0.5	1500	1.6	90.5	6.7	22.2
MgO-400	275	450	0.5	1500	3.1	52.2	57.2	16.0
MgO-500	250	450	0.5	1500	1.4	50.7	66.3	8.4
MgO-500	275	450	0.5	1500	6.7	39.6	86.9	12.9
La_2O_3	250	450	0.5	3000	1.8	76.8	14.8	0.4
La_2O_3	250	450	0.5	1500	2.5	71.8	17.0	13.6
La_2O_3	275	450	0.5	3000	4.4	59.8	27.6	16.2
La_2O_3	275	750	0.5	3000	5.8	66.0	23.2	13.5

Table 5.3: Summary of the effect of support on the performance of Rh catalysts at 30atm. hydrogen/CO=2.

Support	Temp(C)	GHSV	%CO conv.	% Oxyg.	%C2+ oxyg
Al_2O_3	250	3000	6	30	83
SiO_2	250	1500	1	58	94
TiO_2 -300	235	4500	7.6	26	90
TiO_2 -500	235	4500	8.1	27	90
MgO-400	250	1500	3.1	52	66
MgO-500	250	1500	1.5	50	66
La_2O_3	250	3000	1.8	77	15

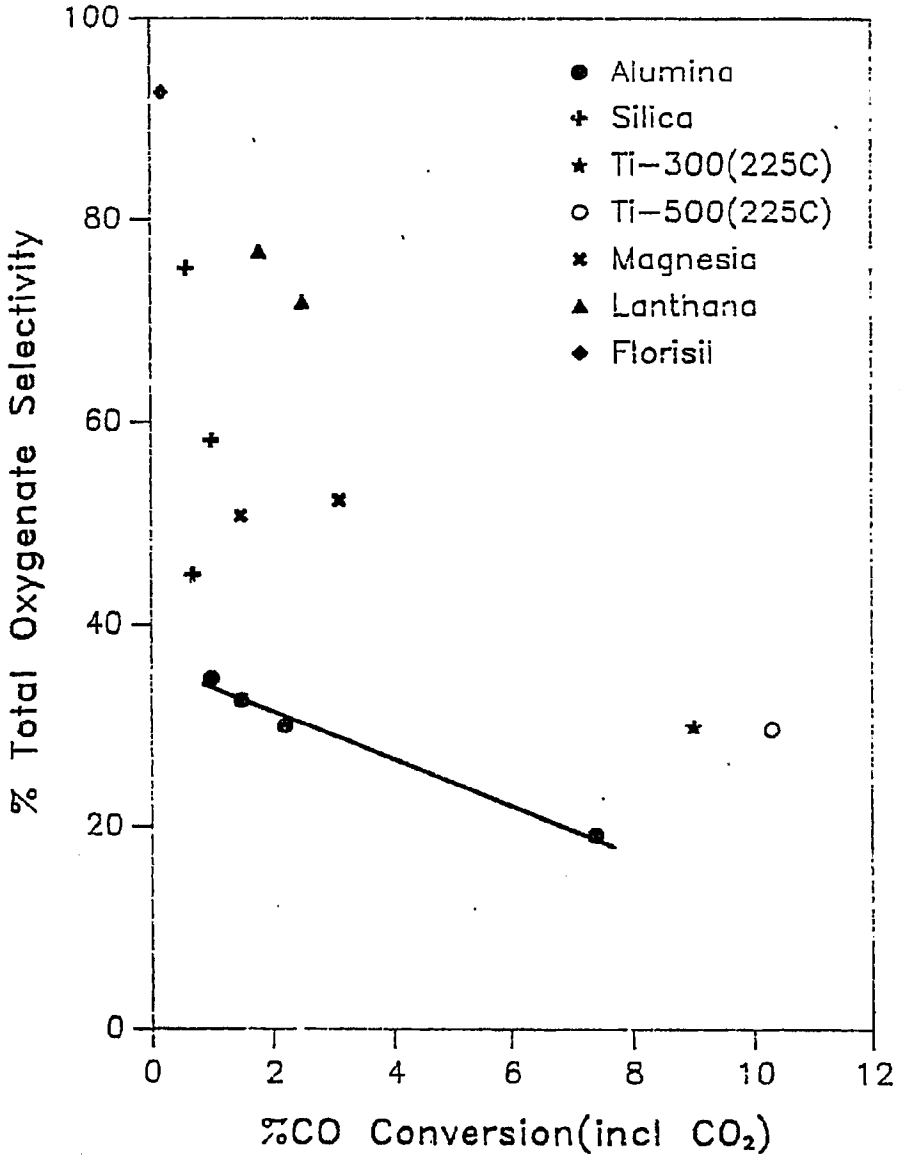

Figure 5.2: Selectivity-Conversion plot for various supported Rh Catalysts at 250C. CO/Hydrogen=0.5 and 30atm

also reduced at 500C to convert it into the SMSI state. The Ti-500 catalysts were much more active than the Ti-300 catalysts. The selectivity to oxygenates is increased, the %C2– oxygenate selectivity is also increased. However, the amount of carbon dioxide formed decreases. In comparison, addition of molybdena increases the activity of Rh/Al_2O_3 . The selectivity to oxygenates is increased and the selectivity to C2– oxygenates decreases since lot of methanol and dimethyl ether is formed. Also, addition of Ce to Rh/Al_2O_3 decreases the activity for CO hydrogenation and the selectivity to oxygenates increases, and the selectivity to C2+ oxygenates decreases. The addition of Sn decreases the activity for CO hydrogenation and no oxygenates are formed. Large amounts of carbon dioxide is formed on Mo and Sn modification.

Here again the selectivity-conversion plot given in figure 5.3 shows the effect of additives on CO hydrogenation on Rh/Al_2O_3 . The figure clearly shows that Sn-modified Rh/Al_2O_3 catalysts are not selective to oxygenates. Also the selectivity to oxygenates of the Ti-modified Rh/Al_2O_3 catalysts is similar to Rh/Al_2O_3 . The selectivity to oxygenates on the Ce-modified Rh/Al_2O_3 is higher than Mn-modified Rh/Al_2O_3 , and the selectivity to oxygenates of Mn-modified Rh/Al_2O_3 is higher than the Rh, Al_2O_3 . The Mo-modified Rh/Al_2O_3 catalysts are unique because of the higher activity, as seen by the lower temperature, i.e. 225C instead of 250C. The Mo-modified Rh/Al_2O_3 catalysts has a selectivity-conversion plot that is much higher and far apart from the selectivity-conversion plot of other modifiers on Rh/Al_2O_3 and Rh/Al_2O_3 catalysts. The above remarks are for 1Modifier:1Rh atom only.

5.3.3.2 Rh/SiO_2

The effect of modifiers such as Mn and Mo on Rh/SiO_2 is shown in table 5.6. The addition of Mn and Mo to Rh/SiO_2 accelerates the water gas shift reaction. This is evident from the increase in carbon dioxide formed during reaction. There

Table 5.4: Effect of modifier(1 modifier atom : 1 Rh atom) on alumina supported rhodium catalysts

cata	temp C	pres psi	$CO:H_2$	GHSV	%CO conv	% TOT oxyg	%C2– oxyg	C% to CO_2
None	250	450	0.5	3000	6.6	22.6	72.3	3.9
Mn	250	450	0.5	3600	3.7	31.0	81.4	0.5
Mn	275	450	0.5	3600	11.6	17.6	85.5	0.9
Mn	275	750	0.5	3600	13.5	17.9	86.6	1.2
1:3Mn	250	450	0.5	3000	3.8	30.9	59.0	4.8
1:3Mn	250	450	0.5	1500	6.4	32.7	76.7	5.9
1:3Mn	275	750	0.5	1500	18.2	24.4	85.6	2.4
Ti-300	275	450	0.5	3600	15.9	12.9	82.6	1.2
Ti-300	275	750	0.5	3600	17.7	14.3	85.3	1.4
Ti-500	250	450	0.5	3600	8.7	20.8	94.6	0.4
Ti-500	250	750	0.5	3600	10.6	22.6	95.0	0.5
Mo	225	450	0.5	3000	9.0	58.7	41.6	21.5
Ce	250	450	0.5	3000	2.8	46.6	48.4	5.2
Ce	250	450	0.5	1500	5.0	39.9	57.1	6.3
Ce	250	750	0.5	1500	5.2	45.2	59.4	6.2
Ce	250	450	0.5	1500	3.6	39.3	57.2	5.3
Sn	250	450	0.5	1500	0.4	0.0		22.6
Sn	275	450	0.5	1500	0.9	0.0		33.0
Sn	275	750	0.5	1500	1.1	-0.0		36.6

Table 5.5: Summary of the effect of modifier on the performance of Rh/Al_2O_3 catalysts at 30atm and 250C with 1 atom modifier/1 atom Rh

Modifier	Activity	Selectivity	
		Oxygenates	C2– Oxygenates
Mn	Sl. Lower	Sl. Higher	Equal
Ti-300	Equal	Sl. Lower	Equal
Ti-500	Higher	Sl. Lower	Equal
Mo	Higher	Higher	Lower
Ce	Higher	Higher	Lower
Sn	Lower	0	0

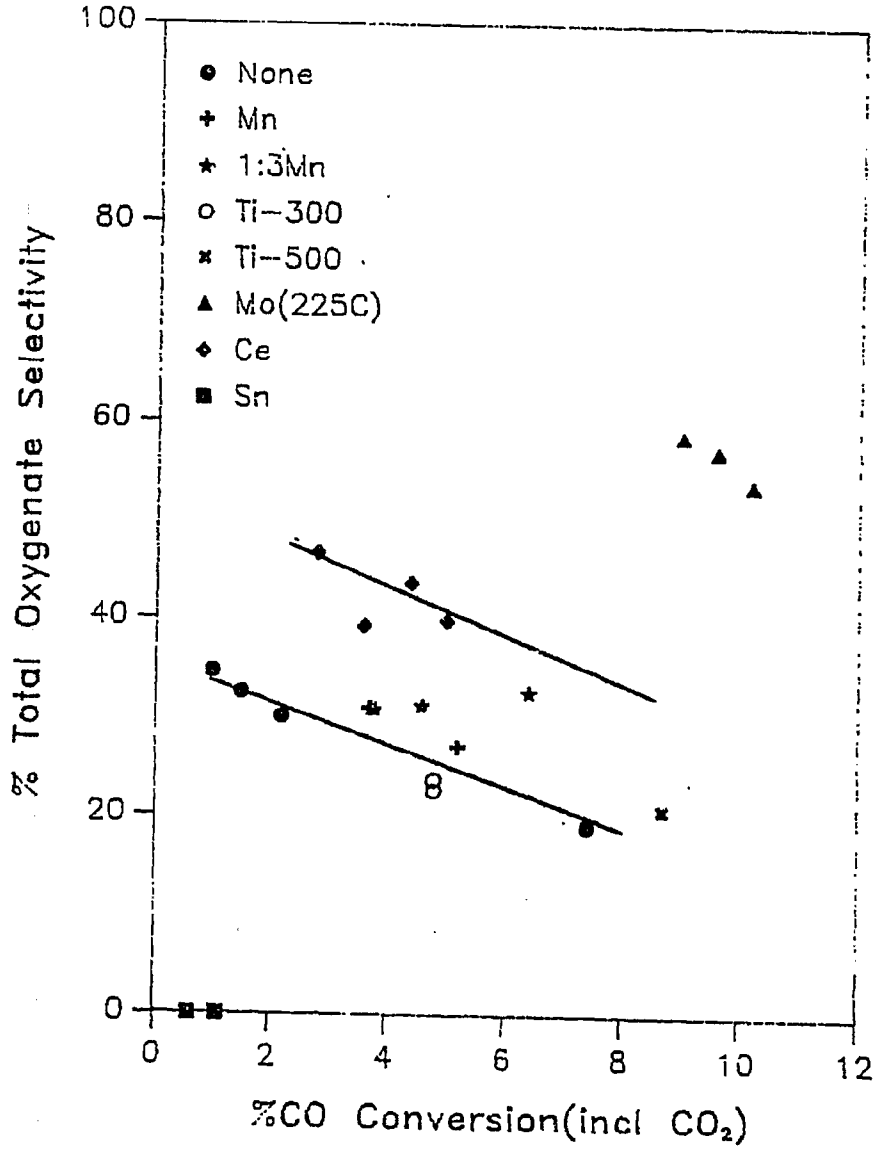

Figure 5.3: Selectivity-Conversion plot of Modified Rh/Al_2O_3 Catalysts. 1 modifier: 1 Rh atom, 250C, CO/hydrogen=0.5 and 30atm

is a large increase in the activity of the catalysts on addition of Mn and Mo. For example, at 275C, 750psi and CO/hydrogen=1, the conversion of carbon monoxide on Rh/SiO_2 is 1.5% at 1500GHSV, in contrast, under similar conditions, the CO conversion on Rh-Mn-Mo/SiO_2 is 9.8% at 4800GHSV. The total oxygenate selectivity and the C2+ oxygenate selectivity is not drastically changed on Mn-Mo promotion. In general, the acetaldehyde-ethanol ratio decreases on Mn-Mo addition, i.e., lot of acetaldehyde formed get hydrogenated to ethanol.

To see whether the presence of silica in alumina affects the catalytic properties of supported Rh catalysts, a 3%Rh 0.3%Mn 0.3%Mo/ silicated Al_2O_3 catalysts was prepared. The catalysts showed slightly better oxygenate selectivity than the alumina supported catalysts but lower than the silica supported catalysts. Because of the acidity of the silicated Al_2O_3 , the majority of the MeOH is converted to MeOMe.

5.3.3.3 Rh/TiO_2

In view of the high activity of Rh/TiO_2 catalysts for CO hydrogenation, the effect of modifiers on titania supported catalysts was investigated with the aim that the modifier would increase the selectivity to oxygenates at the same time still retaining the higher activity. To see the effect of SMSI state, all the TiO_2 supported catalysts were tested after two different reduction temperatures, 300C and 500C.

Table 5.7 shows the performance of modified Rh/TiO_2 catalysts. Addition of lanthanum to Rh/TiO_2 decreases the activity for CO hydrogenation. For example, at 450psi, CO/hydrogen=0.5, the %CO conversion for Rh/TiO_2 is 10.3 at 225C and 2250GHSV, and the %CO conversion for Rh-La/TiO_2 (La) is 5.9 at 250C and 1800GHSV. The total oxygenate selectivity is same in both the catalysts. The table shows that the total oxygenate selectivity is higher for La-catalysts than for

Table 5.6: Effect of modifiers on the performance of silica supported rhodium catalysts

cata	temp C	pres psi	$CO:H_2$	GHSV	%CO conv	% TOT oxyg	%C2– oxyg	C% to CO_2
None	250	450	0.5	3000	0.7	44.9	94.2	0.0
None	250	450	0.5	1500	1.0	58.2	94.2	0.0
None	275	450	0.5	1500	2.9	63.4	94.8	0.4
None	250	450	0.5	1500	0.6	75.2	95.2	0.0
None	275	750	0.5	1500	3.1	68.7	88.8	1.8
None	275	750	1	1500	1.5	77.7	89.9	1.8
Mn-Mo	225	450	0.5	3600	3.8	36.5	81.2	13.3
Mn-Mo	225	450	1	2400	3.3	57.4	84.9	13.2
Mn-Mo	251	450	1	2400	9.6	55.5	91.9	18.8
Mn-Mo	224	450	1	2400	1.7	64.1	92.2	20.2
Mn-Mo	275	450	1	2400	25.1	40.7	94.0	35.4
Mn-Mo	249	450	1	1200	13.6	61.2	94.0	22.1
Mn-Mo	251	750	1	4800	4.0	70.5	93.4	10.7
Mn-Mo	275	750	1	4800	9.8	50.1	93.2	21.8
Mn-Mo	275	200	1	2400	15.9	36.7	96.2	27.9
Mn-Mo	250	200	1	2400	4.0	49.5	96.6	13.2
Mn-Mo	250	450	1	4800	3.1	59.5	94.2	9.3

Rh/TiO_2 . but the conversion is also higher for Rh/TiO_2 . The water gas shift reaction is accelerated in $Rh/La/TiO_2$ catalysts compared to Rh/TiO_2 . There are two sets of lanathanum modified catalysts: La-300 and La-500. These two catalysts were reduced respectively at 300C and 500C for 1 hour under hydrogen respectively. Also two other lanthanum modified catalysts were prepared. The second set of lanthanum modified catalysts are coded as La-300* and La-500*. This second set of catalysts were prepared by sequential impregnation of TiO_2 by lanthana and rhodium. There is no change in activity between La-300 and La-500. In contrast, there is a big difference in the reactivity between La-300* and La-500*. For example, at 250C, 450psi and CO/Hydrogen=2 and GHSV=1800, the %CO conversions for La-300, La-500, La-300* and La-500* are 5.1%, 5.9%, 6.0% and 9.0% respectively. A comparison of the amount of carbon dioxide formed show the following trends: La-500*< La-300* and La-500< La-300. The reduction at 500C reduces the amount of carbon dioxide formed on these catalysts. The %C2+ oxygenates increases with reduction at higher temperatures. For example, the %C2+ oxygenates vary as La-500* > La-300* and La-500> La-300.

The activity for $Rh\text{-}Ti/Al_2O_3$ is lower than Rh/TiO_2 reduced at both 300C and at 500C. The total oxygenates selectivity is lower for $Rh\text{-}Ti/Al_2O_3$ than for Rh/TiO_2 -300C and Rh/TiO_2 -500. In contrast $Rh\text{-}Mo/TiO_2$ is more active than Rh/TiO_2 . The water gas shift reaction is accelerated on molybdena addition to Rh/TiO_2 . Unlike the Rh/Al_2O_3 system, the total oxygenate selectivity and %C2+ oxygenate decreases on molybdena addition to Rh/TiO_2 .

Figure 5.4 shows the selectivity-conversion plot of CO hydrogenation on various modifiers on Rh/TiO_2 catalysts. As seen from the figure, all the additives except Mo lie within the same selectivity-conversion envelope. The higher selectivity of the Rh-Mo is because of the lower temperatures used. The higher activity of these catalysts permits the use of lower temperatures.

Table 5.7: Effect of modifiers on the performance of titania supported rhodium catalysts

cat-lysts	temp C	pres psi	$CO:H_2$	GHSV	%CO conv	% TOT oxyg	%C2– oxyg	C% to CO_2
None-300	235	450	0.5	4500	7.6	26.2	89.4	2.8
None-300	235	750	0.5	4500	9.2	27.0	86.0	2.9
None-300	225	750	0.5	2250	12.0	30.9	87.3	3.5
None-500	225	450	0.5	2250	10.3	29.7	90.2	2.7
None-500	225	750	0.5	2250	11.4	31.1	90.6	2.1
La-300	225	450	0.5	3600	1.6	50.2	36.2	9.0
La-300	250	450	0.5	1800	5.1	41.5	65.6	8.9
La-500	275	750	0.5	1800	16.9	25.2	86.2	9.6
La-500	250	450	0.5	1800	5.9	48.9	83.1	4.4
La-300*	250	450	0.5	3600	4.9	40.1	52.0	9.6
La-300*	250	450	0.5	1800	6.0	40.0	62.5	9.0
La-500*	250	450	0.5	1800	10.0	35.4	88.1	4.8
La-500*	250	750	0.5	1800	9.6	38.4	85.6	4.9
Ti/Al_2O_3	275	750	0.5	3600	17.7	14.3	85.3	1.4
Ti/Al_2O_3	250	450	0.5	3600	8.7	20.8	94.6	0.4
Mo	225	450	0.5	4680	11.8	50.8	22.6	36.9
Mo	225	450	0.5	4680	11.4	54.7	20.3	35.5

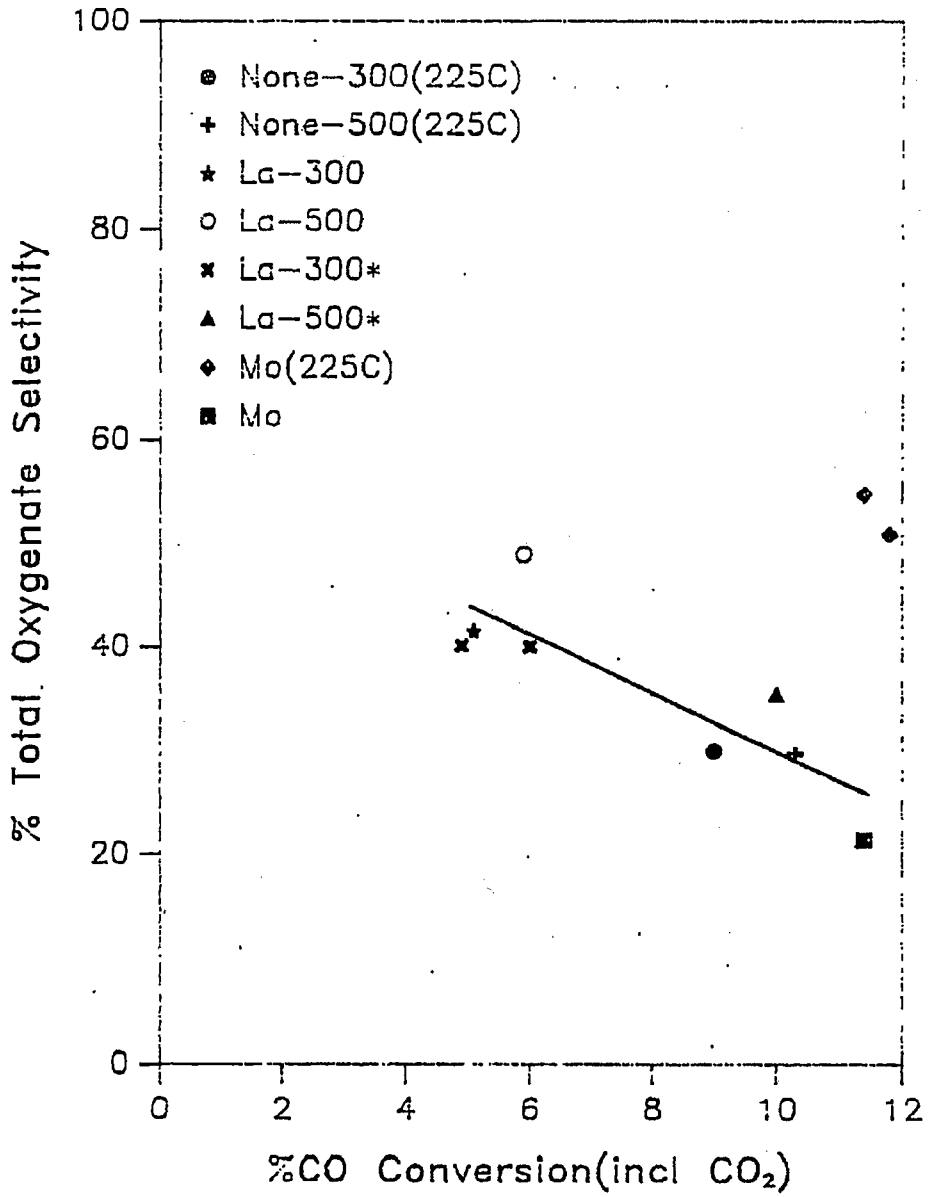

Figure 5.4: Selectivity-Conversion plot of Various modifiers on Rh/TiO_2 Catalysts. 250C, CO/hydrogen = 0.5 and 30atm

5.3.3.4 Rh/Florisil

Table 5.8 summarizes the performance of modified Rh Florisil catalysts. This is the first reported investigation of the use of florisil supported catalysts for CO hydrogenation. Rh/Florisil catalysts have low activity compared to the other supported rhodium catalysts. However, the selectivity to oxygenates is high. Hence, it was decided to add activity enhancing modifiers to these supported catalysts. Two Mn and Mo modified Rh/Florisil catalysts were tested. The composition of these catalysts were similar to the silica supported catalysts. The first catalysts 2.5%Rh 1%Mn 1%Mo/Florisil was decomposed in helium(Mn-Mo-He) while the second one was air calcined by the usual approach. The Mn and Mo modification increases the activity of Rh/Florisil catalysts substantially. For example, at 250C, 450psi and CO/hydrogen=2, the CO conversion on Rh/Florisil catalyst at 3000GHSV is 0.2%, and in comparison the CO conversion on Rh-Mn-Mo/Florisil is 1.1% at 3600GHSV. The %C2+ oxygenates increases dramatically on Mn and Mo modification. There are no C2+ oxygenates formed on Rh/Florisil, in comparison the %C2+ oxygenates on Rh-Mo-Mn/Florisil is 15-40%. Also, there is no substantial effect of addition of Mn and Mo on the water gas shift reaction, since the florisil is a good water gas shift reaction. There is no substantial difference in the performance of the Mn-Mo catalysts and Mn-Mo-He catalysts.

Also, in table 5.8, the data for titania coated Rh-Mn-Mo/Florisil catalysts are given. The first catalysts 3%Rh 2%Mo/TiO_2 /florisil (Mo/TiO_2 -S) was prepared by sequential impregnation of Rh and Mo on TiO_2 /Florisil. The second catalyst 1.5%Rh 6%Mo/TiO_2 /Florisil(Mo/TiO_2) was prepared by coimpregnation by the usual method. The coimpregnated catalyst is reactive compared to Rh Al_2O_3, and the Mn-Mo catalysts. The % total oxygenates formed is lower than in Mn-Mo catalysts. Also, substantial amount of C2+ oxygenates are formed. This is one of the few catalysts where large amounts of C2+ oxygenates

are formed. Comparison of this catalysts with Rh Mo TiO_2 catalysts shows that in Rh-Mo/TiO_2 -Florisil larger fraction of the oxygenates is C2− oxygenates. In contrast, the activity of coimpregnated catalysts is much lower. The %C2+ oxygenates formed on the coimpregnated catalysts is also low. However because of the large amount of molybdenum, the water gas shift reaction is accelerated more than in Mo/TiO_2 -S.

5.3.4 Alloying with Pd

Since Pd catalysts are well-known to be selective in the conversion of syngas to methanol, Rh-Pd bimetallic was investigated to find the effect of Pd on the activity and selectivity of supported Rh catalysts. A comparison of the Rh/SiO_2 , Pd/SiO_2 and Rh-Pd/SiO_2 catalysts shows that the activity of the catalysts does not change appreciably in the bimetallic system, see table 5.9. The water gas shift reaction is slow on the bimetallic system. However the fraction of C2+ oxygenates formed is high. The Rh-Pd/Al_2O_3 catalysts is much more active for CO hydrogenation than Rh-Pd/SiO_2 catalysts. For example, table 5.9 shows that at 250C, 450psi,and CO/hydrogen=0.5, the %CO conversion for Rh-Pd/Al_2O_3 is 8.6% at 1730GHSV and is 2.5% for Rh-Pd/SiO_2 at 1500GHSV. The water gas shift reaction is accelerated on the alumina supported bimetallic catalysts, the overall selectivity of oxygenates and the %C2+ oxygenates decrease on the Rh-Pd/Al_2O_3 than on Rh-Pd/SiO_2 catalysts. No synergistic effects were observed.

5.3.5 Modification by Sodium

An exploratory series of prepared and purchased rhodium catalysts have been tested for CO hydrogenation with interesting results. The results are summarized in table 5.10 The typical test conditions for the catalysts reported in table 5.10 are 250C, 30 atm. Hydrogen/CO=2 and 4000 GHSV.

Table 5.8: Effect of modifiers on the performance of florisil supported rhodium catalysts

catalyst	temp C	pres psi	$CO:H_2$	GHSV	%CO conv	% TOT oxyg	%C2– oxyg	C% to CO_2
None	250	450	0.5	3000	0.2	92.5	0.0	7.7
None	275	450	0.5	1500	0.4	82.9	0.0	18.0
Mn-Mo-He	225	450	0.5	3600	1.1	94.8	14.9	5.5
Mn-Mo-He	250	450	0.5	3600	1.1	86.7	33.4	7.0
Mn-Mo-He	250	450	1	2400	1.0	91.5	26.5	9.7
Mn-Mo-He	250	750	1	2400	1.2	87.9	37.5	12.3
Mn-Mo-He	275	750	1	2400	3.5	84.1	40.3	15.9
Mn-Mo	250	450	0.5	3000	1.7	78.5	37.3	12.6
Mn-Mo	250	450	1	2000	1.3	82.0	46.3	17.4
Mn-Mo	275	750	1	2000	4.0	72.0	56.5	19.2
Mo/TiO_2 -S	225	450	0.5	3000	5.1	62.3	67.1	20.8
Mo/TiO_2 -S	225	450	0.5	1500	9.3	69.2	71.7	21.8
Mo/TiO_2 -S	225	450	0.5	1500	5.6	64.7	66.6	23.0
Mo/TiO_2 -S	250	450	0.5	3000	10.6	52.3	74.2	24.2
Mo/TiO_2 -S	250	750	0.5	3000	11.6	55.3	69.3	27.8
Mo/TiO_2 -S	250	450	1	2000	7.5	62.4	77.1	27.9
Mo/TiO_2	250	450	0.5	1800	1.4	51.4	34.6	41.9
Mo/TiO_2	275	450	0.5	1800	4.3	42.3	42.2	43.2
Mo/TiO_2	275	450	0.5	1800	3.9	46.0	44.5	39.6

Table 5.9: Effect of alloying with palladium on the performance of alumina and silica supported rhodium catalysts

catalyst	temp C	pres psi	$CO:H_2$	GHSV	%CO conv	% TOT oxyg	%C2– oxyg	C% to CO_2
Rh/Al_2O_3	275	450	1	2000	8.8	22.0	88.6	2.1
$Rh\text{-}Pd/Al_2O_3$	250	450	0.5	1731	8.6	18.0	74.6	3.0
$Rh\text{-}Pd/Al_2O_3$	250	450	0.5	1731	7.7	20.7	82.1	1.7
$Rh\text{-}Pd/Al_2O_3$	275	450	0.5	3462	9.5	15.8	79.7	1.1
$Rh\text{-}Pd/Al_2O_3$	275	750	0.5	3462	12.6	15.7	81.0	1.7
$Rh\text{-}Pd/Al_2O_3$	250	750	0.5	3462	4.1	25.3	81.1	1.5
Pd/SiO_2	250	450	0.5	3000	0.2	100.0	0.0	0.0
Pd/SiO_2	250	450	0.5	1500	0.4	100.0	0.0	4.4
Pd/SiO_2	250	750	0.5	1500	0.5	100.0	0.0	6.6
Pd/SiO_2	275	750	0.5	1500	1.2	100.0	0.0	7.6
Rh/SiO_2	250	450	0.5	1500	1.0	58.2	94.2	0.0
Rh/SiO_2	275	450	0.5	1500	2.9	63.4	94.8	0.4
Rh/SiO_2	250	450	0.5	1500	0.6	75.2	95.2	0.0
Rh/SiO_2	275	750	0.5	1500	3.1	68.7	88.8	1.8
Rh/SiO_2	275	750	1	1500	1.5	77.7	89.9	1.8
$Rh\text{-}Pd/SiO_2$	250	450	0.5	3000	0.4	28.2	100.0	0.0
$Rh\text{-}Pd/SiO_2$	275	450	0.5	1500	2.5	48.5	90.2	0.9
$Rh\text{-}Pd/SiO_2$	275	450	0.5	1500	2.0	51.8	86.1	0.8

Rhodium alumina catalysts are moderately active. for example, 6% CO conversion at the above conditions. Selectivity of CO to oxygenates is typically 30% with the balance being methane. An important feature of the oxygenates are the high amounts of C2– oxygenates including ethanol, acetic acid and methyl and ethyl acetates.

The addition of sodium or potassium lowered the activity considerably. However for the highest sodium level tested, (2 wt. % Na) selectivity to oxygenates increased to 55-75%, though the CO conversion was only about 1% to 2.5%. The high temperatures and low space velocity needed to achieve reasonable conversion show that the Tamaru catalysts[2] 5%Rh/Al_2O_3 prepared from Na_3RhCl_6 are less active.

Also, Na was added as NaOH to prereduced Rh/Al_2O_3 to test the idea that sodium would act differently from when codeposited with rhodium(1:3 Na-R). The activity and the selectivity of these catalysts is similar to the catalysts prepared by codeposition method.

5.3.6 Modification by Molybdena

Because the addition of small amounts of molybdena to Rh/Al_2O_3 (1Mo:1Rh) gave the best performance(see table 5.5) among various modifiers, it was decided that large amounts of molybdena should be added to Rh/Al_2O_3 (1Mo:1Rh=2-5). The addition of large amounts of molybdena to $Rh.Al_2O_3$ catalysts was found to increase CO hydrogenation activity by a factor of ten. Also, under standard test conditions the selectivity to oxygenates is increased from about 35% to about 85%. The C1/C2 oxygenates ratio is increased. C1 oxygenates include MeOH, MeOMe and MeOEt. The $Rh/Mo/Al_2O_3$ catalysts also show high activity for water-gas shift reaction.

Table 5.10: Performance of various Rh-Na Al_2O_3

catalyst	temp C	pres psi	$CO:H_2$	GHSV	%CO conv	% TOT oxyg	%C2– oxyg	C% to CO_2
Na_3RhCl_6	250	450	0.5	2000	0.9	21	30	24.2
Na_3RhCl_6	450	275	2	2000	1.5	17	<50	24.9
Nit	250	450	0.5	3000	6.6	22.6	72.3	3.9
Nit	250	450	0.5	3000	5.7	28.9	82.4	0.9
Nit	250	450	0.5	1500	9.1	27.5	87.9	1.4
1:1K	250	450	0.5	3273	1.6	37.6	74.4	3.0
1:1K	250	750	0.5	3273	1.9	45.3	80.9	2.6
1:1Na	250	450	0.5	3000	2.3	33.4	85.5	2.7
1:1Na	250	450	0.5	1500	4.4	29.8	85.3	2.5
1:3Na-He	250	450	0.5	3600	0.9	70.5	37.1	31.0
1:3Na-He	276	450	0.5	3600	1.7	57.2	47.9	32.8
1:3Na	250	450	0.5	1500	1.0	70.7	40.4	23.3
1:3Na	275	450	0.5	1500	3.3	53.6	63.7	21.7
1:1.3Na-R	250	450	0.5	1500	3.1	54.6	38.7	27.5
1:1.3Na-R	275	450	0.5	1500	4.5	33.2	71.2	9.6

Mo/Al_2O_3 tested under similar conditions(250C, 30atm. hydrogen. CO=2, 3000 GHSV) displayed low activity and only hydrocarbons are produced.

In $Rh/Co/Mo/Al_2O_3$, the catalyst showed high activity, no unusual results were attributable to the presence of cobalt. Rh/TiO_2 was the most active catalysts among the catalysts tested. The influence of catalyst composition on the selectivity is of special interest. First, note that addition of molybdena greatly increases the water gas shift reaction. Indeed, with the higher amounts of Mo, 20 to 35% of CO reacted under the test conditions was converted to carbon dioxide. The water needed for the shift reaction came from the synthesis of hydrocarbons and higher alcohols.

5.4 Conclusions

The effect of the support on CO hydrogenation on supported rhodium catalysts was investigated. The titania supported catalysts reduced at 500C were the most active catalysts among the differents supports used, i.e. Al_2O_3 , SiO_2 , La_2O_3 , and MgO supported catalysts. However the selectivity to oxygenates was the highest on MgO supported catalysts among the different supports investigated. but MgO had low activity. The modified Rh/SiO_2 catalysts in general were more selective for oxygenates but had less overall activity than modified Rh/Al_2O_3 catalysts. Addition of Mo, particularly large amounts(Mo:Rh=5) increased the rate of CO hydrogenation Rh/Al_2O_3 , Rh/TiO_2 and Rh/SiO_2 catalysts. The selectivity to oxygenates was also increased. Addition of Na to Rh/Al_2O_3 decreased the activity but increased the C2− oxygenate selectivity. Alloying Pd with Rh in Rh/SiO_2 and Rh/Al_2O_3 catalysts gave the best C2− oxygenate selectivity. The selectivity to total oxygenates was high on Rh/Florisil, but the overall activity was low. $Rh/Mo/TiO_2$ /Florisil catalysts had a good selectivity to oxygenates and a good overall selectivity. In conclusion, there are many interesting effects of the

Table 5.11: Performance of molybdena modified Rh Al_2O_3 and Rh TiO_2 catalysts at 30 atm pressure and hydrogen CO=2

Catalysts	Temp C	GHSV	%CO conv	%CO conv. to CO_2	oxyg	C2– OXYG
Rh/Al_2O_3	250	4000	6	1	33	80
$Rh/2.8\%Mo/Al_2O_3$	225	3000	9	21	59	42
$Rh/7.5\%Mo/Al_2O_3$	200	3000	7	24	86	17
	250	36000	5	25	65	27
$Rh/15\%Mo/Al_2O_3$	200	3000	7	23	91	21
	225	3000	27	37	83	14
$15\%Mo/Al_2O_3$	225	3000	<1	61	0	-
	250	3000	2	50	0	-
	275	3000	5	51	0	-
$Rh/Mo/Co/Al_2O_3$	250	3000	1	0	58	94
Rh/SiO_2	250	3000	1	0	58	94
Rh/TiO_2	225	2500	9		27	90
$Rh/6\%Mo/TiO_2$	225	4700	11	33	56	19

modifier on supported rhodium catalysts that need further detailed kinetics and characterization study. These investigations were carried out with molybdena and sodium modified catalysts and are discussed in chapters 6 to 9.

REFERENCES

1. G.M. DaCruz, G. Djega-Mariadassou and G. Bugli, Appl. Catal. 1985, 17, 205.

2. S. Kagami, S. Naito, Y. Kikuzono and K. Tamaru, JCS Chem. Commun. 1983, 256.

3. E.K. Poels, P.J. Magnus, J. van Welzen and V. Ponec, 8th Intl. Congr. Catal., 1984, Berlin, pII-59.

4. A.J. Dennis, G.E. Harrison and J.P. Wyber, European patent appl. 96987, assigned to Davy McGee, 1984.

5. S.D. Worley, C.A. Rice, G.A. Matson, C.W. Curtis, J.A. Guin and A.R. Tarrer, J. Chem. Phys. 1982, 76, 20.

6. K. Gilhooley, S.D. Jackson and S. Rigby, Appl. Catal.1986, 21, 349.

7. J.R. Katzer, A.W. Sleight, P. Gajardo, J.B. Mitchel, E.F. Gleason and S. McMillan, Far. Dis. Chem. Soc. 1981, 72, 121.

8. B.J. Kip, Ph.D. thesis, Eindhoven University of Technology, The Netherlands, 1987.

9. T.P. Wilson, P.H. Kasai and P.C. Ellgen, J. Catal. 1981, 69, 193.

CHAPTER 6
PERFORMANCE OF SODIUM MODIFIED RHODIUM/ALUMINA CATALYSTS

Recently, there has been much interest in modified rhodium catalysts for conversion of syngas to higher oxygenates. Addition of alkali modifier is known to increase the selectivity to oxygenates. However, almost all the previous work on alkali modified rhodium catalysts was done on silica supported systems. Alumina is a much better industrial support than silica because of its mechanical strength. Also the properties of alumina can be changed over a wide range by adding a third component.

In this chapter, the kinetics and the performance of sodium modified rhodium/alumina catalysts is discussed. The chapter is divided into two parts. In the first part the catalyst preparation and the catalysts testing results are discussed. In the second part the delplot method, developed in chapter 3, is applied to carbon monoxide hydrogenation on sodium modified rhodium/alumina catalytic system to separate products according to their rank.

6.1 Catalysts Preparation

The catalysts were prepared by using Air Products CATAPAL alumina extrudate ground to a particle size of 60-100 mesh. The support was then calcined at 500C under flowing air (Matheson UHP grade) for two hours. The surface area of the support is approximately $200m^2/gm$. The Rh/Al_2O_3 catalysts were prepared by using a no-excess solution impregnation technique, using a sulfate-

free rhodium nitrate solution from Engelhard. The impregnated catalysts was then held at room temperature for two hours, dried at 110C for 12 to 16 hours, then calcined under flowing air at 500C for 2 hours. Alkali was added as nitrate by co-impregnation unless otherwise specified. The catalysts were reduced in the reactor at atmospheric pressure at 200C for 1/2 hour, at 350C for 1/2 hour and at 500C for 1 hours under flowing hydrogen. The reactor and the details of the procedure are described in chapter 3. Some sodium modified catalysts were prepared by sequential impregnation of sodium and rhodium to investigate the effect of method of preparation. Unless, otherwise specified, all runs test were run with hydrogen/CO=2 and the same amount of catalysts was used.

6.2 CO Hydrogenation

Catalyst testing was done in a micro-flow reactor described in chapter 3 with down stream analytical system. After reduction, the catalyst the reactor was cooled to the reaction temperature (200-275C) and the reactor was pressurized to 30 atm pressure under hydrogen. Carbon monoxide flow was started and the reaction was run for 12-16 hours before collecting data to avoid initial transients.

6.2.1 Activity

Table 6.1 on page 210 shows a typical set of data for sodium modified catalysts. Addition of sodium to Rh/Al_2O_3 decreases the rate of carbon monoxide hydrogenation substantially. As seen from table 6.1, addition of 1:1 atomic ratio of Na:Rh to Rh/Al_2O_3 decreases the conversion from 6% to 2.5% at 250C and 30atm. Also, the conversion decreased from 18% to 7% at 275C and 30atm pressure. The difference in the carbon monoxide conversion decreased with the increase in pressure as observed by changes in conversion in the third row in table 6.1. The overall selectivity to oxygenates and the % C2+ oxygenate selectivity is not

appreciably affected. Conversion of carbon monoxide is reported on a total basis. Here again, the selectivity is reported on a carbon basis excluding carbon dioxide. Carbon monoxide converted to oxygenates is reported as %oxygenates and the fraction of oxygenates greater than C_1 is reported as %C2+OXYG.

The details of activity and selectivity of rhodium/alumina catalysts were discussed in the chapter 5. Addition of sodium to rhodium/alumina decreases the rate of carbon monoxide hydrogenation.

The addition of sodium decreases the overall rate exponentially with the amount of sodium added, see figure 6.1. This is because the sodium added first poisons the most active sites. As seen in Table 6.2 the overall carbon monoxide conversion decreases from 6% for Rh/Al_2O_3 to 2.5% for Rh-0.67%Na/Al_2O_3 to 1% for Rh-2%Na/Al_2O_3 at 250C and 30atm. Also, at 275C and 30atm, the overall conversion decreased from 18% to 7% to 1.4%(corrected for GHSV) and at 275C and 47.5atm the overall conversion decreased from 13% to 9.4% to 1.4%, as seen in table 6.2. Here again, the extent of changes in the activity on sodium addition decreased with increase in reaction pressure. These results are consistent with other investigations on similar systems[1-5].

6.2.2 Product Distribution

Table 6.3 on page 214 shows the effect of sodium addition on the detailed product distribution. The water gas shift reaction is accelerated on addition of sodium as evidenced by the increase in carbon dioxide formed from 0.6% to 22%. The amount of methane and ethane formed decreases. Unlike Rh/Al_2O_3 no propene, propane and butanes are formed. Addition of sodium increases the selectivity to methanol substantially. Unlike Rh/Al_2O_3 no ethers are formed, this is because the acidic sites on alumina are neutralized by addition of alkali modifier. The carbon selectivity to C2 oxygenates is doubled with ethanol the predominant

Table 6.1: Effect of addition of sodium on carbon monoxide hydrogenation on 3%Rh/Al_2O_3 . hydrogen/CO=2. 4000 GHSV.

Catalysts	Press atm	Temp C	% CO Conv.	% oxy-genates	% C2– oxyge-nates
3%Rh/Al_2O_3	30	250	6	33	80
	30	275	18	17	75
	47.5	275	13	22	75
3%Rh 0.67%Na/	30	250	2.5	35	75
Al_2O_3	30	275	7	25	75
	47.5	275	9.4	30	85

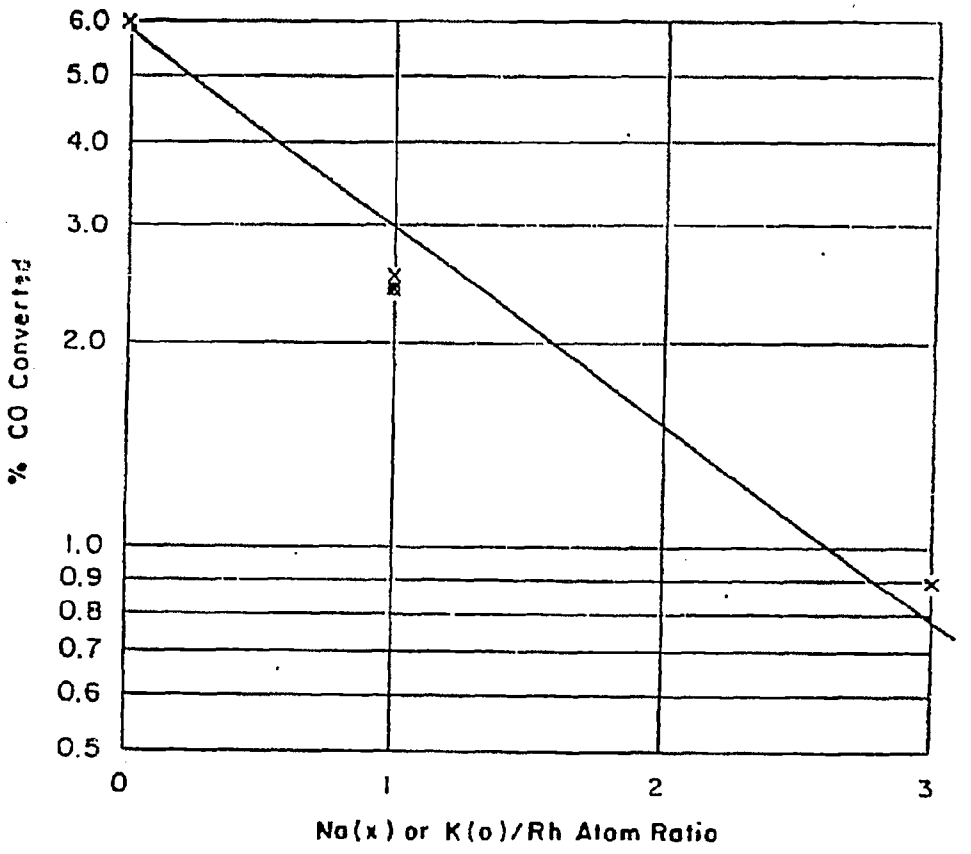

Figure 6.1: Poisoning of Rh Al_2O_3 by the addition of alkali for carbon monoxide hydrogenation at 30 atm. 250C and 4000 GHSV.

Table 6.2: Effect of the amount of sodium added on carbon monoxide hydrogenation 3%Rh/Al_2O_3 , hydrogen/CO=2.

Catalysts	Press atm	Temp C	GHSV 1./hr	%CO conv.	% oxygenates	%C2– oxygenates
3% Rh/Al_2O_3	30	250	4000	6	33	80
	30	275	4000	18	17	75
	47.5	275	4000	13	22	75
3%Rh 0.67%Na	30	250	4000	2.5	35	75
Al_2O_3	30	275	4000	7	25	75
	47.5	275	4000	9.4	30	85
3%Rh 2%Na	30	250	4000	1	70	33
Al_2O_3	30	275	2000	2.8	53	50
	47.5	275	2000	2.8	52	40

product. The carbon selectivity to propanol is also increased from 2.4% to 6.4%. Also, the amount of esters formed decreased.

Even though the selectivity to oxygenates increases on sodium addition, the productivity to oxygenates, defined as the total rate to oxygenates decreases substantially. This is because of the much lower activity of the sodium modified Rh/Al_2O_3 catalysts and because of the high amounts of carbon dioxide formed on $Rh\text{-}Na/Al_2O_3$ as compared to Rh/Al_2O_3. Chapter 5 shows that the hydrocarbons follow a Schulz-Flory distribution for CO hydrogenation on Rh/Al_2O_3 catalysts. Here again, the oxygenate products are C1, C2 and sometimes C3 products or any secondary products such as EtOAc derived from C1 and C2 products. Because C2 oxygenate products correspond to the C1-component of the oxygenate SF distribution[6], there are only two data points for oxygenate SF distribution in these systems. Hence fitting of SF distribution was not done because of lack of oxygenates higher than C3. It is interesting to note that unlike Cu/ZnO based catalysts, no isobutanol was formed in these systems. The absence of MeOMe in the product distribution is because of the lower acidity of the $Rh\text{-}Na/Al_2O_3$ catalysts. Also, the high amounts of carbon dioxide formed is particularly useful when the syngas is coal-based. The optimum gasifier hydrogen/CO ratio for a coal-based gasifier is 0.5-1. The rate of CO hydrogenation on these catalysts is lowered at these high partial pressure of CO. The water gas shift reaction not only generates hydrogen in-situ, thus increasing the hydrogen/CO ratio, but also removes water from the product by converting it into carbon dioxide, thus partially solving the water separation problem.

The selectivity to oxygenates for Rh/Al_2O_3 catalysts is plotted in figure 6.2 on page 216 as a function of carbon monoxide conversion. While the curve is fairly flat, the selectivity increases from 20 to 37% when conversion decreases from 18% to 2%. For selectivity comparisons between catalyst to be valid, it is deemed necessary to refer to equal conversions. This is frequently not done in

Table 6.3: Detailed product distribution of carbon monoxide hydrogenation on 3%Rh·Al_2O_3 and 3%Rh 2%Na Al_2O_3 .

	3%Rh/Al_2O_3	3%Rh 2%Na Al_2O_3
Temp(C)	250	275
GHSV(1/hr)	3000	1500
% CO conv.	5.4	3.3
% CO to CO_2	0.6	22
% CO to Oxygenates	31	53
%CO to C2+ Oxygenates	89	64
%C selectivities to		
Methane	59	43
Ethane	3.5	3.4
Propene	1.5	0
Propane	4.0	0
Butane	1.6	0
Methanol	0.9	18
MeOMe	0.4	0
MeCHO	4.2	2.7
EtOH	10.4	20.4
MeOAc	4.5	3.4
AcOH	0	2.4
MeOEt	2.2	0
PrOH	2.4	6.4
EtCHO	0.1	0
EtOAc	8.4	0

the current literature on similar systems. The addition of 1 sodium or potassium atom per rhodium atom reduces the activity to about one-half and the addition of 3 sodium atoms per rhodium atom to one-sixth of the unpromoted catalysts. It is remarkable that these relatively small amounts of alkali have such a profound deactivating effect, particularly considering the extensive alumina surface. As mentioned above, the activity decreases as if the addition of sodium is poisoning the performance of Rh/Al_2O_3 catalyst. From the selectivity to oxygenates versus conversion plots, clearly the low conversion data ($< 6\%$) for the sodium modified catalysts shows higher selectivity, while the high conversion data shows selectivity similar to Rh/Al_2O_3 catalysts. Similar results were obtained on $Ru\text{-}Na/SiO_2$ by Gonzalez et al.[7, 8].

A more detailed examination of the changes in the product distribution shows that the alkali deactivates hydrocarbon formation more than that of oxygenates. This is shown in table 6.4 on page 217 where it is shown that while the amount of C2+ oxygenates are decreasing from 1.6 to 0.2 C atoms/ 100 C atoms fed of the total carbon monoxide. In contrast on $Rh\text{-}Na/SiO_2$, Tamaru et al.[9, 10] observed no changes in the methanation rate on sodium addition. However, the amount of methanol remains constant at 0.4 C atoms/100 C atoms fed. Using delplot analysis MeOH will be shown to be a primary product. Thus, under differential conditions, the amount of carbon converted to MeOH is proportional to the rate of conversion of carbon monoxide to methanol. Thus the rate of methanol formation is not affected by the presence of alkali addition. In contrast, the rate of higher oxygenates and hydrocarbon formation are drastically affected.

6.2.3 Effect of Catalysts Pretreatment

Although the standard preparation method consisted of coimpregnation, air calcination and reduction under hydrogen, several variation of catalysts preparation and catalysts pretreatment were also investigated. Table 6.5 on page 220

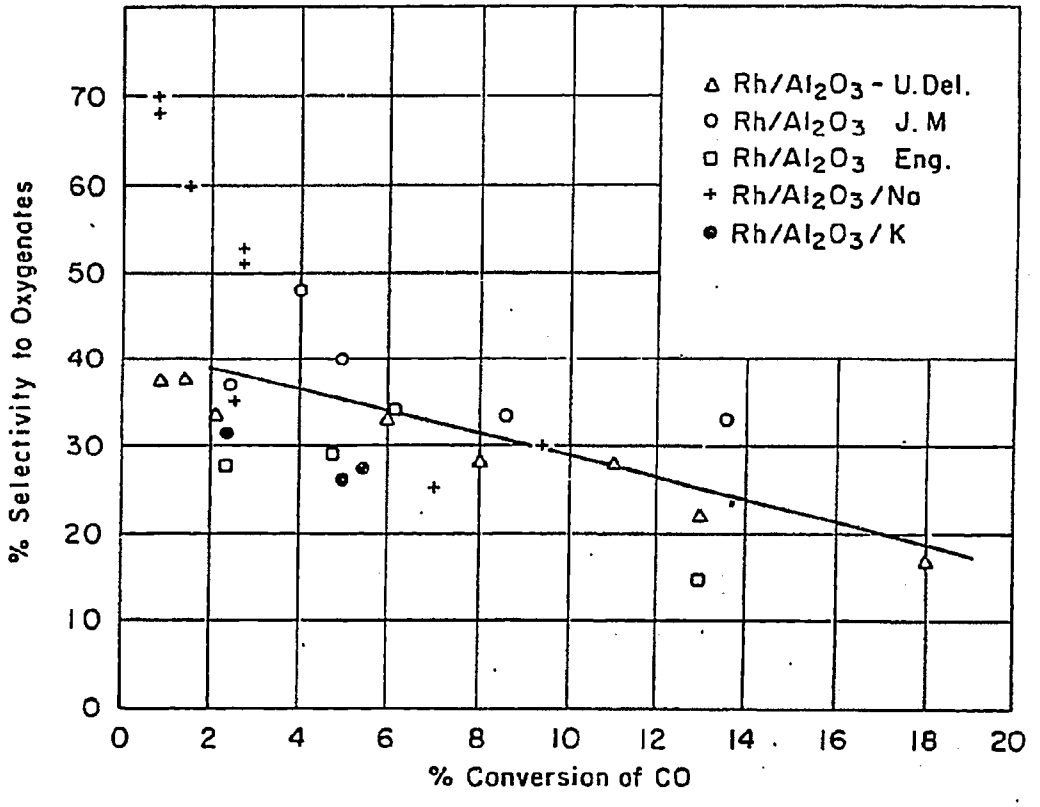

Figure 6.2: Effect of alkali addition on the conversion on the selectivity to oxygenates on Rh/Al_2O_3 catalysts.

Table 6.4: Effect of sodium on the product categories in carbon monoxide hydrogenation on $3\%Rh/Al_2O_3$.

Na:Rh atomic ratio	% CO conv.	C in Hydro-carbons	C in oxygenates	C in C2– oxygenates	C in MeOH
0	6	4	2	1.6	0.4
3	0.9	0.27	0.63	0.2	0.4

summarizes the data from these runs. Catalyst that were reduced without air calcination had the same activity as the catalyst which were calcined before being reduced. There was no substantial change in the selectivity pattern at 250C. However, the selectivity was markedly different at 275C. The reasons for these changes are not clear. The air treatment was carried out by taking a used catalysts and exposing it to air. The catalysts was then rereduced at 500C.

The effect of air treatment after use was drastic. The activity of the catalyst remained the same but the selectivity to oxygenates decreased substantially. At the same time the fraction of C2+ oxygenates increased. Methanol formation was suppressed by the air treatment. The XRD results shown in chapter 7, show that on air treatment the rhodium crystallites grow or agglomerate. This is consistent with the observation that the agglomeration of rhodium crystallite occurred on air treatment and that the formation of methanol does not require an ensemble of sites. Thus, on air treatment larger ensembles are created that lead to decrease in the number of highly dispersed sites. These highly dispersed sites are responsible for formation of methanol. This is consistent with the results of Arakawa et al.[11], in which the effect of particle size was investigated on the selectivity to methanol.

Table 6.6 on page 221 shows the effect of sodium addition to prereduced Rh/Al_2O_3 catalysts. A comparison of table 6.6 with tables 6.1 and 6.2 shows that there no substantial effect of sequence of sodium addition on the performance of these catalysts.

6.2.4 Selectivity and Productivity

Figure 6.3 on page 222 shows a plot of carbon selectivity of various C2 oxygenates versus the carbon monoxide conversion. The carbon selectivity to C2 oxygenates and in particular ethanol, acetaldehyde, acetic acid and methylacetate decrease with conversion. The decrease in the acetaldehyde selectivity was the

steepest. Based on a similar analysis, Underwood and Bell[12] reported that acetaldehyde was the primary product for carbon monoxide hydrogenation on Rh La_2O_3. It is interesting to note that the selectivity versus conversion curve for MeOAc follow the AcOH curve closely. This indicates that the formation of MeOAc is limited either by formation of AcOH or any precursor to AcOH. In contrast, the ethylacetate selectivity increases with conversion. Thus ethylacetate is clearly a secondary product. The delplot method is used in the next section to reach the same conclusion using a quantitative and rigorous analysis. Also, all the C2 oxygenate product give a finite asymptotic value at high conversion.

Figure 6.4 shows the productivity of C2 oxygenate products versus conversion. The productivity is defined as the carbon monoxide conversion multiplied by the product selectivity. The productivity-conversion plots show the changes in the total amount of product formed as a function of conversion. The productivity of all C2 oxygenates increases with conversion. This is a direct consequence of the of finite asymptotic value of the selectivity-conversion plots. Here again, acetaldehyde has the highest change in the productivity-conversion plots from low conversion to the high conversion region. The productivity of EtOAc jumps form zero to a high value.

6.3 Transport Limitations

The heat and mass transfer effects are evaluated in Appendix A and are shown to be insignificant under the reactor conditions used in this chapter.

6.4 Basic Delplot Analysis

In this section the basic delplot method is applied to the kinetic analysis of carbon monoxide hydrogenation on sodium modified Rh/Al_2O_3 . As explained in

Table 6.5: Effect of calcination and redispersion on carbon monoxide hydrogenation on 3%Rh 2%Na/Al_2O_3 , hydrogen/ CO=2.

Treatment	Press atm	Temp C	GHSV 1/hr	%CO conv.	% oxygenates	%C2+ oxygenates
reduced	30	250	4000	0.8	70	30
without	30	275	4000	1.5	60	30
calcination						
reduced	30	250	4000	1	70	35
after	30	275	2000	2.8	53	50
calcination	50	275	2000	2.8	52	40
used	30	275	375	12.6	33	90
catalysts	30	275	750	6.0	38	93
exposed to	30	275	1500	3.1	46	91
to air	30	275	2250	1.7	43	90
re-reduced	30	275	3000	1.5	45	90
at 500C	30	275	3600	0.8	51	90

Table 6.6: Effect of sodium addition on passivated 3 % Rh/Al_2O_3 catalysts*

Press atm	Temp C	%CO conv.	% oxy-genates	% C2+ oxy-genates
30	250	2.7	61	42
30	250	1.9	58	
30	275	4.3	34	73
50	275	7.2	35	76
50	250	1.6	57	55
30	250	0.8	55	64

* - 3%Rh/Al_2O_3 catalysts was first reduced, passivated, then 1%Na was impregnated from a NaOH solution. The catalysts was then dried and reduced without air calcination.

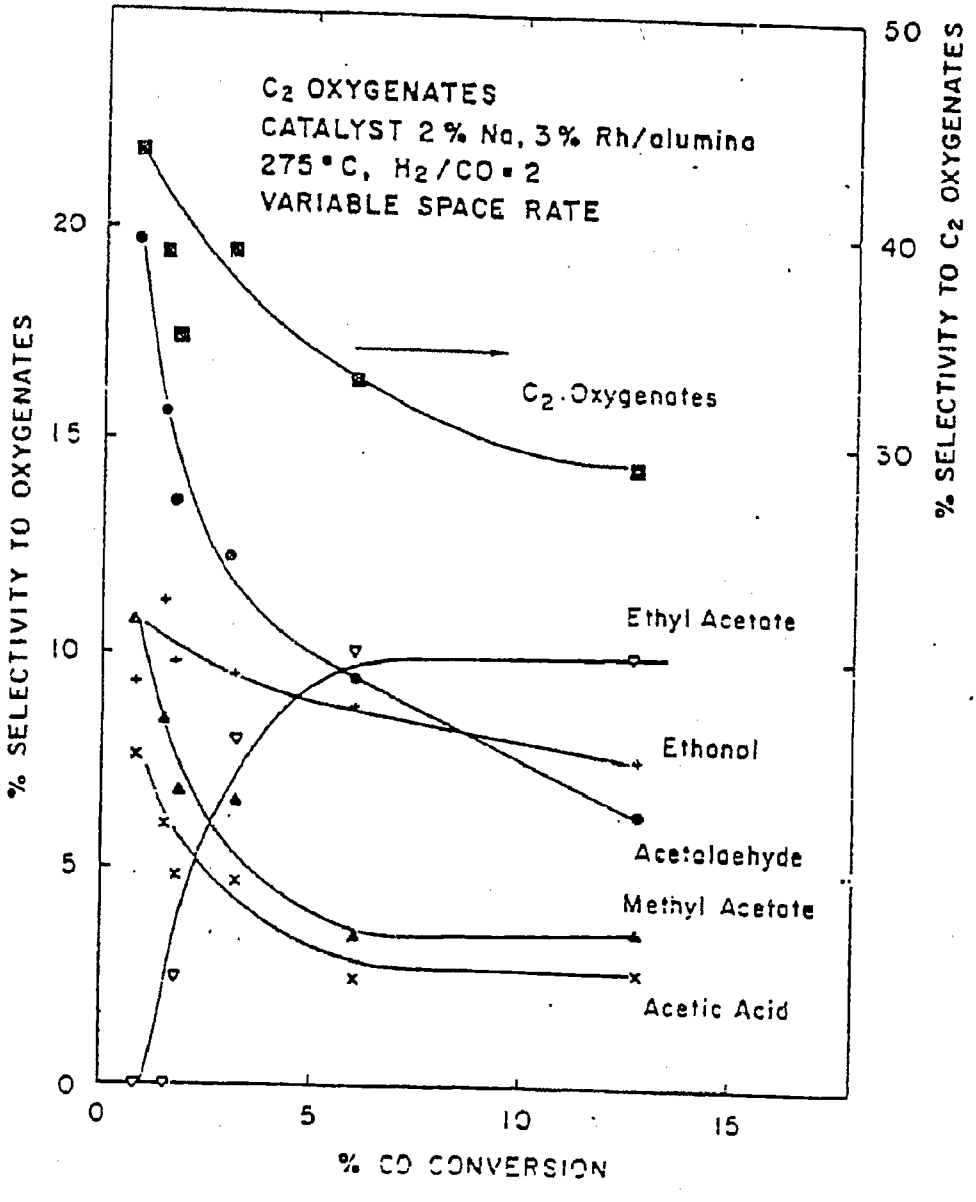

Figure 6.3: Effect of conversion on the selectivity of oxygenates on 3% Rh 2% Na Al_2O_3 catalyst at 275C, 30 atm and hydrogen/CO=2.

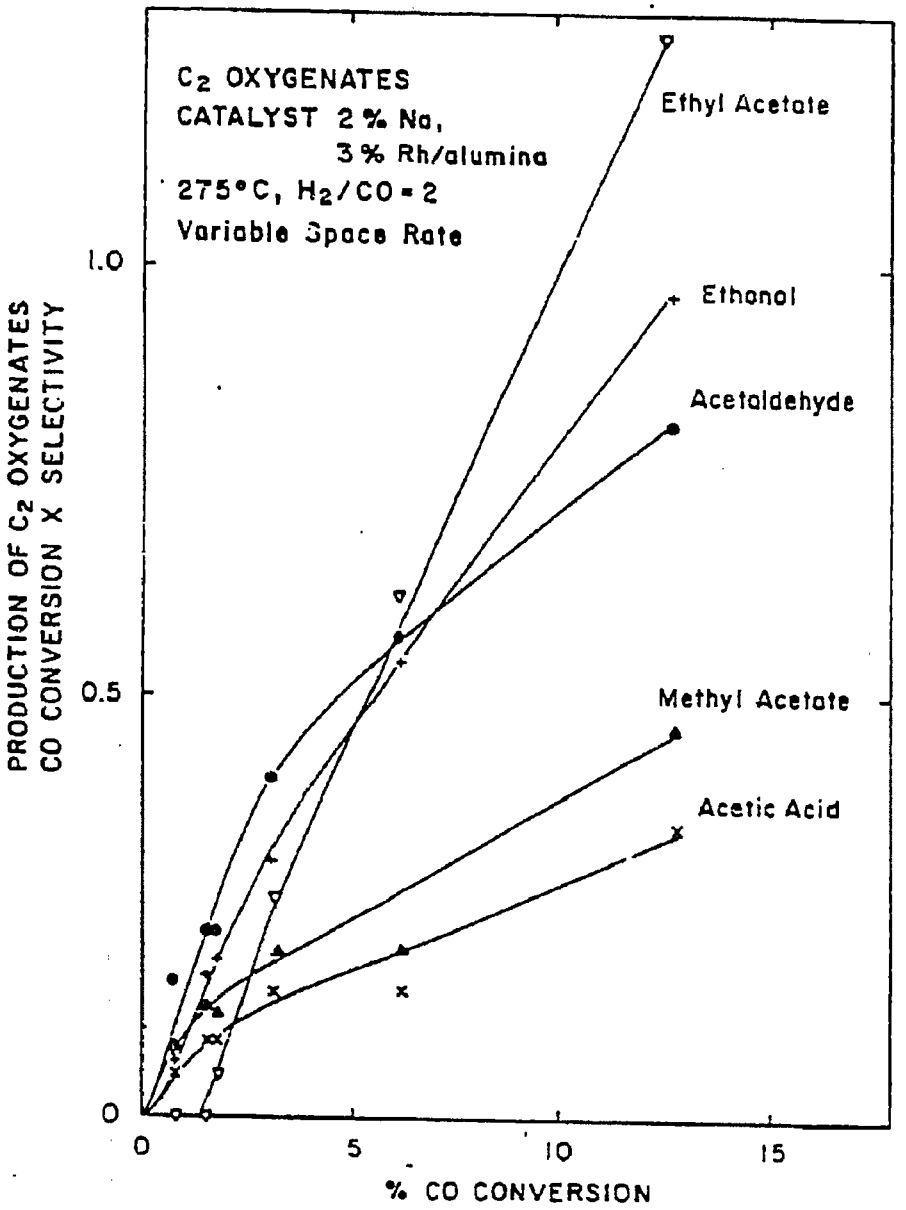

Figure 6.4: Effect of conversion on the productivity of the oxygenates on 3%Rh 2%Na, Al_2O_3 catalyst at 275C, 30 atm and hydrogen, CO=2.

chapter 6. the delplot method sorts products according to their rank. The reactant A, in the delplot method is carbon monoxide. The molefraction of a the product conversion of CO is plotted against the conversion of carbon monoxide. Figures 6.5 to 6.10 on pages 225 to 230 shows the delplots for various products on carbon monoxide hydrogenation on Rh-Na/Al_2O_3 catalysts. Table 6.7 on page 232 tabulates the products and their delplot intercepts.

From figure 6.5 on page 225 methane is a primary product on the time scale investigated. This implies that there is only one slow step in methanation on these catalysts. The large value of the intercept suggests the large amount of methane formed. The intercept is the ratio of the initial rate of formation of methane to the sum of all initial rates. From figure 6.6 the basic delplot of carbon dioxide has a small but finite intercept. Thus carbon dioxide is a primary product. However carbon dioxide is formed from the water gas shift reaction. Water is the reactant in water gas shift reaction, this water is formed as a by-product from hydrocarbon and higher oxygenate formation reactions. Many secondary reactions such as ester and ether formation also give water. Many of the reactions in which water is formed have only one slow step because the products are kinetic primary products. Thus CO_2 is a primary product if the water gas shift reaction is fast on the process time scale.

Figure 6.7 indicates that ethane is a secondary product. Thus there are two slow steps in ethane formation from carbon monoxide and hydrogen. Similarly, from figure 6.8 on page 228 methanol is also a primary product. Surprisingly, ethanol, acetic acid and acetaldehyde all have finite delplot intercepts. This implies that there is only one slow step for formation of of each of these products. This analysis does not preclude the formation of ethanol from acetic acid and acetaldehyde. This analysis only indicates that if there are any steps between the primary products then these steps should be very fast on the process time scale or else the product will not be primary products. Figure 6.9 shows the

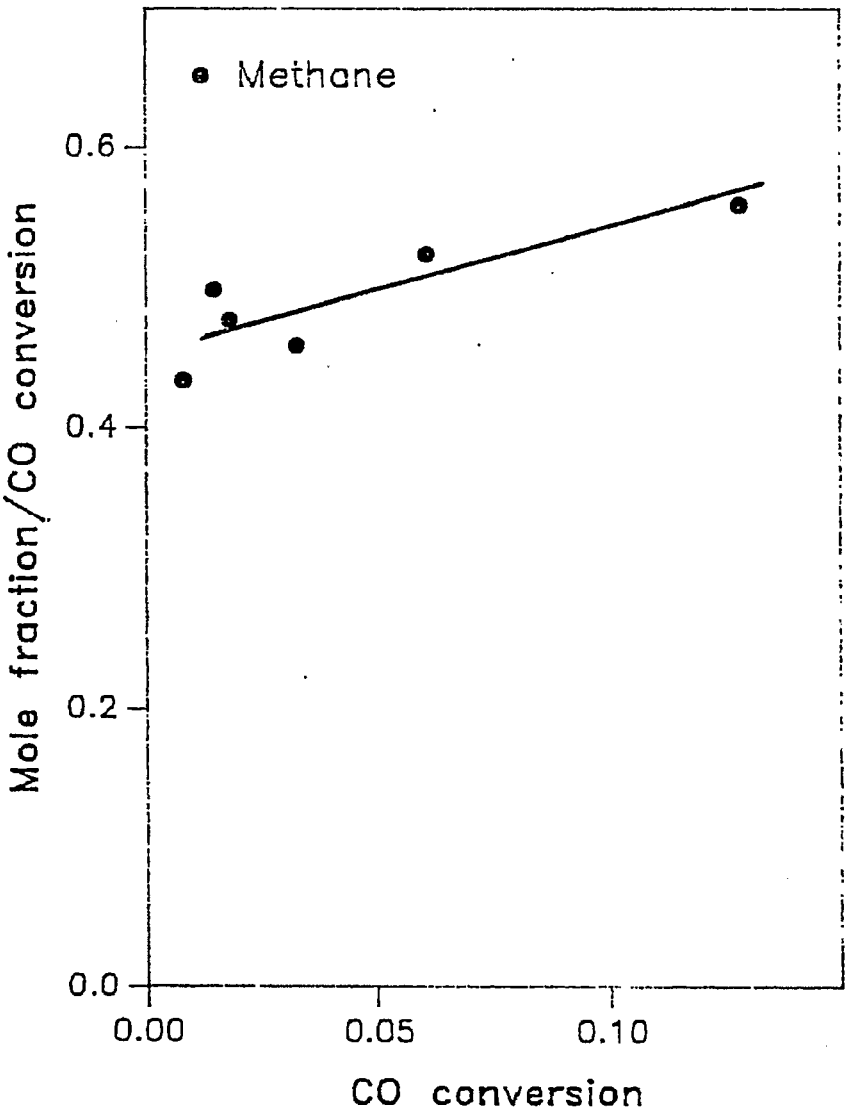

Figure 6.5: Basic delplot of methane on 3%Rh 2%Na/Al_2O_3 at 30 atm. 275C and hydrogen/CO=2.

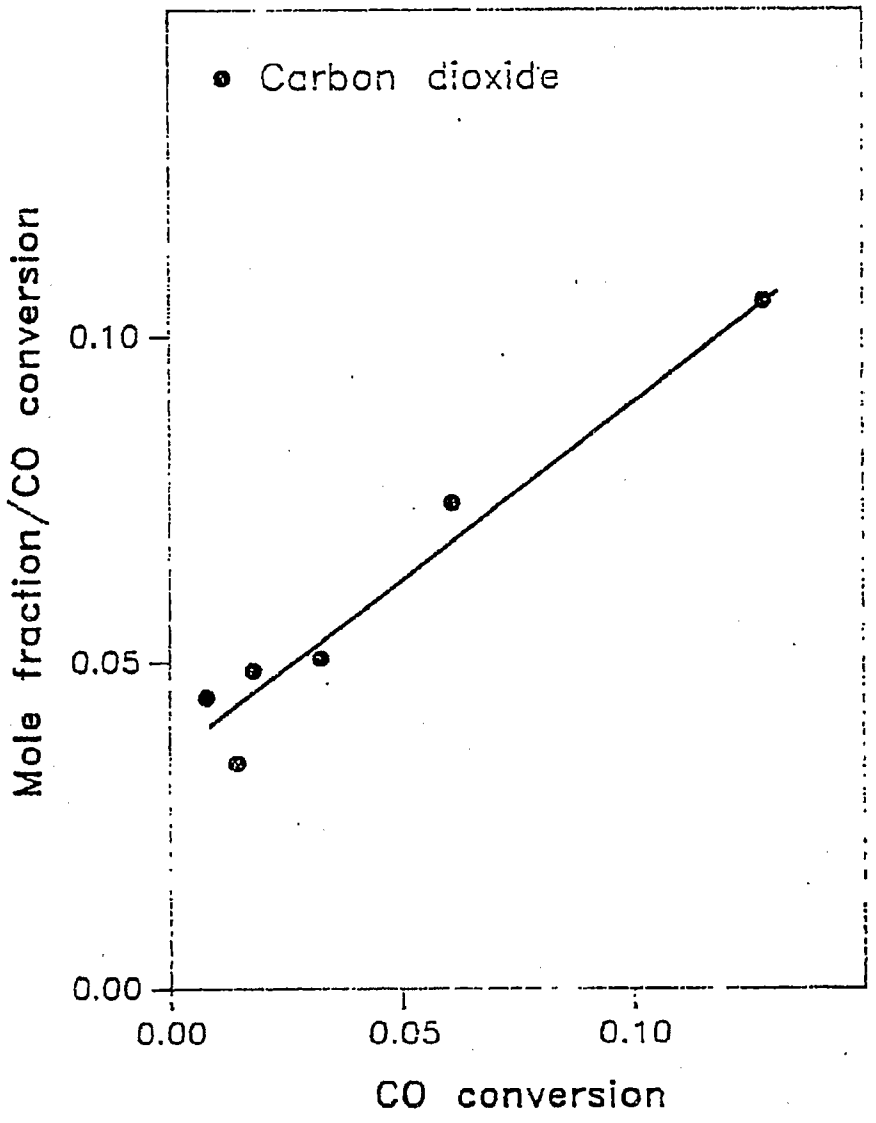

Figure 6.6: Basic delplot of carbon dioxide on 3%Rh 2%Na/Al_2O_3 at 30 atm, 275C and hydrogen/CO=2.

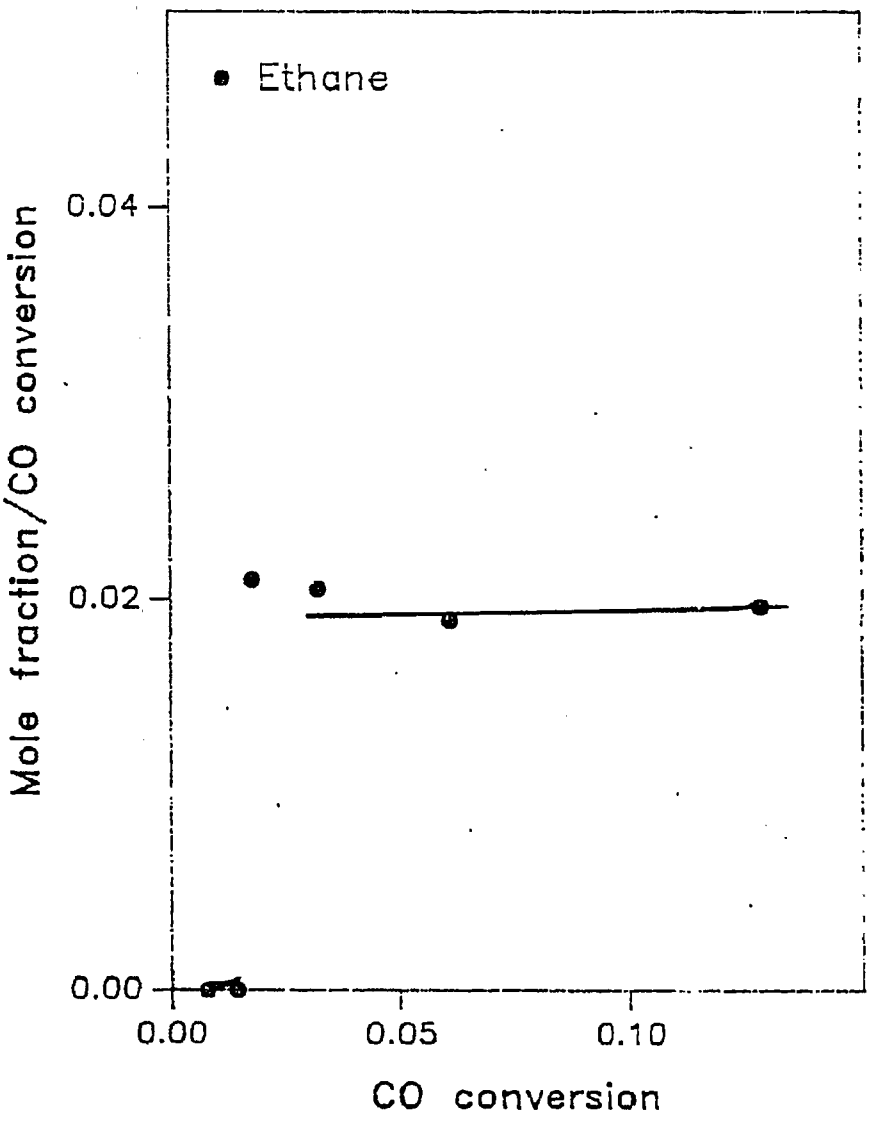

Figure 6.7: Basic delplot of ethane on 3%Rh 2%Na/Al_2O_3 at 30 atm, 275C and hydrogen/CO=2.

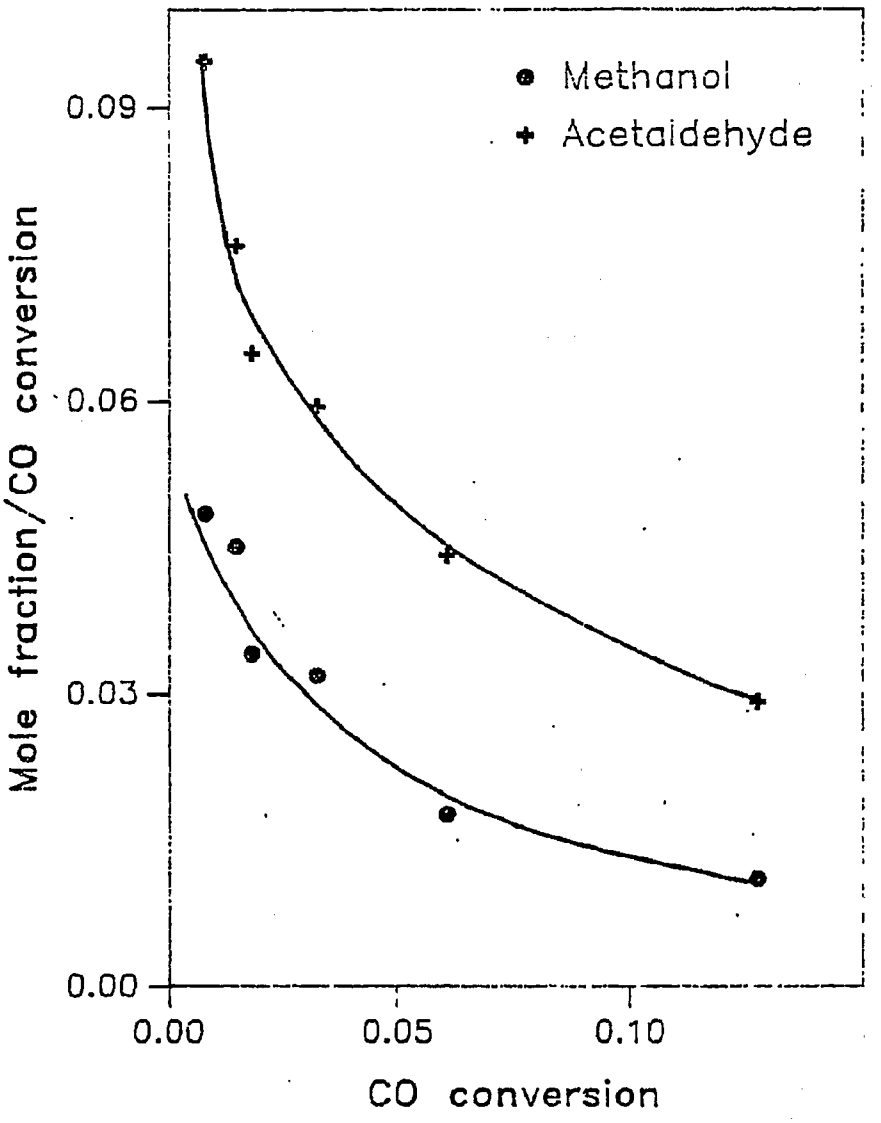

Figure 6.8: Basic delplot of methanol and acetaldehyde on 3%Rh 2%Na/Al_2O_3 at 30 atm, 275C and hydrogen/CO=2.

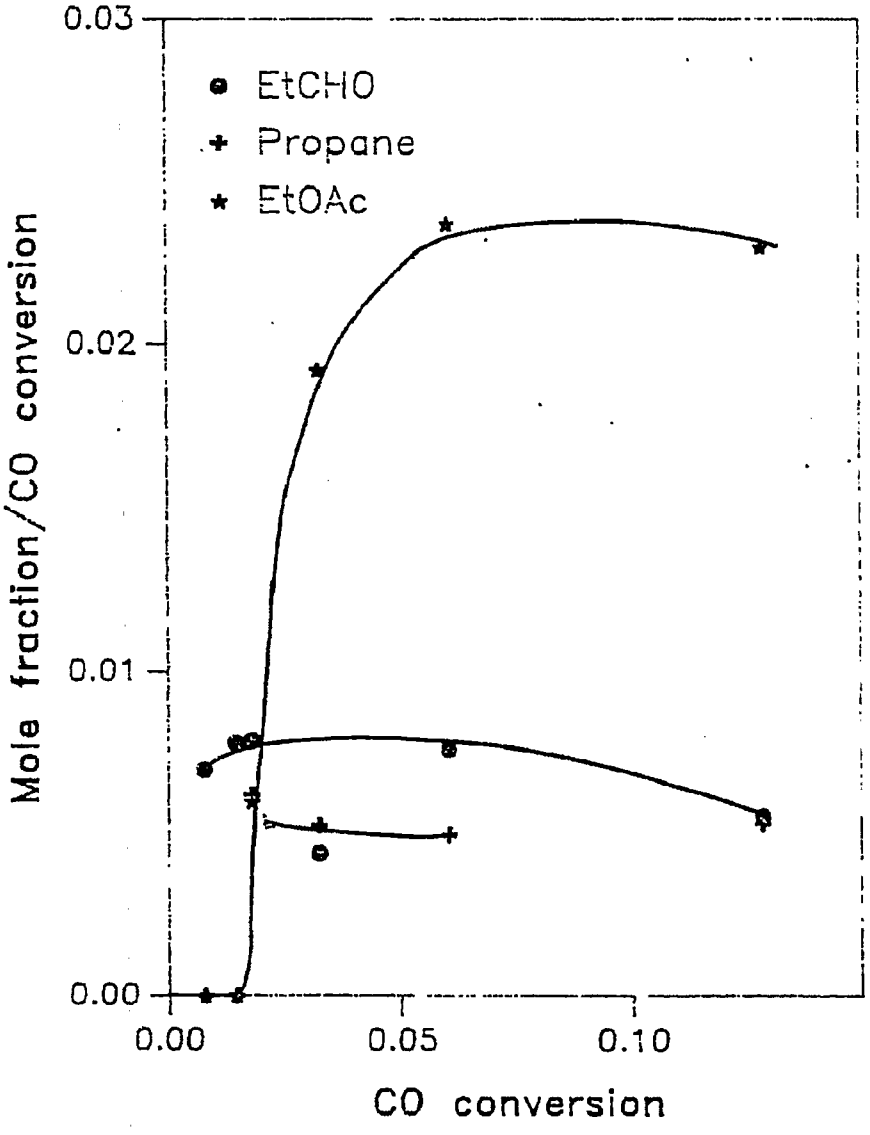

Figure 6.9: Basic delplot of propionaldehyde, propane and ethylacetate on 3%Rh 2%Na/Al_2O_3 at 30 atm, 275C and hydrogen 'CO=2.

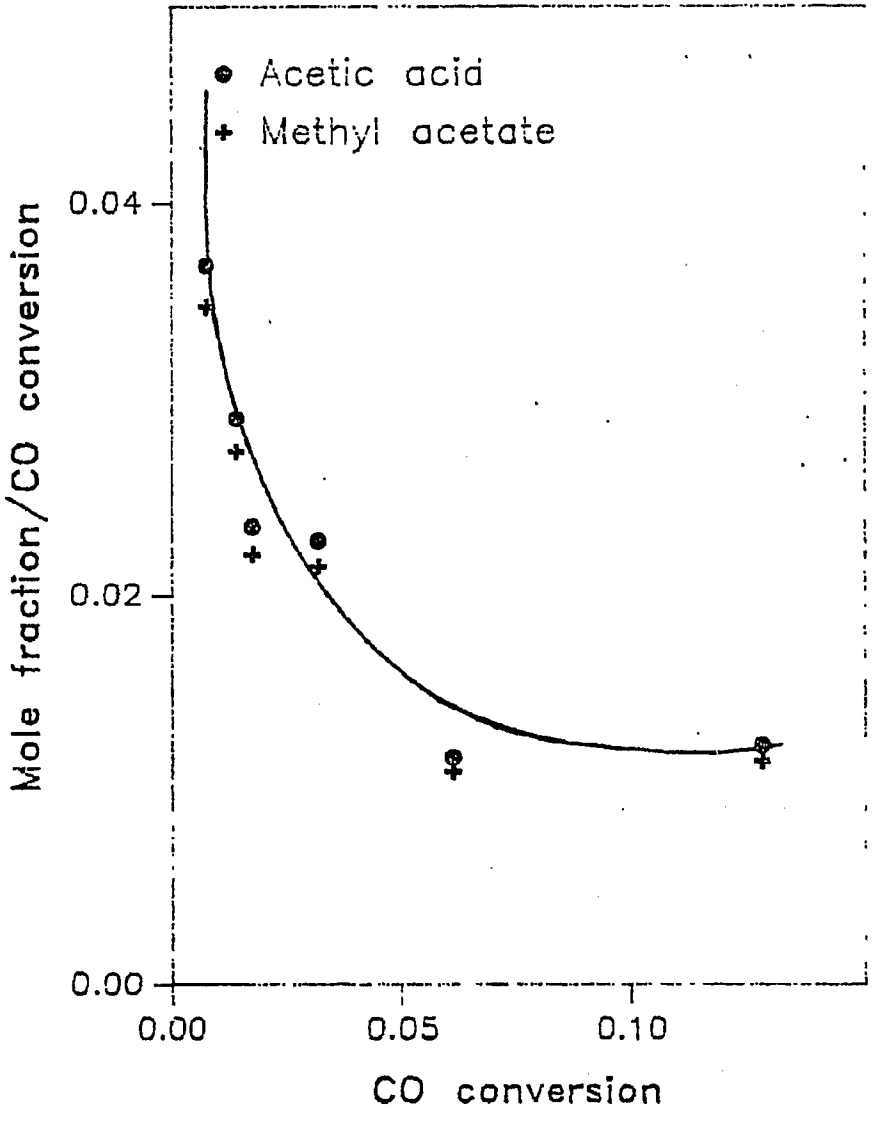

Figure 6.10: Basic delplot of acetic acid and methylacetate on 3% Rh 2%Na/Al_2O_3 at 30 atm, 275C and hydrogen/CO=2.

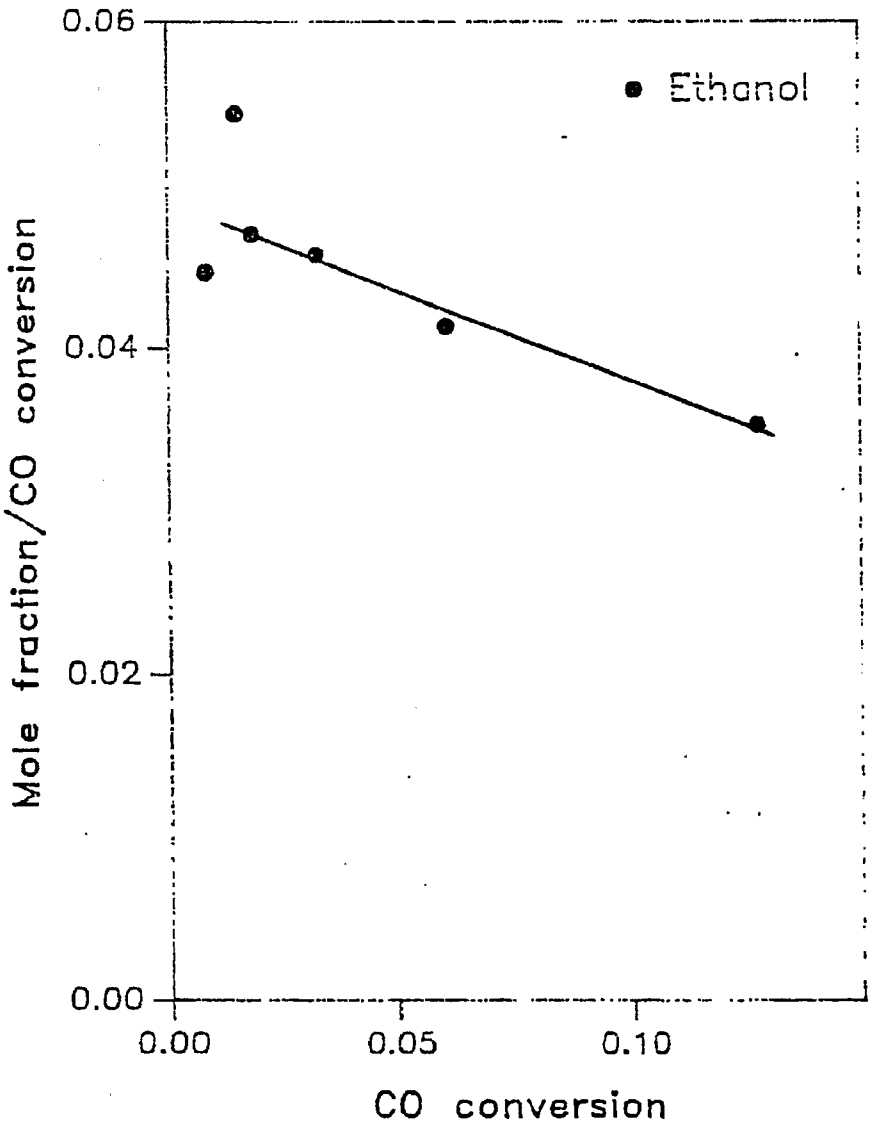

Figure 6.11: Basic delplot of ethanol on 3%Rh 2%Na/Al_2O_3 at 30 atm, 275C and hydrogen/CO=2.

Table 6.7: Delplot intercepts of products formed on CO hydrogenation on 3%Rh 2%Na/Al_2O_3 catalysts at 275C. 30atm and hydrogen/CO=2.

Product	Delplot	Rank	ν_i
Methane	0.45	primary	1
MeOH	0.06	primary	1
EtOH	0.125	primary	2
MeCHO	0.047	primary	2
AcOH	0.038	primary	2
CO_2	0.039	primary	1
Ethane	0	secondary	2
Propane	0	secondary	3
EtCHO	0	secondary	3
EtOAc	0	secondary	4
MeOAc	0.045	primary	3

delplot of EtCHO, propane and EtOAc. Propane and EtCHO are non-primary products. The delplot for EtOAc follows a S-shaped curve. This plot indicates that EtOAc is a non-primary product. Figure 6.10 is the delplot of AcOH and MeOAc on carbon monoxide hydrogenation on Rh-Na/Al_2O_3 . The delplot curve for AcOH and MeOAc follow each other closely. Both MeOAc and AcOH are primary products. This implies that the reaction between MeOH and AcOH is limited by equilibrium. The analysis is limited by the quality of the data at the low conversion.

Chapter 4 shows that the sum of stoichiometrically corrected delplot intercepts should be unity. This sum is the limit of the mass balance of the reactant. Here the reactant is carbon monoxide. Table 6.7 lists the various delplot intercepts and their stoichiometric coefficients. Since no other observable carbon containing species is present, the stoichiometric coefficients are found from the carbon balance. Equation (6.1) shows the sum of stoichiometrically corrected delplot intercepts. The sum is close to 1 within experimental limits. This sum provides an independent check of the delplot analysis. From table 6.7, we get

$$\sum_{j=1}^{n} \frac{{}^{1}P_{CO}^{j} \times \nu_i^{CO}}{\nu_i^j} = 1.065 \qquad (6.1)$$

which follows rule 3 of basic delplot.

6.5 Extended Delplot Analysis

The extended delplot method is useful when many products with rank greater than one are formed. In carbon monoxide hydrogenation on Rh-Na/Al_2O_3 catalyst, very few products are secondary or tertiary. Furthermore, it is very crucial to have good kinetic data at low conversions. Here again, the conversion is based on carbon monoxide. Figure 6.12 on page 235 shows the second rank

delplot for propionaldehyde, which consists of plotting molefraction·conversion^2 versus conversion. The delplot diverges to large values. First, propionaldehyde is a secondary product and not tertiary. Chapter 4 shows that a diverging second rank delplot of a non-primary product suggests that the product is secondary and the order of the second slow step is between 0 and 1 with respect to the reactant. Figure 6.13 on page 236 shows the second rank delplot for propane and ethylacetate. Propane and ethyl acetate follow the same trend as propionaldehyde i.e., they are secondary products and their second rank delplot diverges.

6.6 Conclusions

This study shows the marked effect of addition of alkali modifier on the decrease in the reactivity of the catalysts. Sequential addition of large amounts of sodium follows a typical poisoning model, i.e., the semi-log plot of rate versus amount of sodium added is linear. The addition of alkali modifier to Rh/Al_2O_3 decreases the rate of hydrocarbon formation more than the rat of formation of oxygenates. The selectivity to oxygenates was increased and there were subtle changes in the product distribution on addition of sodium. The data for Rh/Al_2O_3 and $Rh\text{-}Na/Al_2O_3$ follow the same selectivity versus conversion plot, indicating that the major effect of sodium addition is a decrease in the activity and not a change in primary product distribution. Large amounts of C2 oxygenates such as acetaldehyde, ethanol, acetic acid and methyl acetate were also formed on sodium addition. Large amounts of water was formed on sodium addition. Low amount of ethers were formed because of the lower acidity of $Rh\text{-}Na/Al_2O_3$ catalysts. Air treatment of the catalysts had a marked effect on the product distribution. Large amount of hydrocarbons were formed on redispersion, and the fraction of C2+ oxygenates was increased, the amount of methanol formed decreased on redispersion.

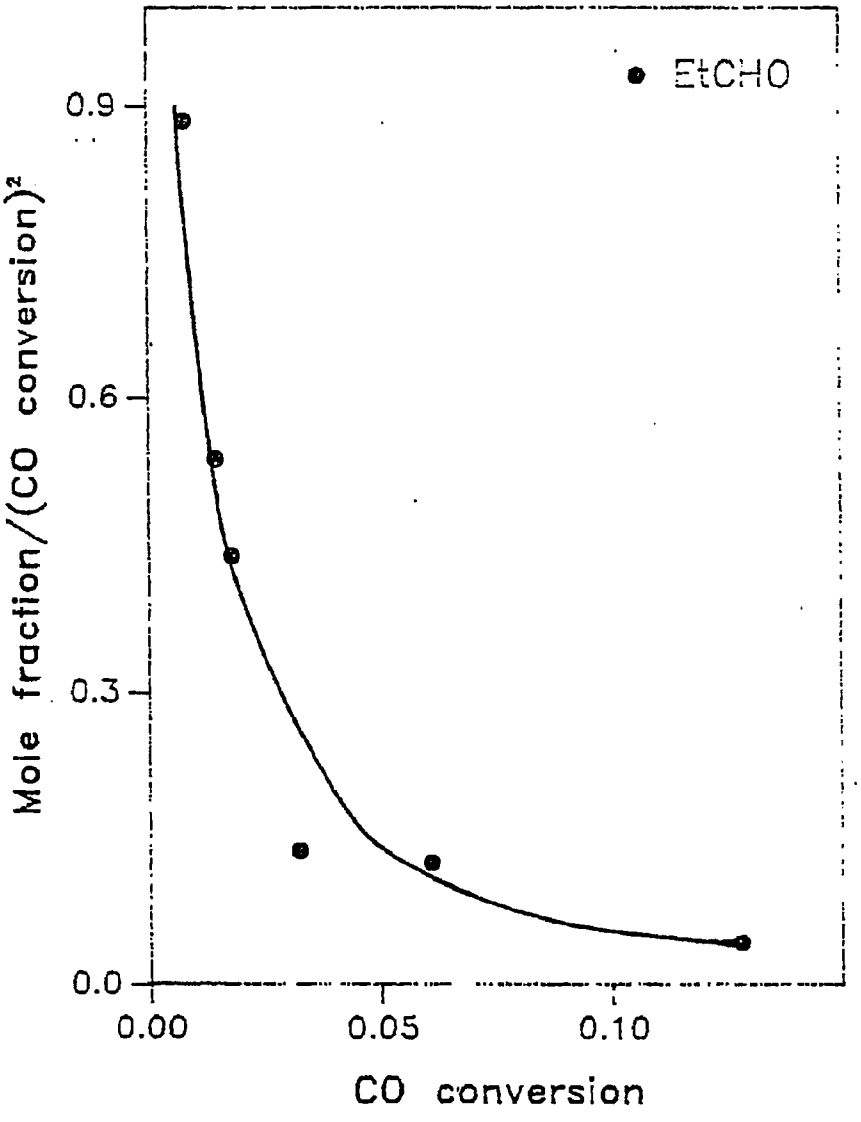

Figure 6.12: Second rank delplot of propionaldehyde on carbon monoxide hydrogenation on 3%Rh 2%Na/Al_2O_3 at 275C. 30atm and hydrogen/CO=2.

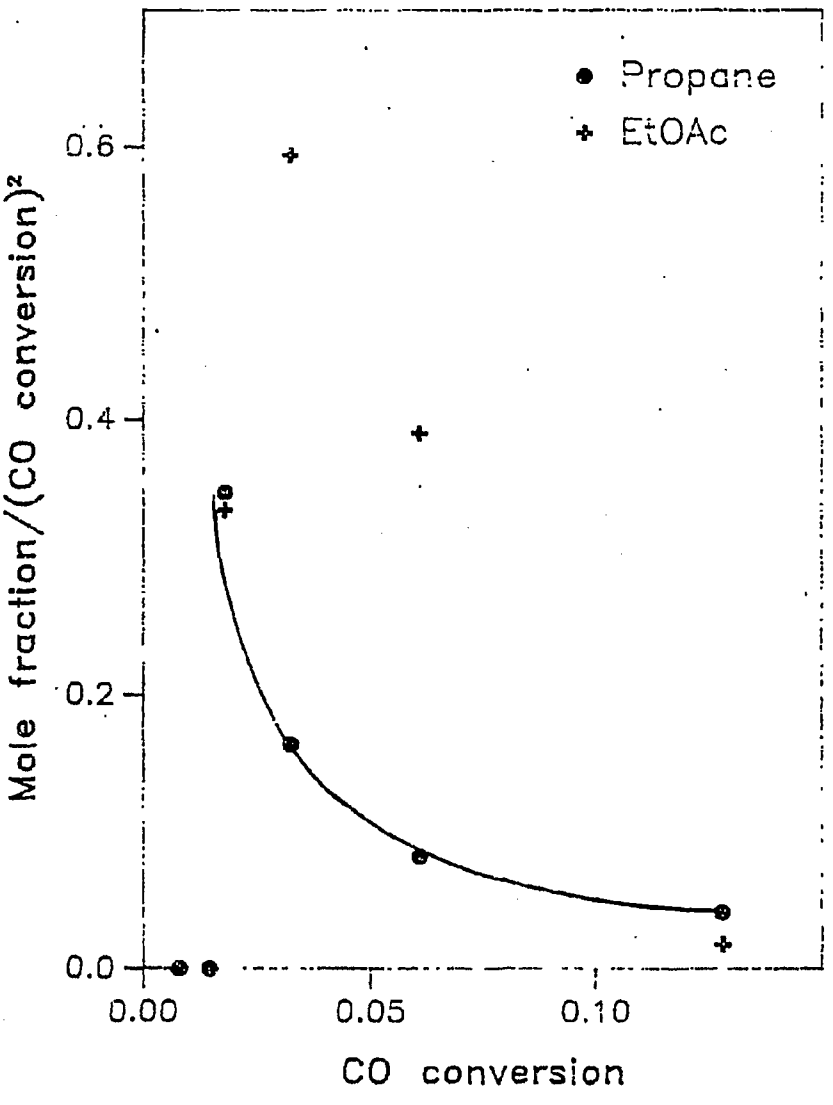

Figure 6.13: Second rank delplot of propane and ethylacetate on carbon monoxide hydrogenation on 3%Rh 2%Na/Al_2O_3 at 275C, 30 atm and hydrogen/CO=2.

The number of slow steps on the process time scale in between the reactants and each product was also found. The formation of MeOAc from AcOH and MeOH precursor was fast on the process time scale. In contrast, the formation of EtOAc was slow on the process time scale. Ethane, propane and propionaldehyde were non-primary products.

REFERENCES

1. D. Kitselmann, W. Vielstich and T. Dittrich, Chem. Ing. Tech. 1977, 49, 463.

2. R.B. Anderson, in Catalysis, Vol. IV, ed. P.H. Emmett, Reinhold, New York, 1956.

3. S.C. Chuang, J. G. Goodwin, Jr., and I. Wender, J. Catal. 1985, 95, 435.

4. W.J. Bartley, T.P. Wilson and P.C. Ellgen, USP 4,235,798, to Union Carbide, 1980.

5. T.P. Wilson, W.J. Bartley and P.C. Ellgen, "Advances in Catalytic Chemistry", Proc. Conf. Salt Lake City, Utah, 1982.

6. F.G.A. van den Berg, Ph.D. thesis, University of Leiden, The Netherlands, 1984.

7. M.M. McClory and R.D. Gonzalez, J. Catal. 1984, 89, 392.

8. H. Miura and R.D. Gonzalez, J. Catal. 1982, 77, 338.

9. S. Kagami, S. Naito, Y. Kikuzono and K. Tamaru, J. Chem. Soc. Chem. Comm. 1983, 256.

10. H. Orita, S. Naito and K. Tamaru, Chem. Letts. 1983, 1161.

11. H. Arakawa, T. Fukushima, M. Ichikawa, S. Natsushita, K. Takeuchi, T. Maatsuzaki and Y. Sugi, Chemistry Letters Japan, 1985, 881.

12. R.P. Underwood and A.T. Bell, Appl. Catal. 1986, 21, 157.

CHAPTER 7
CHARACTERIZATION OF SODIUM MODIFIED RHODIUM/ALUMINA CATALYSTS

This chapter discusses the characterization of the sodium modified rhodium/alumina catalysts. The aim of this investigation is to elucidate, the structure of the catalysts, the role of sodium in modifying the structure of the catalyst, and its related implications on the reactivity of sodium modified rhodium/alumina catalysts. First the investigation of particle size was performed using chemisorption, and x-ray diffraction. Then the bonding of various adsorbed species form the in-situ infrared studies will be discussed. The next stage consists of investigation of the chemical state of rhodium and sodium. X-ray photoelectron spectroscopy is used to find chemical state of various elements in these catalysts. Temperature programmed desorption and temperature programmed reduction results will be elaborated to give an insight into the reducibility of these systems. Lastly the silanization of these surface and its relevance to the stability of adsorbed carbonyl species is discussed.

7.1 Hydrogen Chemisorption

The dispersion of rhodium was measured using hydrogen chemisorption on fresh and used catalysts. The hydrogen chemisorption was done in a static mode and the results of hydrogen chemisorption are summarized in table 7.1. CO chemisorption was not used because of lack of unique stoichiometric coefficient.

The total and the reversibly adsorbed hydrogen was measured after the reduction of the catalysts. The irreversibly adsorbed hydrogen was then calculated. The total hydrogen adsorbed was found by volumetric titration on the reduced catalysts. The catalysts was then evacuated for 1/2 hour to remove all the reversibly adsorbed hydrogen. The reversibly adsorbed hydrogen was then measured by volumetric titrations. The increment in the total hydrogen adsorbed and the reversible hydrogen adsorbed was then measured at higher pressures. Figure 7.1 shows the amount of total and reversibly adsorbed hydrogen on 3%Rh 0.67%Na/Al_2O_3 .

Table 7.1: Amount of hydrogen chemisorbed on Rh-Na/Al_2O_3 catalysts

Catalysts	Treatment	Irreversible Hydrogen μmoles/gm	Reversible Hydrogen μmoles/gm
3%Rh/Al_2O_3	fresh	93.1	57.5
3%Rh/Al_2O_3	used	26.8	14.5
3%Rh 0.67%Na/Al_2O_3	used	23.6	14.2
3%Rh 2%Na/Al_2O_3	fresh	46.0	44.9

The hydrogen chemisorption results shows a decrease in the amount of both the reversible and the irreversible hydrogen chemisorption on sodium addition. For example, the amount chemisorbed on 3%Rh 2%Na/Al_2O_3 is approximately half the amount chemisorbed on 3%Rh/Al_2O_3 . This decrease in the hydrogen chemisorption can be caused by (a) increase in particles size (b) blocking of the rhodium surface and (c) change in the oxidation state of rhodium caused by the addition of sodium. The next sections on x-ray diffraction, infrared

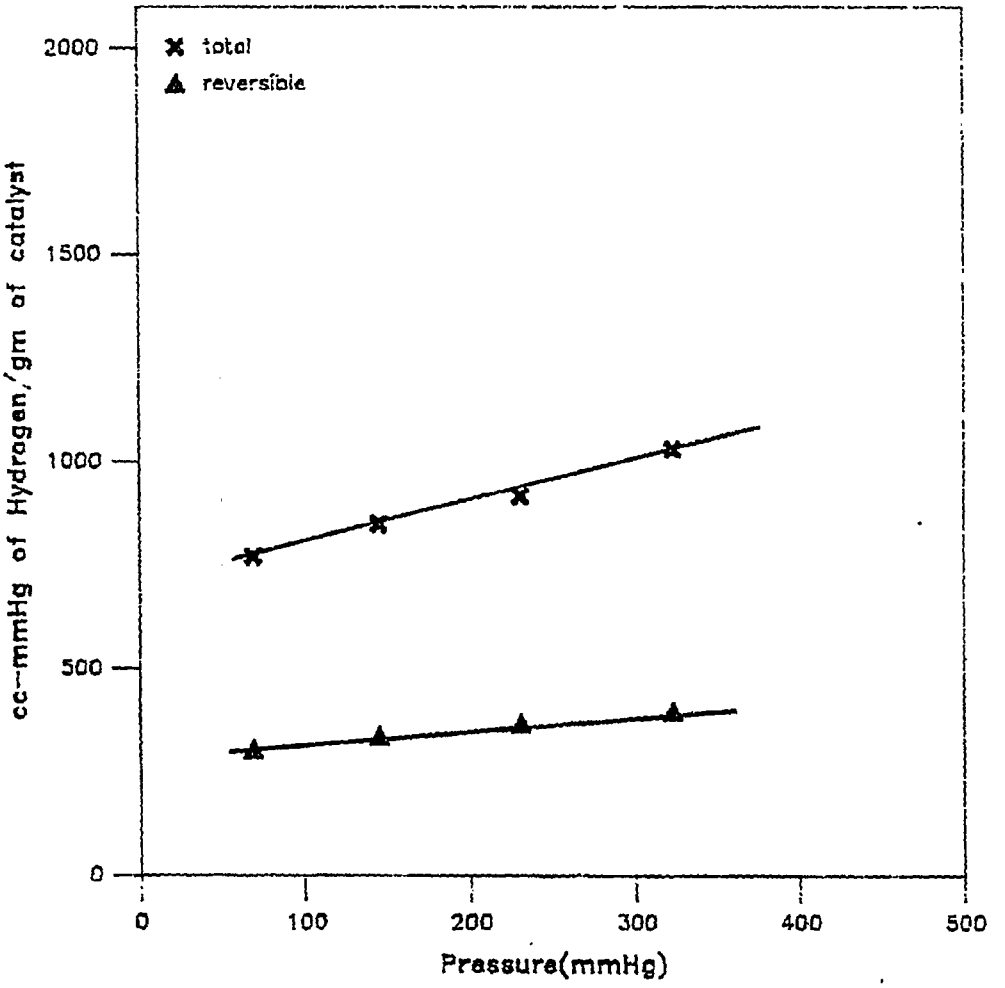

Figure 7.1: Amount of reversible and irreversible hydrogen on 3% Rh 0.67% Na Al_2O_3 catalysts

spectroscopy and x-ray photoelectron spectroscopy show that scheme (a) and (c) are not consistent with the experimental results.

Also, a large decrease in the irreversibly adsorbed hydrogen is observed on used catalysts. This is due to deposited carbon on the surface. Sintering can be ruled out because XRD showed that there was no concomitant increase in particle size of used catalysts. These results agree qualitatively with Blackmond et al.[1].

7.2 X-Ray Diffraction

Different phases of mixed oxide, transition metals, and transition metal oxide phases are investigated in finger printing mode. Whenever a phase is detected, its average crystallite size is calculated from the line broadening of the predominant crystallite reflection. The theory of calculation of average crystallite given elsewhere[2,3].

Table 7.2 shows the expected d values and the two-theta values of various phases of interest for a Cu K_α x-ray source[4]. These phases include sodium rhodate, sodium oxide, sodium carbonate, rhodium, rhodium oxide, aluminum rhodate and γ-Al_2O_3 for a copper K_α x-ray source. Figure 7.2 shows the x-ray diffraction pattern of 3%Rh 2%Na/Al_2O_3 catalysts which were calcined, reduced and use in a reactor. Typically, carbon monoxide hydrogenation was done on a used catalysts for 24-48 hours. In the same figure a x-ray diffraction pattern of 3%Rh 1.14%K/Al_2O_3 used catalysts is also plotted. The diffraction pattern does not show any detectable signal corresponding to rhodium oxide, rhodium, sodium oxide, sodium rhodate or aluminum rhodate phases. The absence of any peak implies that the particle size of any of the above phases is less than 30Å.

Figure 7.3 shows the difference in the x-ray diffraction pattern of the same catalyst which is subjected to a oxidation/reduction cycle. The drastic changes

in the reactivity of the catalyst on air treatment was elaborated in chapter 5. Comparison of these two spectra clearly show a peak at two-theta of approximate 41 degrees from the rhodium crystallite (111) reflection. The metal crystallite is not completely oxidized on exposure to air. This implies that there is a passivation of the catalysts.

Recall from chapter 6, that the air treatment of used catalysts gave a much higher selectivity to hydrocarbons. The XRD pattern of this catalysts before and after the air treatment shown in figure 7.3 clearly shows that the rhodium particles have agglomerated. The presence of a detectable Rh XRD pattern after the air treatment confirms this hypothesis. X-ray line broadening calculations give an average particle size of 120Å. These results are consistent with Arakawa et al.[5] on Rh/SiO_2 , where they observed that the selectivity to hydrocarbons increased with increase in particle size.

7.3 Infrared Spectroscopy

Infrared spectroscopy is a very valuable tool for determining the local environment around an atom in an oscillator. A series of low pressure IR experiments were done to investigate the effect on sodium modified Rh/Al_2O_3 catalysts of following parameters:

(i) the adsorptive behavior of used catalysts as compared to adsorptive behavior of fresh catalysts

(ii) the temperature stability of the different adsorbed carbonyl species on the surface of the catalysts and

(iii) the stability of these species as a function of partial pressure of CO.

Table 7.2: X-ray diffraction pattern of various phases of interest for Rh-Na/Al_2O_3 system

Phase	d Å	2θ
γ-Al_2O_3	2.663	33.65
	2.421	37.13
	2.294	39.27
	1.5213	60.87
	1.4335	65.06
$NaRhO_2$	5.67	15.63
	2.62	34.22
	2.50	35.92
Rh	2.20	41.03
	1.90	47.88
	1.15	84.19
Rh_2O_3	2.57	34.91
	2.73	32.81
	3.68	24.18
Na_2O	1.97	46.07
	2.78	32.19

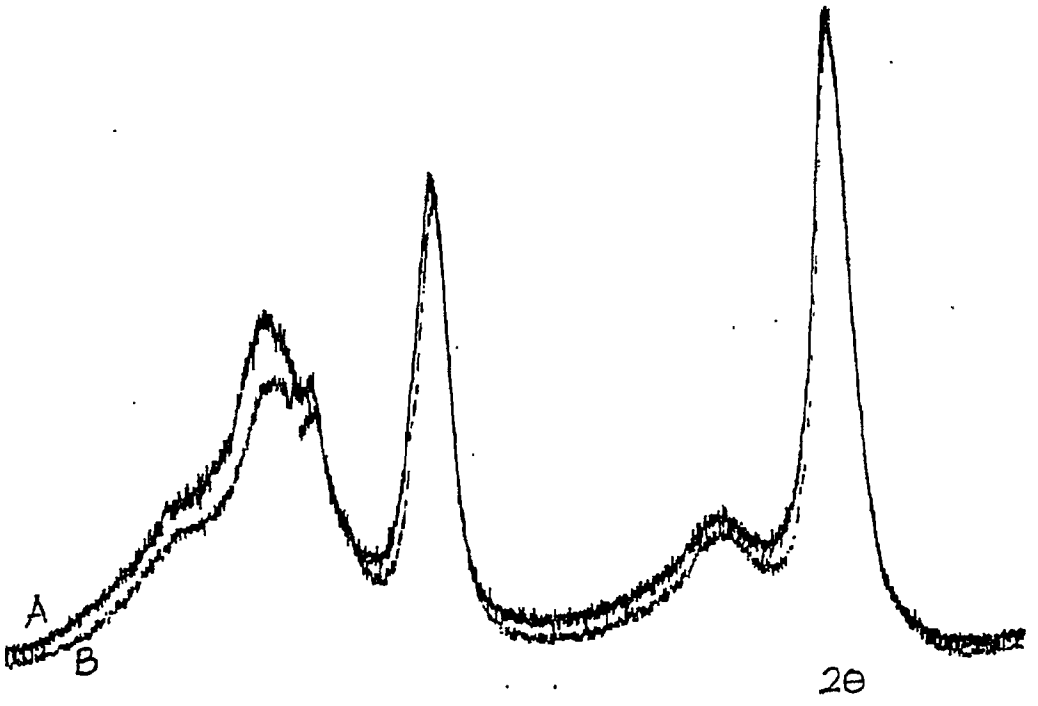

Figure 7.2: X-ray diffraction pattern of used (A) 3%Rh 2%Na Al_2O_3 catalysts and (B) 3%Rh 1.14%K/Al_2O_3 catalysts.

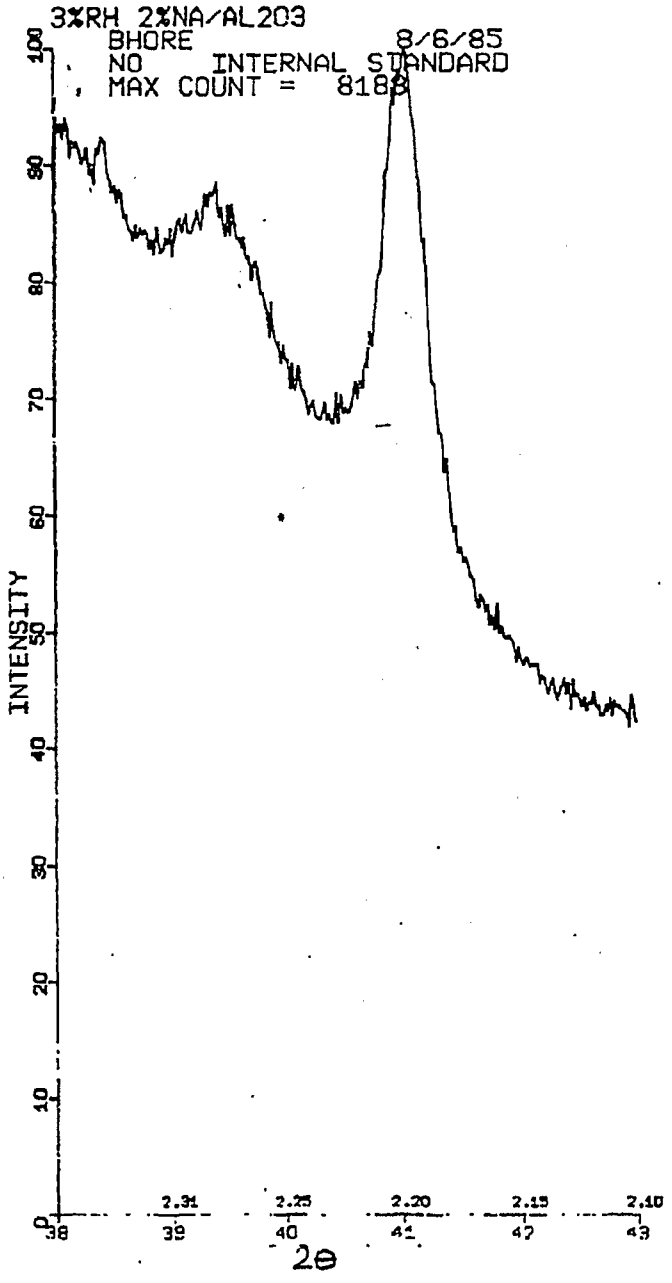

Figure 7.3: X-ray diffraction pattern of reduced-oxidized-rereduced 3% Rh 2% Na · Al_2O catalysts

No shifts in the frequency of linear and gem-dicarbonyl species were observed on fresh sodium containing catalysts.

7.3.1 Stability of Adsorbed CO Species

Figure 7.4 shows the IR spectra of CO adsorbed on 3%Rh/Al_2O_3 and 3%Rh 2%Na/Al_2O_3 at 30C after hydrogen reduction at 400C. Two sets of spectra are shown for each sample, one just after outgassing and the second one after 10 minutes outgassing. Figure 7.3-A shows the IR spectra of CO adsorbed on 3%Rh/Al_2O_3 just after evacuation at 30C. The predominant species is the linear species. but a clear shoulder is seen at the gem-dicarbonyl positions. In contrast, no clear shoulder is seen for 3%Rh 2%Na/Al_2O_3 in figure 7.4-C. On outgassing the sample for 10 minutes, a substantial portion of the linear species disappears and the gem-dicarbonyl species appears as shown in figure 7.4-B. In contrast, the band corresponding to gem-dicarbonyl species is very weak on similar treatment on 3%Rh 2%Na/Al_2O_3 . At 50C, the formation of gem-dicarbonyl species is accelerated. This is seen in spectra in figure 7.5. At 50C, after a similar treatment the IR spectra shows only gem-dicarbonyl bands on 3%Rh/Al_2O_3 and a strong gem-dicarbonyl band on 3%Rh 2%Na/Al_2O_3 . Thus the stability of the linear and bridged species at 30C and 50C varies as 3%Rh 2%Na/Al_2O_3 >3%Rh 0.67%Na/Al_2O_3 >3%Rh/Al_2O_3 and the ease of formation of gem-dicarbonyl species varies as 3%Rh 2%Na/Al_2O_3 <3%Rh 0.67%Na/Al_2O_3 <3%Rh/Al_2O_3 .

7.3.2 Effect of Temperature

Figure 7.6 shows effect of temperature on the adsorbed CO species on 3%Rh 2%Na/Al_2O_3 . The IR spectra at 30C shows the presence of linearly adsorbed species. With increase in temperature to 50C substantial portion of the linearly adsorbed species is converted to gem-dicarbonyl species and at 100C almost all

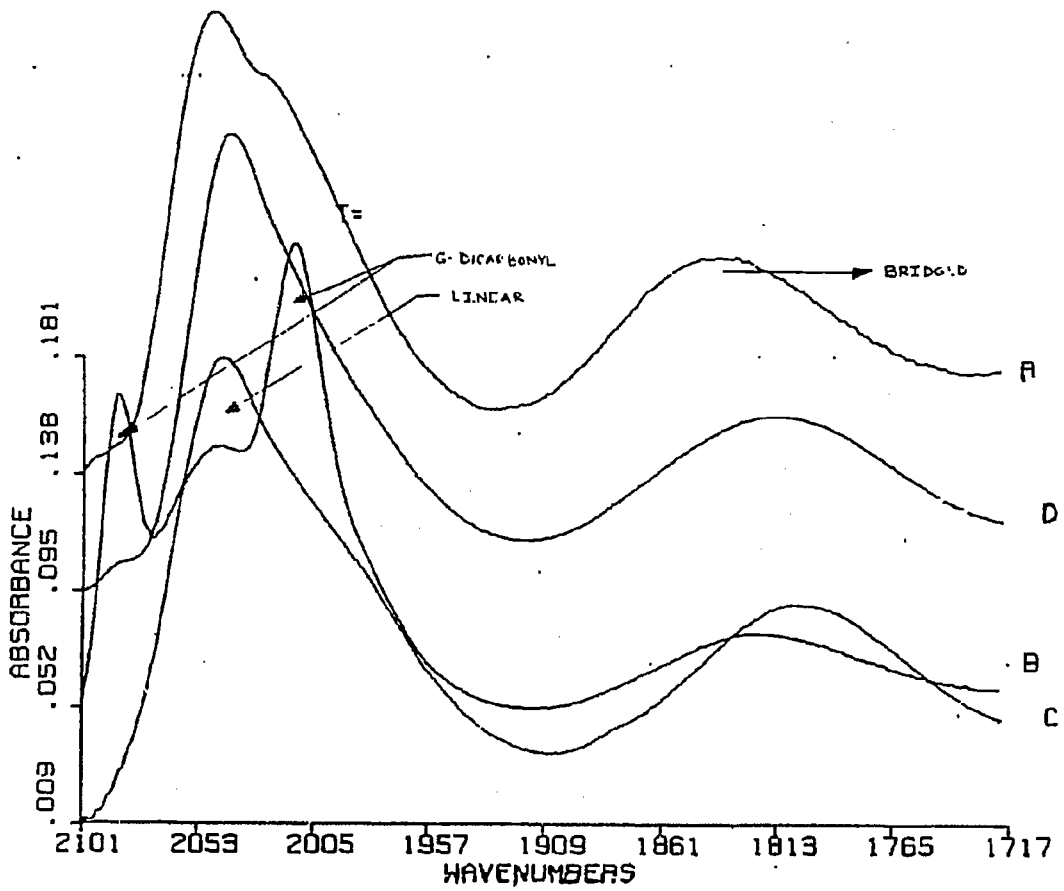

Figure 7.4: IR spectra of adsorbed CO at 30C on (A) 3% Rh Al_2O_3 after outgassing, (B) 3%Rh/Al_2O_3 10 minutes after outgassing, (C) 3% Rh 2%Na/Al_2O_3 after outgassing and (D) 3% Rh 2% Na Al_2O_3 10 minutes after outgassing

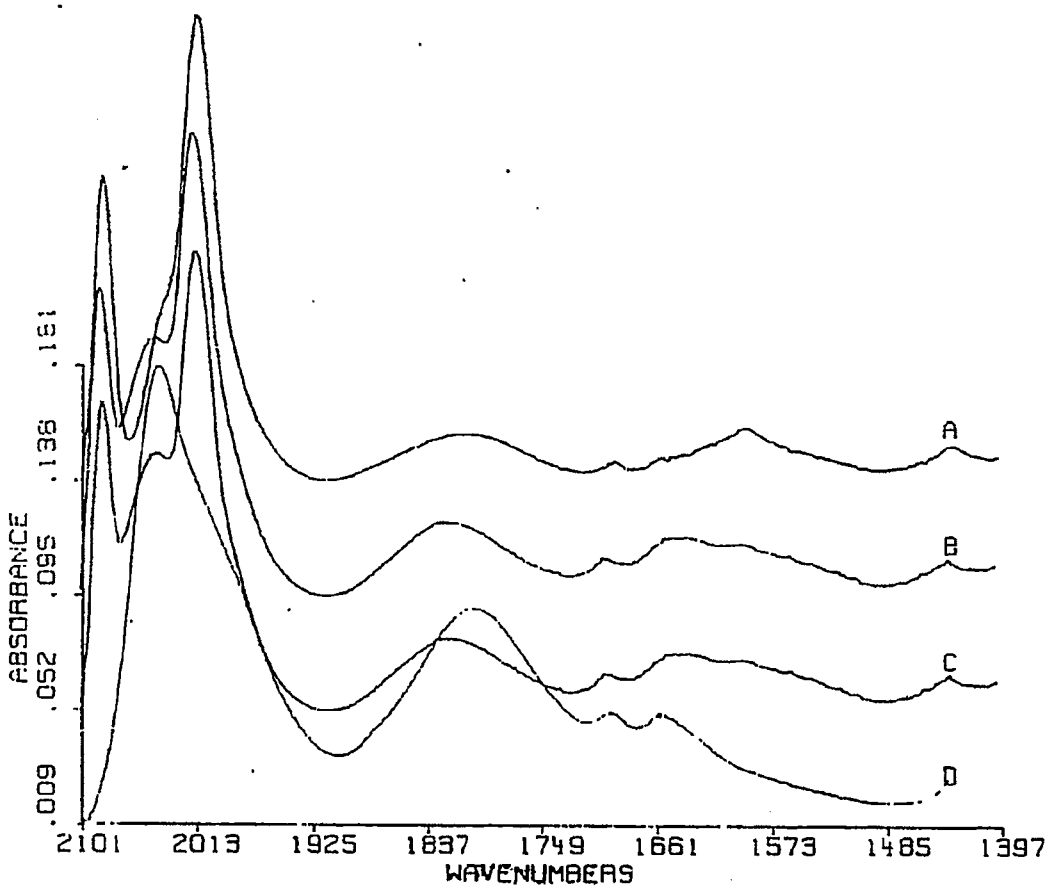

Figure 7.5: IR spectra of adsorbed CO at 50C on (A) 3%Rh. Al_2O_3 after outgassing. (B) 3%Rh Al_2O_3 10 minutes after outgassing. (C) 3%Rh 2%Na Al_2O_3 after outgassing and (D) 3%Rh 2%Na. Al_2O_3 10 minutes after outgassing

the carbonyl species is in gem-dicarbonyl form. This is consistent with other investigations on similar systems[6-8].

7.3.3 Effect of Reaction

A summary of the stability of used and fresh catalysts is given in table 7.3.

In sodium modified system at 30C, the linear species is much more stable than on the Rh/Al_2O_3 catalysts at a pressure of CO of about 0.001torr. Unlike the the linear species on Rh/Al_2O_3 catalysts, the linear species is stable at 50C for the $Rh/Na/Al_2O_3$ catalysts. Two other bands at 1699cm^{-1} and 1656cm^{-1} associated with the formate species appear on sodium addition.

7.4 X-Ray Photoelectron Spectroscopy

The XPS investigation was carried out to investigate the chemical state of rhodium after various treatments on the catalysts. These treatments included, reduction, carbon monoxide adsorption and carbon monoxide hydrogenation reactions. The effect of the amount of sodium added on the chemical state of rhodium is also investigated. Using the peak areas of the various elements, the physical state, i.e., the state of aggregation of various components, is probed. Finally, XPS is used to elaborate silanization reaction on sodium modified rhodium/alumina.

The x-ray photoelectron spectra was collected for Rh(3d), Na(1s), C(1s), O(1s) and Al(2p) regions. Also, for the silanization studies additional data was collected for Si(2p) and N(1s) regions. The intensity of the peaks in the carbon and rhodium region was low inspite of the large number of the scans collected. Hence there is a large error($\pm$0.3eV) in the binding energies of the peaks in the carbon and the rhodium region. The signal/noise in the XPS peak areas is low, and hence quantitative XPS has substantial errors, i.e., noise and drift, up to 30%.

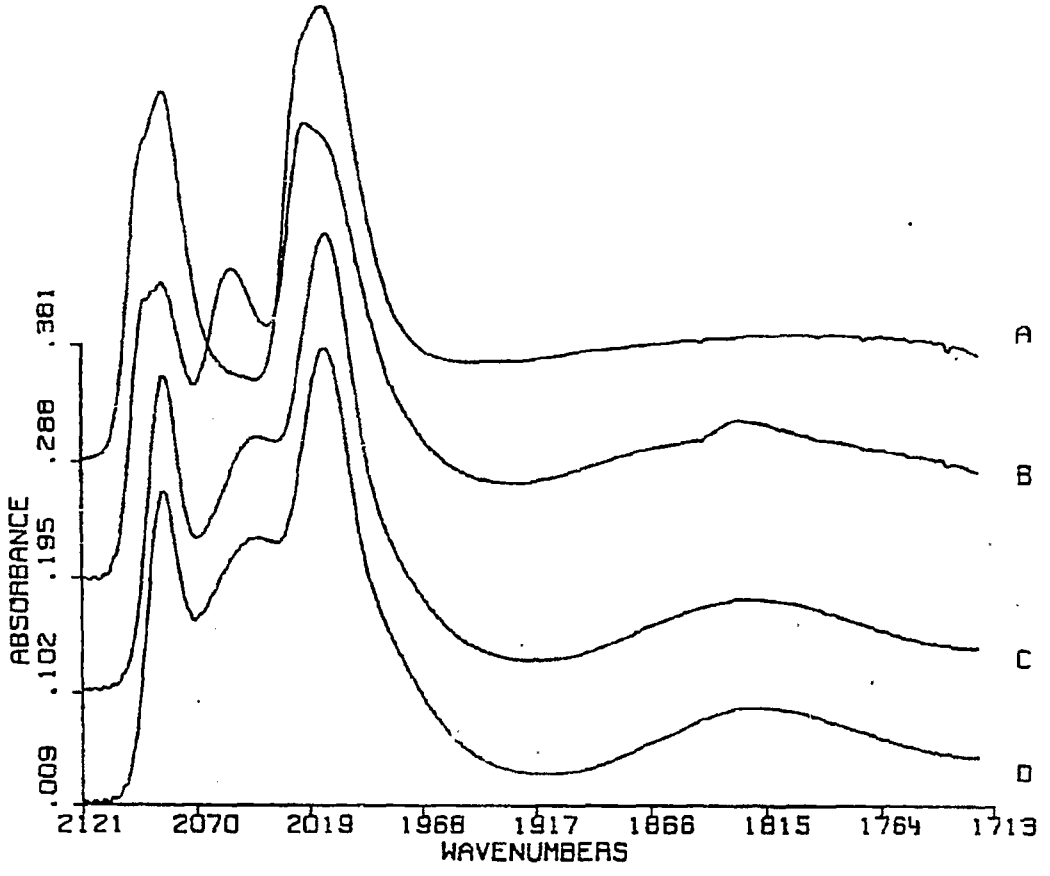

Figure 7.6: IR spectra of adsorbed CO on reduced 3% Rh 2% Na Al_2O_3 at (A) 100C, (B) 75C, (C) 50C and (D) 30C.

Table 7.3: IR results for sodium modified Rh. Al_2O_3

Treat-ment	3%Rh/ Al_2O_3	3%Rh 0.67%Na/ Al_2O_3	3%Rh 2%Na Al_2O_3	2%Na/ Al_2O_3
1	gem-dicarbonyl linear bridged	linear(S) gem-dicarbonyl bridged	linear bridged only	no band in 1750- 2100 cm^{-1}
2	g-dicarbonyl only	g-dicarbonyl(S) linear bridged	linear(S) bridged g-dicarbonyl	
3	linear(S) complete reversibility	g-dicarbonyl linear	linear bridged	

Key to catalysts treatments

1. Catalysts is reduced at 200C for 1/2 hour, and at 400C for 3 hours, then cooled to 400C under hydrogen and dosed with CO at room temperature and the sample is then outgassed.

2. The sample at the end of the above treatment is heated to 150C, and then dosed with CO again and the sample is again outgassed.

3. The sample at the end of the previous treatment is cooled to room temperature under flowing hydrogen.

Because alumina is an insulator, it is charged on photoelectron emission. This charging causes problems with the precise physical and chemical interpretation of the spectra. As explained in Chapter 2, the spectra will be referenced internally with respect to the Al(2p) peak at 74.7eV. All the data reported henceforth is internally referenced. The peak area is measured by using a sloping baseline. Wherever aluminum metal is seen from the sample holder as a shoulder, the peaks are manually deconvoluted and the actual area from the aluminum from the support measured.

7.4.1 Chemical State of Rhodium

Figure 7.7 shows the x-ray photoelectron spectra of Rh(3d) region of 3%Rh 2%Na/Al_2O_3 in calcined and reduced state. It is clear from figure 7.7 that rhodium exists in +3 oxidation state in both calcined catalysts. After reduction both catalysts were reduced to rhodium metal/rhodium(I). This is seen from the shift in rhodium binding energies from 310.3 eV to 307.9eV. Because of a low signal/noise ratio, high charging, surface heterogeneity and the small difference in the binding energies between Rh(0) and Rh(1), these two oxidation states cannot be discriminated from XPS data. However, whether the rhodium is in oxidation state zero or one is inconsequential to this investigation. As mentioned in chapter 2 and as shown in the earlier sections on infrared spectroscopy, the interchange between Rh(0) and Rh(1) depends on the gas phase environment above the catalysts. For example, the presence of carbon monoxide in gas phase converts Rh(0) to Rh(1). Furthermore, passing hydrogen over the catalysts changes Rh(1) back to Rh(0). Thus under reaction conditions, the gem-dicarbonyl species associated with Rh(I) is not present.

The data in table 7.4, show that there is no discernable difference between the oxidation state of rhodium in calcined 3%Rh/Al_2O_3 , 3%Rh 0.67%Na/Al_2O_3 and 3%Rh 2%Na/Al_2O_3 . There is also no change in the chemical state of

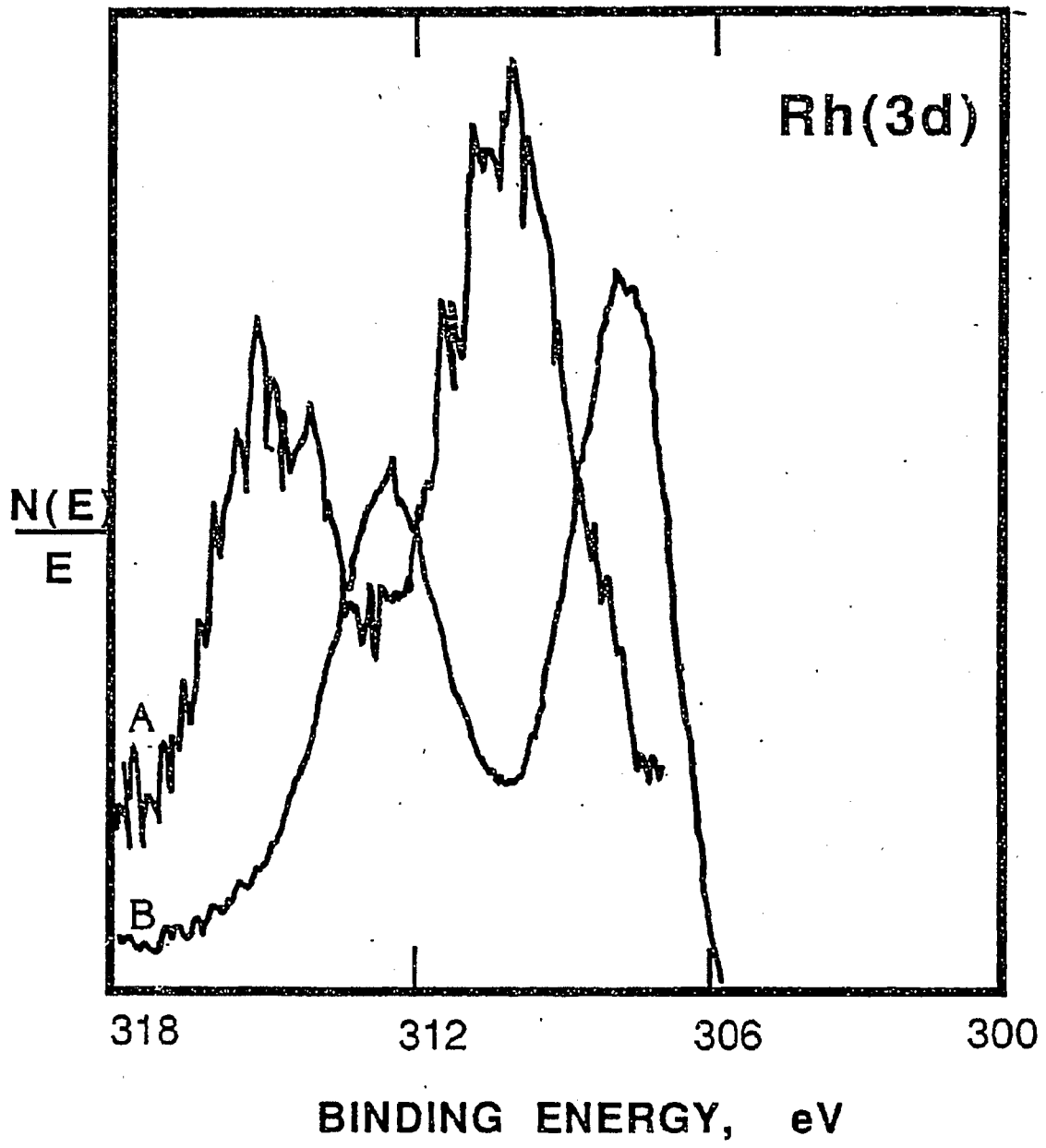

Figure 7.7: X-ray photoelectron spectra of Rh(3d) region of (A) calcined 3%Rh 2%Na/Al_2O_3 and (B) reduced 3%Rh 2%Na/Al_2O_3

rhodium on subsequent treatments such as reaction under carbon monoxide and hydrogen at 200C.

Also. in table 7.4 are the binding energies of catalysts after use in the high pressure reactor. Then the reactor was cooled and the catalysts slowly exposed to air at room temperature. The binding energies of Rh in the used catalysts show that the catalysts were passivated and the entire rhodium metal crystallite was not oxidized.

Shyu et al.[9] have measured binding energy shifts in Ru(3d) photoelectron in Ru-K/SiO_2 catalysts. However in this investigation. because of the low signal/noise ratio, no such shifts were detected.

7.4.2 Chemical State of Sodium

Figure 7.8 shows the XPS spectra for calcined and reduced Na/Al_2O_3 and $Rh\text{-}Na/Al_2O_3$ in the Na(1s) binding energy region. Peak locations are given in table 7.4. The binding energy for Na(1s) photoelectron is 1071.5 ± 0.3 for sodium halides, sodium carbonates and sodium nitrates[11]. However the binding energy for Na(1s) photoelectron is 1072.7 ± 0.2eV. All the binding energies of Na(1s) photoelectron in Na/Al_2O_3 and $Rh\text{-}Na/Al_2O_3$ catalysts at any loading and under any treatment investigated lies between 1072.6 eV and 1072.9 eV in the sodium oxide region. Thus the chemical state of sodium is similar to that of sodium oxide. Also. the chemical state of sodium is not affected by various treatments and by the presence of rhodium. This indicates that in the catalyst. after calcination most of the sodium exists as a surface compound of alumina or as sodium oxide.

Figure 7.8 shows the Na(1s) region of the x-ray photoelectron spectra of 3%Rh 2%Na/Al_2O_3 and 3%Rh 0.67%Na/Al_2O_3 in calcined and reduced state. As seen from this figure, there is no detectable change in the chemical state of

Table 7.4: Effect of addition of sodium on the chemical state of rhodium

Catalysts	Treatment	Rh($3d_{5/2}$) eV	Na(1s) eV
3%Rh/Al_2O_3	calcined	310.5	
	reduced	307.9	
	CO-chemisorbed	308.1	
	reaction	307.8	
	used	307.6	
3%Rh 0.67%Na/Al_2O_3	calcined	310.0	1072.9
	reduced	307.3	1072.7
	reaction	307.3	1072.9
	used	307.2	1072.9
3%Rh 2%Na/Al_2O_3	calcined	310.3	1072.9
	reduced	307.9	1072.7
	used	307.7	1072.7
0.67%Na/Al_2O_3	calcined		1072.9
1.3%Na/Al_2O_3	calcined		1072.8
2%Na/Al_2O_3	calcined		1072.7
2.67%Na/Al_2O_3	calcined		1072.6
3.33%Na/Al_2O_3	calcined		1072.6

sodium and rhodium on changing the amount of sodium and the chemical state of rhodium.

7.4.3 Silanization Studies

It is clear that the number of hydroxyl groups determine the stability of various adsorbed carbon monoxide species on the surface. These hydroxyl groups are believed to play an important role in oxidative addition of a rhodium particle to form a geminal dicarbonyl species. To test this hypothesis. the surface -OH groups were removed by reaction it with silanes. However. it is not clear if all the HMDS is reacted. It is possible that part of the HMDS forms a donor-acceptor bond with the lewis acid site on the surface. Also, in many other studies on surface silanization. part of the HMDS oxidizes on the surface to form silica instead of surface silanes. This can obviously complicates the interpretation of the results, since the stability of the carbon monoxide adsorbed species will change if part of the rhodium crystallite is covered. Hence a XPS investigation was undertaken to investigate the reactivity of HMDS by monitoring the N(1s) peaks and the silica formation by following the binding energy of Si(2p) peak.

Table 7.5 on page 260 shows a summary of the silanized surfaces. First of all there is no detectable nitrogen in the sample. Using approximate atomic sensitivity factors, and reasonable area detectability limit, the limit of HMDS present is less than 5% of all the silane added. Typical silicon areas for x-ray photoelectron spectroscopy of silylated areas is approximately 300 counts. The minimum detectable limit of a peak with a fwhh of around 2eV is 15 counts. Since same number of cycles were used for nitrogen(1s) and silicon(2p) scans, the maximum amount of silicon as silica can be found from the atomic sensitivity factor. This gives us the maximum amount of undetected silicon as 15 counts. Thus there is less than 5% of the initial HMDS remains either as HMDS or gets converted to silica; most of the HMDS reacts to form surface silane and ammonia.

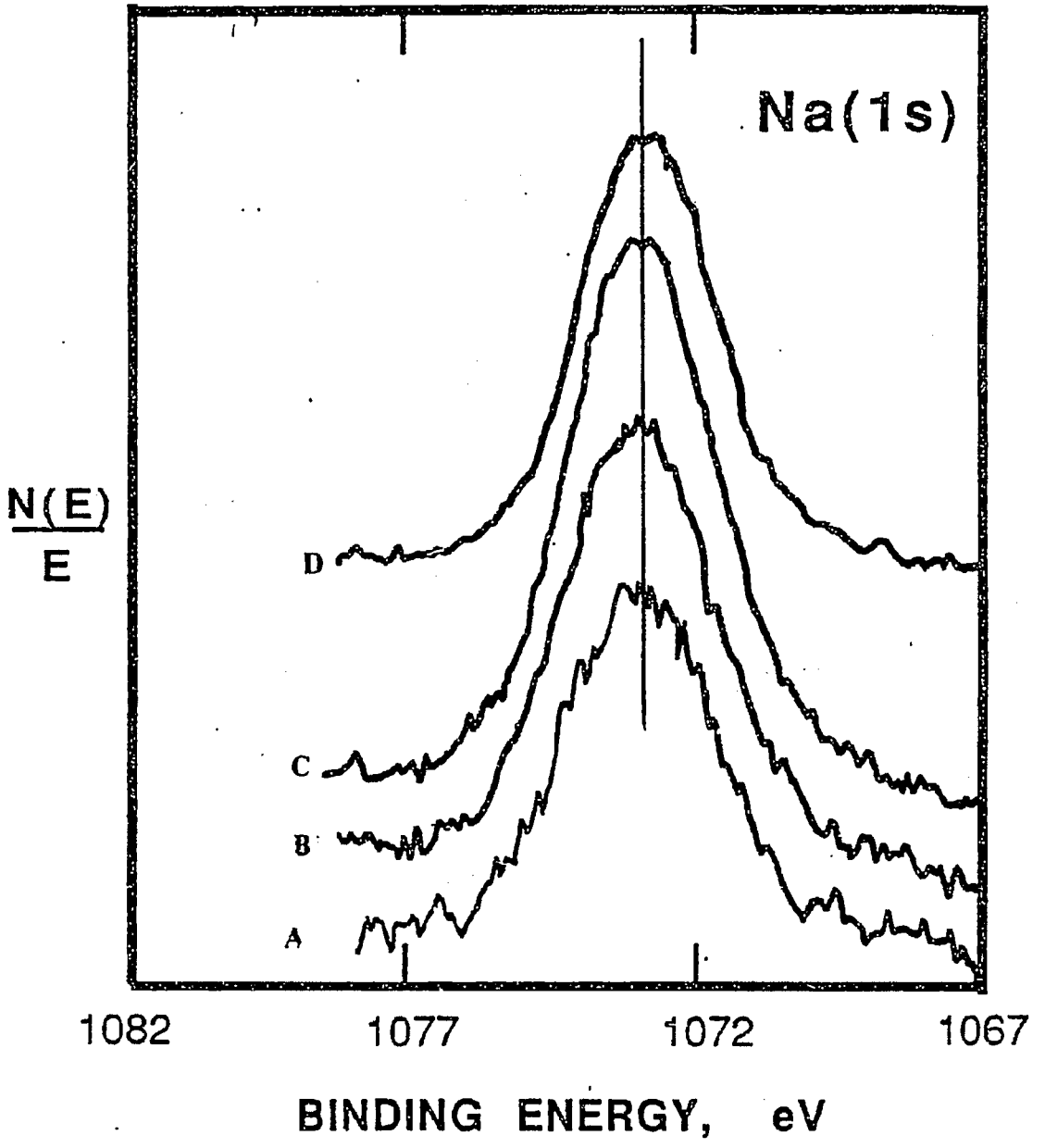

Figure 7.8: X-ray photoelectron spectra of Na(1s) region of calcined (A) 3%Rh 0.67%Na/Al_2O_3 . (B)0.67%Na/Al_2O_3 . (C) 3%Rh 2%Na/Al_2O_3 and (D) 2%Na/Al_2O_3

This proves that the disilazane reacts completely with the surface OH groups The reaction given below was previously investigated by Zaki et al.[10]

$$(CH_3)_3SiNHSi(CH_3)_3 + 2\ Al-OH(s) \longrightarrow 2\ Al-O-Si(CH_3)_3(s) - NH_3$$

As shown in figure 7.9, the binding energy of silicon in both the silanized-Al_2O_3 and silanized-2%Na/Al_2O_3 samples was 101.1eV. This binding energy is close to the binding energy of silicon in HMDS (101.4eV) and in $Me_3SiOSiMe_3$ (101.6eV). The binding energy of silicon in silica is 103.4eV, which is too far away from the observed binding energy of silicon. Thus, silanization of the surfaces produces quantitative conversion of disilazanes and these silanes are stable. They do not form silica. Figure 7.10 shows the C(1s) region of the x-ray photoelectron spectra of silanized Al_2O_3 and Na/Al_2O_3 samples. Unlike the other samples, here the carbon signal is intense. This is due to the carbon atoms in the methyl groups sitting on the top of the silanized surface.

7.4.4 Photoelectronic Responses

The physical state of sodium and rhodium is investigated using the photoelectronic response. The photoelectronic response of an element is defined as the ratio of the area of that element to the area of a standard element. Since the area of the catalysts is large and the photoelectronic mean free path is of the order of 10Å, the signal is obtained from a large number of aluminum atoms. Thus aluminum form a convenient element to form the basis. Oxygen cannot be used as a reference element because some of the modifiers are in the oxidic form. The carbon signal is too weak to be used as a standard. Since the rhodium signal obtained from XPS is very weak and the information of the physical state of rhodium can

Table 7.5: Binding energies of silanized surfaces

Catalysts	N(1s)	$Si(2p_{3/2})$	O(1s)	C(1s)	Ref.
silanized-Al_2O_3	no peaks	100.1	531.8	284.6	this work
silanized-2%Na/Al_2O_3	no peaks	100.1	531.6	285.2	this work
Silicon		98.7			[11]
Silica		103.4			[11]
$Me_3SiOSiMe_3$		101.6			[11]
$Me_3SiNHSiMe_3$		101.4			[11]

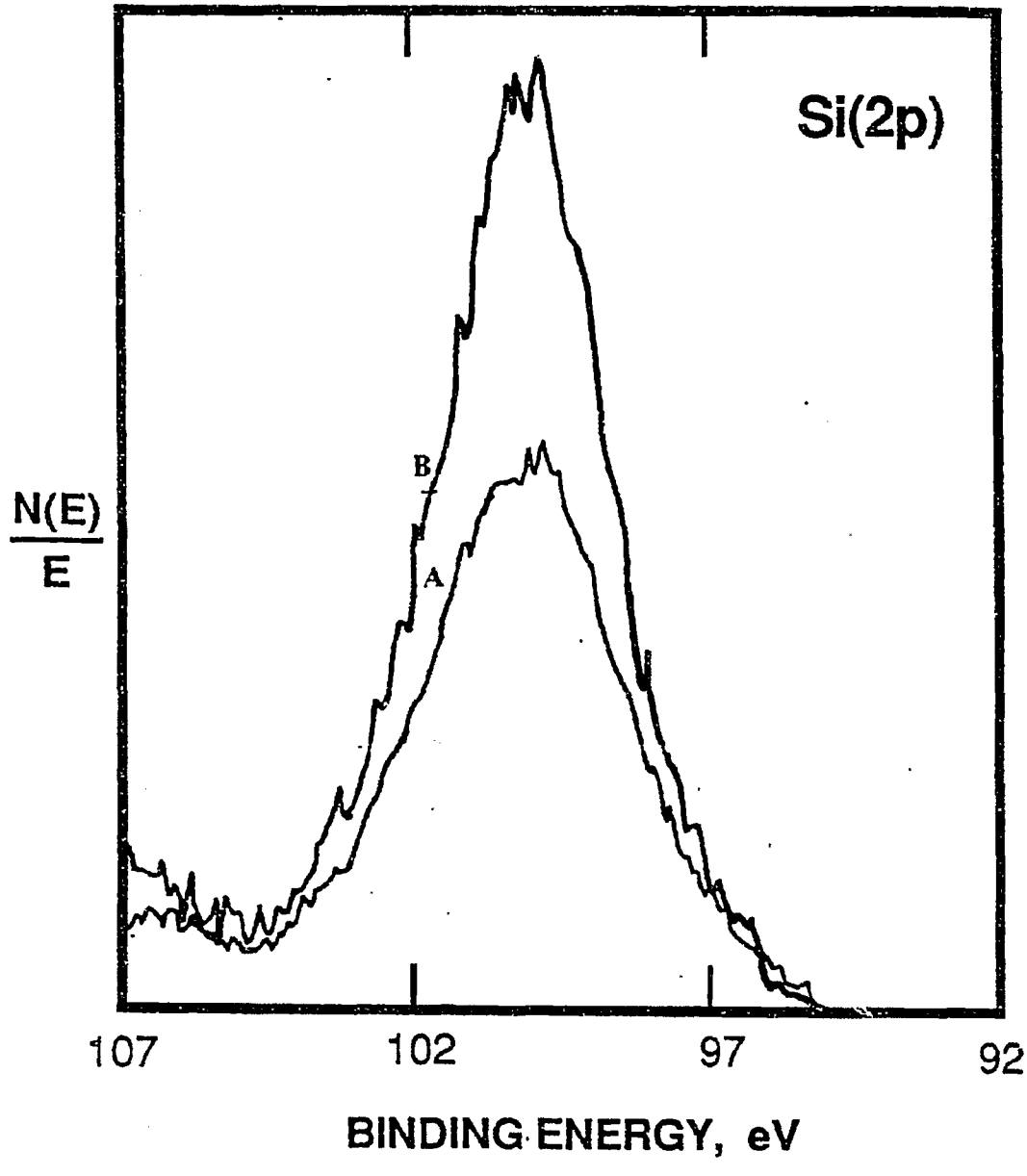

Figure 7.9: X-ray photoelectron spectra of Si(2p) region of (A) silanized-Al_2O_3 and (B) silanized 2%Na/Al_2O_3

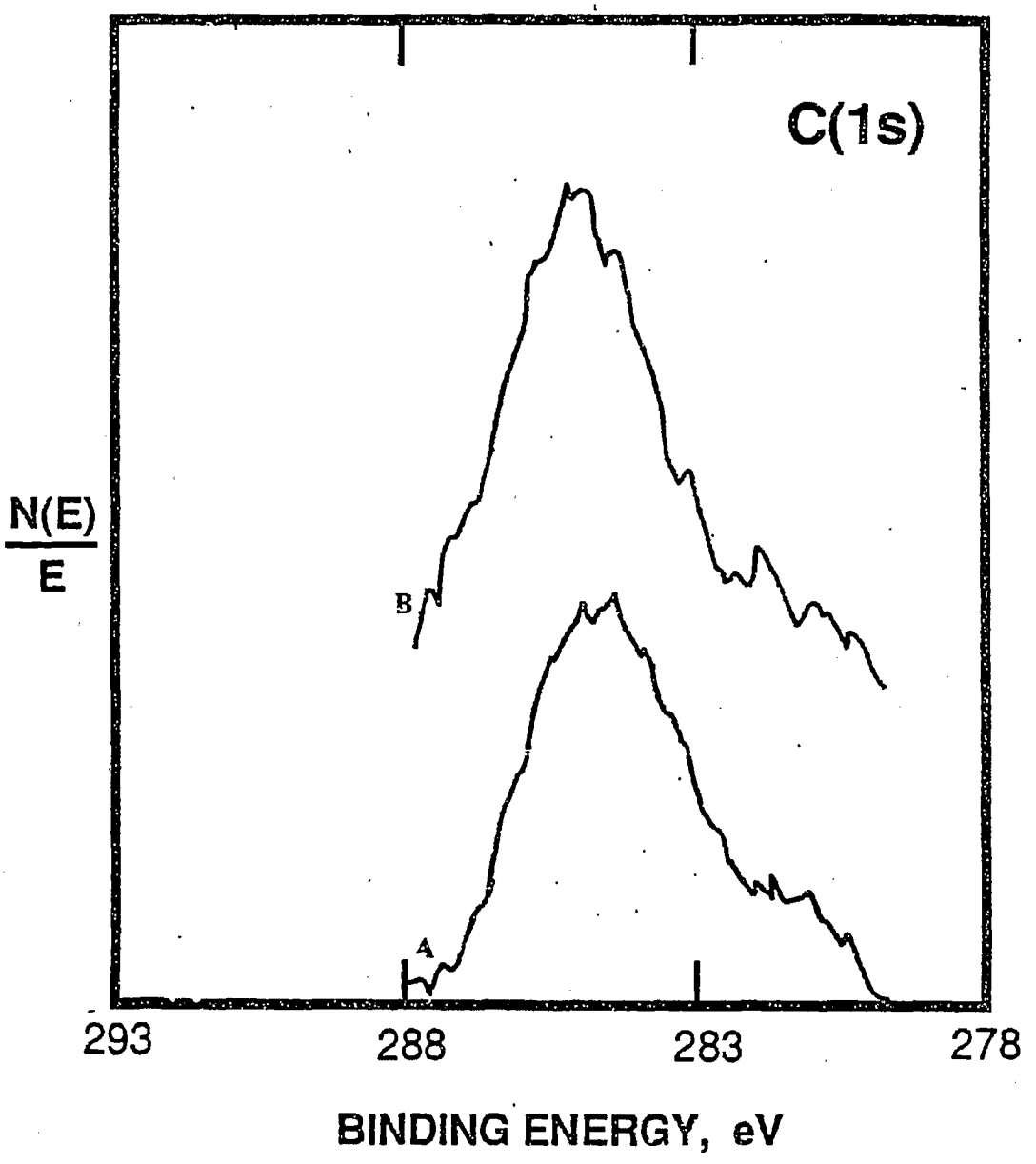

Figure 7.10: X-ray photoelectron spectra of C(1s) region of (A) silanized Al_2O_3 and (B) silanized 2%Na/Al_2O_3

be easily obtained by other methods, the photoelectronic response of rhodium is not used.

The physical state of sodium can be conveniently investigated using the sodium photoelectronic response. Table 7.6 on page 264 shows the sodium photoelectronic responses of the Na/Al_2O_3 and $Rh\text{-}Na/Al_2O_3$ samples. Figure 7.11 shows the sodium photoelectronic response plotted against the weight percent sodium added. This plot is linear. The linearity of the plot indicates that the physical state of sodium or the state of aggregation of sodium is same at the different loading of sodium investigated. The open symbols in the figure 7.11 show the photoelectronic response for $Rh\text{-}Na/Al_2O_3$ catalysts. For a given sodium loading, the Na(1s) photoelectronic response of Na/Al_2O_3 and $Rh\text{-}Na/Al_2O_3$ is same. This implies that the state of aggregation of sodium is same in Na/Al_2O_3 and $Rh\text{-}Na/Al_2O_3$. Thus the physical state of sodium is not affect by the presence of rhodium. Also there is no evidence of aggregation of sodium oxide on these catalysts. Because the photoelectronic response of sodium is not affected by the presence of rhodium, substantial portion of sodium is not being blocked by rhodium crystallites. This is consistent with the results reported by Wilson et al.[12], where they reported that most of sodium sits on the alumina surface.

According to Ratnaswamy and Knozinger[13] the number of surface hydroxyl groups on a $\gamma\text{-}Al_2O_3$ support which is not dehydroxylated is greater than $5 \times 10^{14}/cm^2$. For a typical density and surface area of alumina, this number translates to 10^{21} OH groups/gm of support. For a 3.3 wt. % loading of sodium, there are around 9×10^{20} sodium atoms. Thus the number of sodium atoms is less than the number of OH groups.

Table 7.6: Photoelectronic responses of Na/Al_2O_3 and $Rh\text{-}Na/Al_2O_3$ catalysts

Catalysts	I_{Na}/I_{Al}	I_O/I_{Al}
$0.67\%Na/Al_2O_3$	0.58	7.60
$1.3\%Na/Al_2O_3$	0.77	6.98
$2\%Na/Al_2O_3$	1.40	8.10
$2.67\%Na/Al_2O_3$	1.94	6.51
$3.33\%Na/Al_2O_3$	2.34	7.07
$3\%Rh\ 0.67\%Na/Al_2O_3$	0.69	
$3\%Rh\ 2\%Na/Al_2O_3$	1.56	

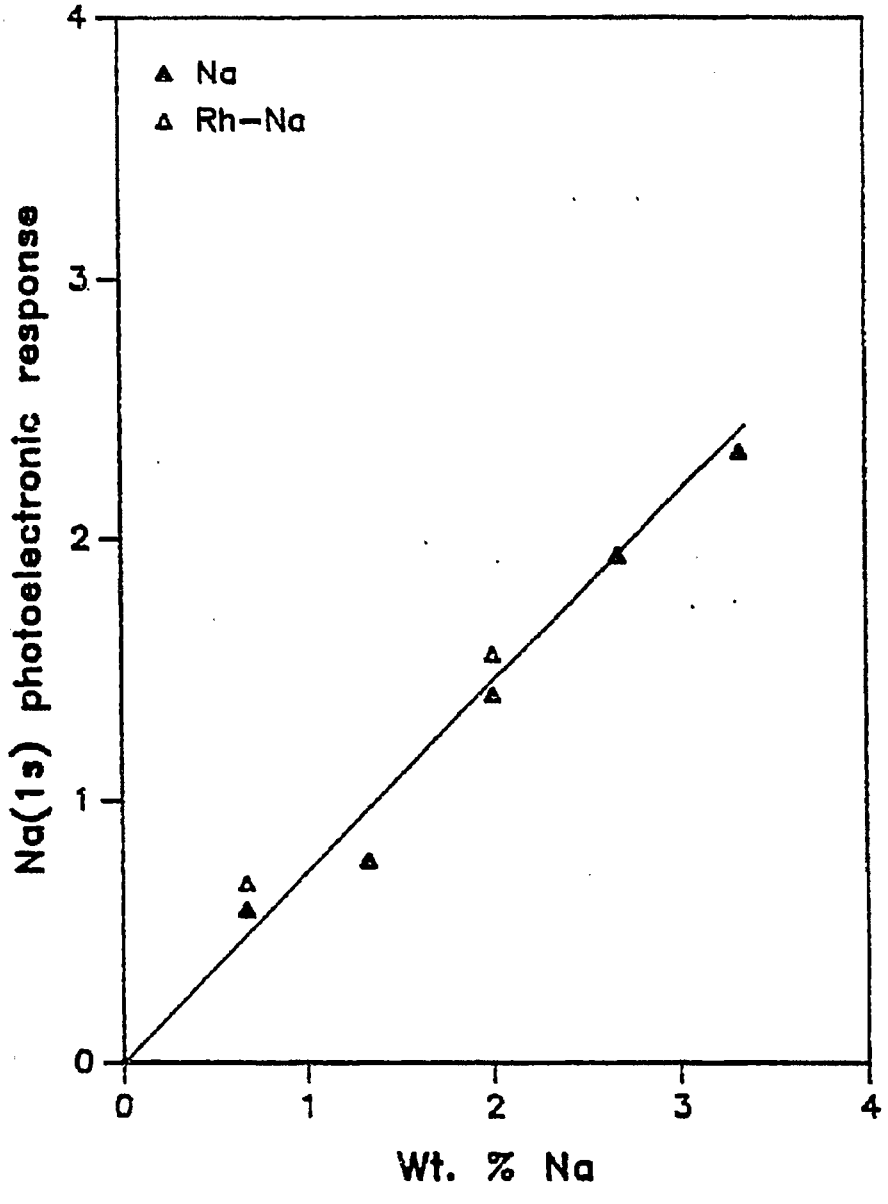

Figure 7.11: Photoelectronic response of calcined Na, Al_2O_3 samples

7.5 Temperature Programmed Methods

The reducibility of rhodium, the adsorption states of hydrogen, and the effect of sintering was investigated on various sodium modified rhodium, alumina catalysts by temperature programmed reduction(TPR) and temperature programmed desorption(TPD) The TPR/TPD data was collected by Dr. S.B. Ziemecki of the Central Research Department at the duPont Experimental Station.

7.5.1 Effect of Sodium on the Reducibility of Rhodium

The rhodium is well dispersed in all cases, as manifested by the diffuse appearance of the TPR profiles. Figure 7.12 on page 268 shows the TPR spectra of Rh-Na/Al_2O_3 catalysts at different sodium loadings. These catalysts were freshly reduced i.e., this is the TPR spectra of the first cycle of reduction. The peaks for all three samples are very broad because of the heterogeneity of the samples and different extent of reduction of various components on the surface. The lowest temperature peak for 3%Rh/Al_2O_3 is centered around 190C. The high temperature region of the spectra contains contributions from many different states. In contrast with other investigation[14], no attempt was made to deconvolute the peaks due to low signal to noise ratio and non-uniqueness of the fit. Inspite of the low signal to noise ratio the reproducibility of TPR is quite good. The hydrogen consumption for the sodium-free catalysts was 31 mV-min corresponding to 3H/Rh. A repeat run with the same catalyst gave a hydrogen consumption of 32 mV-min. This hydrogen consumption corresponds to rhodium as Rh_2O_3: this is consistent with the XPS experiments where rhodium is found in an oxidation state of -3 in the calcined catalysts.

Figure 7.12 on page 268 shows that as the sodium content is increased a peak at 295C becomes more pronounced. This phase may be sodium rhodate. However x-ray diffraction studies do not show any presence of sodium rhodate.

This apparent inconsistency can be explained because the particle size may be less than 30Å, the minimum detectable limit by x-ray diffraction. The XPS experiments showed that the rhodium is completely reduced to metallic state, while the chemical state of the sodium is not affected by oxidation or reduction treatments. Thus if there is any alloying between sodium oxide and the rhodium-component, it will be in the calcined state. A mixed alloy between an oxide and an metal cannot be expected. Thus alloying has to be checked in the calcined state.

Figure 7.14 on page 270 shows the TPR spectra of 3%Rh 0.67%Na Al_2O_3 with various treatments. The fresh catalysts shows a broad peak starting from 120C and ending at 380C. Within this broad peak is the peak at 295C which increases with the amount of sodium added. After the first oxidation treatment, the catalyst is re-reduced and the TPR spectra was collected. The TPR spectra of the second reduction showed an intense peak shifted to a well-defined maximum at 100C. The peak is nearly symmetrical and has a full width at half height of approximately 70C. However there is no substantial decrease in the peak areas, which implies that the same amount of hydrogen is consumed. When the catalyst was sintered, the intensity of the peak in the TPR spectra decreased substantially as shown in Figure 7.13. The peak shifted to lower temperature and the heterogeneity decreased as manifested by the low full width at half height of 45C. Figure 7.13 shows the effect of oxidation/reduction cycle on 3%Rh/Al_2O_3 . As seen in the figure the TPR spectra of 3%Rh/Al_2O_3 in the first cycle is very broad and diffuse. The TPR spectra of first reduction consists of many convoluted peaks. The peak with the lowest temperature and also with the best defined profile appears at 180C. The second reduction, similar to 3%Rh 0.67%Na/Al_2O_3 shows a well-defined peak centered at 100C. The full width at half height of the second reduction spectra is 80C. The TPR peak areas for 3%Rh 0.67%Na/Al_2O_3 after different catalyst treatment is given in table 7.7.

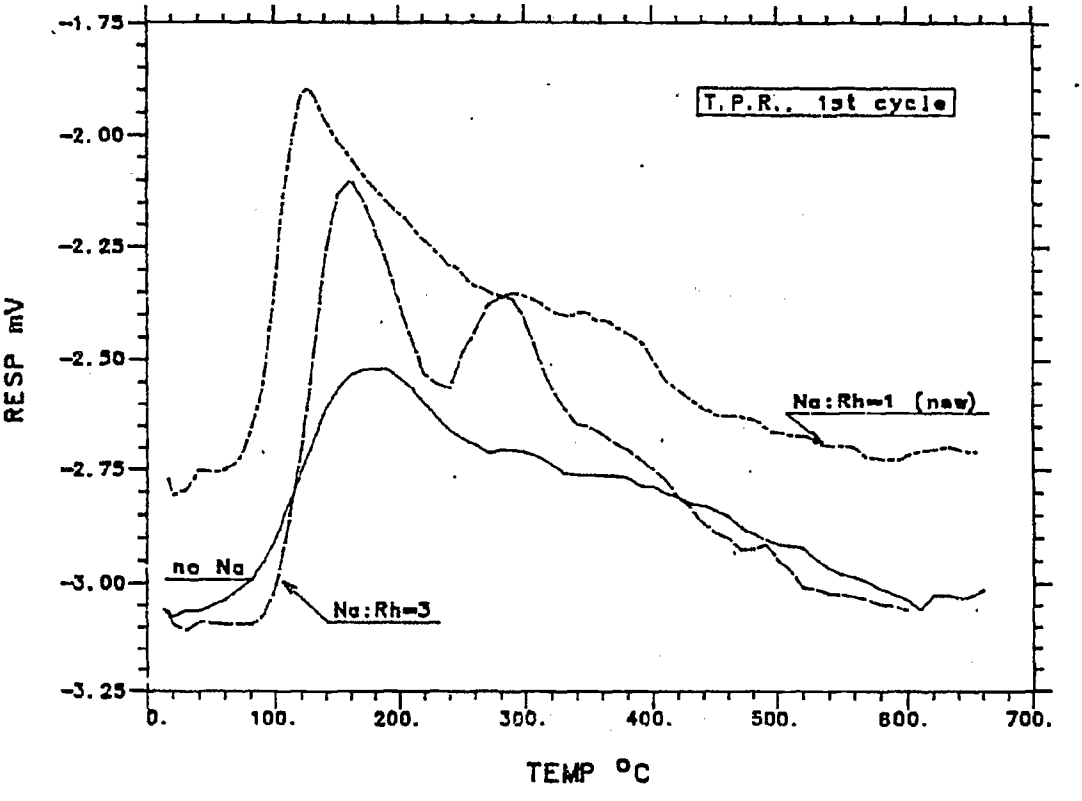

Figure 7.12: Effect of addition of sodium on the TPR of Rh-Na Al_2O_3 catalysts

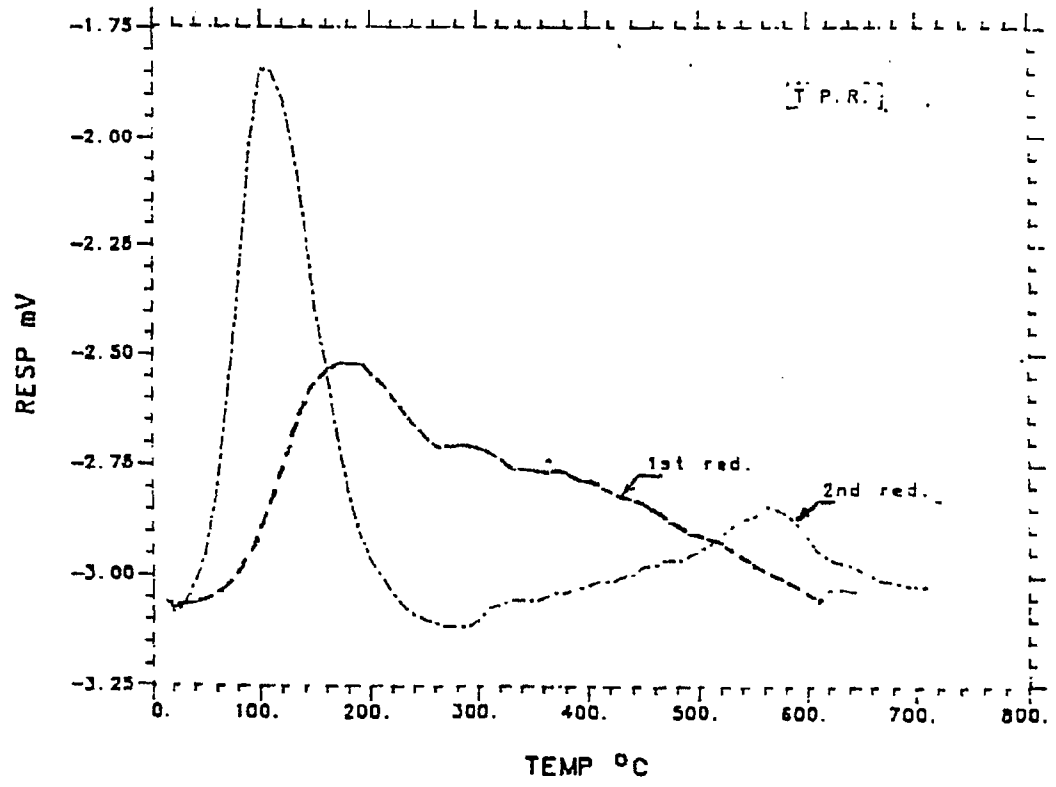

Figure 7.13: Effect of various treatments on the TPR spectra of 3%Rh. Al_2O_3 catalysts

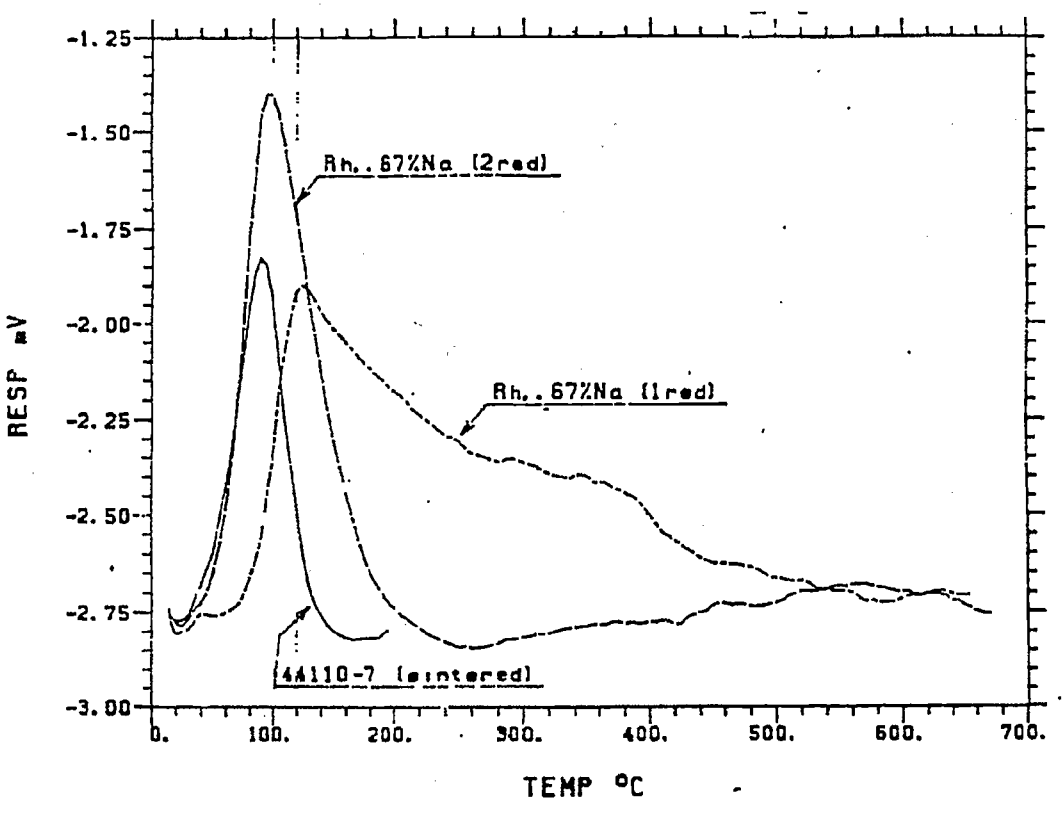

Figure 7.14: Effect of various treatments on the TPR spectra of 3% Rh 0.67% Na /Al_2O_3 catalysts

Table 7.7: Intensities of TPR peaks for 3% Rh 0.67% Na Al_2O_3

Treatment	TPR area in mV-C
First reduction	157.0
Second reduction	101.7
Sintered catalysts	47.6

LeMaitre has listed the possible reasons for shifts in the TPR spectra on adding a second component [15]. They are

i) The second component may form an alloy which reduces at a different temperature

ii) The second component may form the nucleating agent for the reduction of the first component.

iii) The second component may generate activated hydrogen which then more easily reduces the first component

iv) The water formed during the reduction of the second component may act as a nucleating agent for the first component.

Also, there are other possible reasons such as

The second component can cover the support and hence the mobility of the particle is hindered. This is especially true if the particle aggregates during the process of reduction. Also the second component can affect the interface between the metal and the support and hence can change the TPR characteristics.

In the case of Rh-Na/Al_2O_3 the third and fourth reason can be ruled out because the chemical state of sodium is not changed on reduction as observed by

x-ray photoelectron spectroscopy. At this stage, the remaining modes cannot be differentiated based on the experimental data.

7.5.2 Effect of Sodium on Hydrogen Adsorption in Rh-Na/Al_2O_3

The temperature programmed desorption spectra were collected on these samples to investigate the nature of adsorption of hydrogen and to elucidate the possible role of sodium in these catalysts. Figure 7.15 on page 273 shows the TPD spectra of samples containing various amounts of sodium in Rh-Na/Al_2O_3 catalysts. The TPD spectra is broad and diffuse for the samples investigated. The peak positions do not shift on sodium addition.

7.6 Discussions

7.6.1 Reactivity

The role of alkali modifier on supported rhodium catalysts is not clear. The kinetic results shown in chapter 6 indicate that the rate of CO hydrogenation decreases substantially with addition of sodium. The decrease in conversion follows a typical semi-log plot indicating the poisoning of sites.

The selectivity to oxygenates on supported Rh catalysts is a function of the catalysts, temperature, partial pressure of CO and hydrogen and the conversion. Hence the two catalysts have to compared at the same conversion. The catalysts can be compared on a selectivity-conversion plot shown in chapter 5 and 6. Thus even though there is a substantial decrease in the rate of CO hydrogenation there are minor changes in the selectivity to oxygenates. The selectivity versus conversion plots for Rh-Na/Al_2O_3 is similar to the selectivity-conversion plots for Rh/Al_2O_3 . Thus the overall rate of CO hydrogenation decreases, the rate of hydrocarbon formation and the rate of oxygenate formation both decrease.

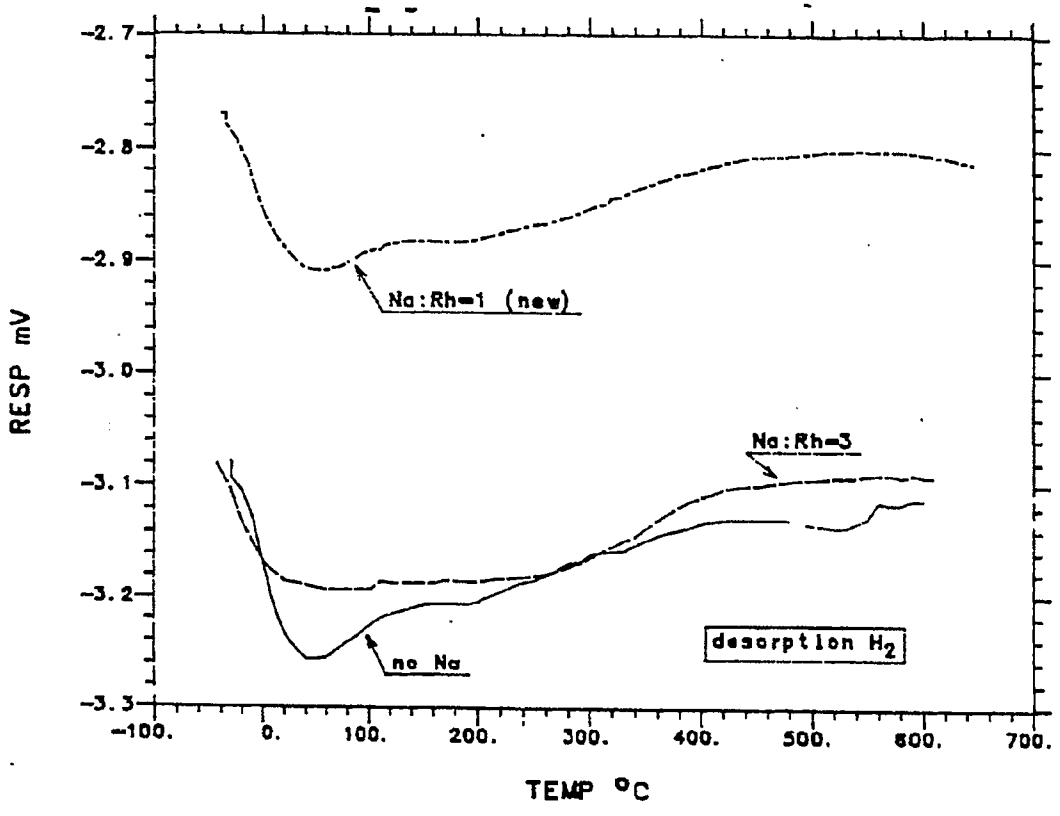

Figure 7.15: Effect of addition of sodium on the hydrogen TPD of Rh-Na/Al_2O_3 catalysts

However, the decrease in the rate of formation of hydrocarbon is much more than the decrease in the rate of formation of oxygenates. These results agree with those reported by McLaughin and Gonzalez[16] on Ru-Na, SiO_2 . In contrast on Rh-Na/TiO_2 , Chuang et al.[17] observe that the rate of formation of hydrocarbons decreases on sodium addition and the rate of formation of oxygenates increases on sodium addition.

7.6.2 Location of Sodium Modifier

Hydrogen chemisorption decreases on addition of sodium. It is also lower on used catalysts. The absence of any diffraction pattern on any of the used catalysts means that the entire decrease in the hydrogen chemisorption cannot be attributed to an increase in particle size. Two possibilities remain. Either part of the rhodium is in an oxidized form and hence cannot adsorb hydrogen or part of the rhodium surface is blocked by the sodium phase. The XPS results show that on reduction, rhodium is metallic. Thus the decrease in hydrogen chemisorption is at least partly the result of the rhodium surface being blocked by sodium oxide.

It is important to recognize that although some of the alkali modifier may block the rhodium surface most of it sits on the alumina support, where it probably forms a surface compound with alumina and thus removing the surface -OH groups. This in turn changes the stability of the various adsorbed species. For example, because of the decrease in the surface -OH groups on Rh-Na/Al_2O_3 , the gem-dicarbonyl species is easily formed on Rh/Al_2O_3 than on Rh-Na·Al_2O_3 . Not only is the number of surface -OH groups important for formation of gem-dicarbonyl species but also their location around the rhodium crystallite important. The reaction of break-up of rhodium crystallite to form isolated gem-dicarbonyl species is given below.

$$Rh - CO(crystallite) + CO + 2Al - OH = 2Al - O - Rh(CO)_2 - H_2$$

Thus the rhodium crystallite slowly disintegrates into gem-dicarbonyl species.

However only a small amount of the alkali modifier sits on the rhodium crystallite. Blackmond et al.[1] have also observed a decrease in bridged and gem-dicarbonyl species on Cs addition to Rh/Al_2O_3 . This differences in IR spectra were attributed to the blocking of redispersion of Rh crystallite to $Rh(CO)_2$. However the exact mode of cesium was not elaborated. The results shown in this chapter show that. the predominant effect of addition of sodium is the removal of blocking of surface -OH groups.

The XPS data on the silanized Al_2O_3 and Na/Al_2O_3 show that all the silicon in the silanized sample is present as silanes. Furthermore because of absence of nitrogen signal there is no unreacted HMDS and thus there is no bond between the lone pair on the secondary nitrogen on the HMDS and the Lewis acid site on the alumina surface.

7.6.3 Chemical State of Rh and Na

The XPS results show that rhodium is completely reduced to metallic state. Also, there is no detectable shift in the binding energies on addition of sodium and on various treatments such as CO adsorption and reaction. No shifts in the binding energy of sodium peak is detected in Na/Al_2O_3 and $Rh\text{-}Na/Al_2O_3$ after various treatments such as reduction. CO adsorption and reaction. Furthermore. the physical state or the state of aggregation of sodium is same in the presence and the absence of rhodium.

The TPR data show that rhodium is reduced to metallic state. The rhodium is well-dispersed. The intensity of the high temperature TPR peak increases substantially with amount of sodium added. The hydrogen TPD spectra of Rh/Al_2O_3 and $Rh\text{-}Na/Al_2O_3$ and diffuse.

7.6.4 Formation of Mixed Oxide

Discussion of phases containing sodium, rhodium and oxygen where the oxidation state of rhodium is greater than 3 is warranted at this stage. Scheer et al.[18] during their investigation of species formed from platinum metals and alkali oxide found that oxides of the type ABO_2 and A_2BO_4 are formed. Here, A is the alkali ion and B is the platinum group metal ion. Most of the compounds formed are of the type A_2BO_4 and are formed by heating a mixture of platinum group metal and alkali carbonate to 1000C under oxygen for 20 hours. The only rhodium compound was Li_2RhO_4. $LiRhO_2$ was formed first, and then converted to Li_2RhO_4. For the mixed oxides containing sodium, only $NaRhO_2$ was formed. The phase Na_2RhO_4 has not been reported in literature in the 30 years since the investigation of Scheer et al.[18]. The reason for absence of A_2BO_4 compounds containing Rh and Na is not clear. The possible reason for non-existence of other compounds of rhodium and sodium oxide may be the absence of oxidation states of rhodium higher than -3. This is relevant to the current investigation, since higher consumption of hydrogen in a TPR spectra can be explained by the presence of mixed oxides containing one transition metal in a higher oxidation state. The amount of hydrogen consumed in the reduction of these catalysts increase with the amount of sodium added. However, when compared to the data of Houalla et al.[19-21] the observed changes are very small. Hence this increase in the hydrogen consumption is not due to increase in the oxidation state of rhodium.

7.6.5 Ensemble Requirement

Thus the overall effect of addition of sodium is to block the rhodium hydrogenation sites. This not only decreases the activity substantially but also reduces the size of many ensembles. A fixed number of rhodium metal atoms in an ensemble required to form hydrocarbons[22,23]. However the ensemble requirement for

CO insertion reaction is less stringent than that for hydrocarbon sites [24]. Because sodium blocks some of the surface sites, the number of ensembles large enough for hydrocarbon formation decrease faster than the number of sites available for CO insertion and MeOH formation. This causes drastic changes in the reactivity and minor changes in the selectivity.

7.7 Conclusions

The addition of sodium to Rh/Al_2O_3 decreases the rate of CO hydrogenation. The rate decrease exponentially with the amount of sodium added. The selectivity to oxygenates is increased slightly.

Hydrogen chemisorption and XRD shows that addition of sodium poisons blocks or poisons the rhodium crystallite. The rhodium is in metallic state under reaction conditions and the oxidation state of sodium is not changed. The formation of gem-dicarbonyl species is hindered due to the lower amount of surface -OH groups. XPS and IR results show that hexa methyl disilazane reacts with the surface -OH groups to form surface silanes. These silylated catalysts show that the formation of the gem-dicarbonyl species is hindered.

REFERENCES

1. D.G. Blackmond, J.A. Williams, S. Kesraoui and D.S. Blazewick. J. Catal. 1986. 101. 496.

2. B.D. Cullity. "Elements of X-Ray Diffraction", Addison-Wesley. Reading. Massachusetts. 1978.

3. J.L. Maitre. P. Govind Menon and F. Delannay, in "Characterization of Heterogeneous Catalysts", Ed. F. Delannay, Marcel Dekker. New York. 1984.

4. "Powder Diffraction File", Alphabetical Index, Inorganic Phases, International Center for Diffraction Data, Swarthmore, Pennsylvania, 1987.

5. H. Arakawa. K. Takeuchi. T. Matsuzaki and Y. Suge, Chem. Letts. Japan. 1984. 1607.

6. F. Solymosi, M. Pasztor and G. Rakhely, J. Phys. Chem. 1988, 110. 413.

7. P. Basu. D. Panayotov, and J.T. Yates, Jr.. J. Phys. Chem. 1987, 91. 3133.

8. C.H. Dai and S.D. Worley, J. Phys. Chem. 1986, 90. 4219.

9. J.Z. Shyu. J.G. Goodwin. Jr., and D.M. Hercules. J. Phys. Chem. 1985. 89. 4983.

10. M.I. Zaki. G. Kunzmann. B.C. Gates and H. Knozinger. J. Phys. Chem. 1987. 91. 1486.

11. C.D. Wagner. W.N. Riggs. L.E. Davis. J.F. Moulders and G.E. Mullenberg. "Handbook of X-ray Photoelectron Spectroscopy". Perkin-Elmer Co.. Eden Prarie. Minnesota. 1979.

12. T.P. Wilson. W.J. Bartley and P.C. Ellgen. "Advances in Catalytic Chemistry". Proc. Conf. in Salt Lake City. Utah. 1982.

13. H. Knozinger and P. Ratnaswamy. Cat. Rev. Sci. Eng. 1978. 17. 31.

14. J.A. Konvalinka, P.H. Van Oeffelt and J.J.F. Scholten, Appl. Catal. 1981. 1. 141.

15. J. LeMaitre, in "Characterization of Heterogeneous Catalysts", Ed. F. Delannay, Marcel Dekker, New York, 1984.

16. M. McLaughlin and R.D. Gonzalez, J. Catal. 1984. 89. 392.

17. S.C. Chuang, J.G. Goodwin, Jr. and I. Wender, J. Catal. 1985, 95. 435.

18. J.J. Scheer, A.E. van Arkel and R.D. Heyding, Can. J. Chem. 1955. 33. 683.

19. M. Houalla, F. Delannay and B. Delmon, J. Phys. Chem.1981. 85. 1704.

20. M. Houalla, J. LeMaitre and B. Delmon, C. R. Acad. Sci. Paris, Ser. C.1979. 289. 77.

21. M. Houalla, J. LeMaitre and B. Delmon, J. Chem. Soc., Faraday Tans.1. 1981. 78, 1389.

22. W.M.H. Sachtler, 8th Intl. Congr. Catal. 1984, Vol. I. 151, Berlin.

23. G.A. Somorjai, Chemical Reviews 1984, 321.

24. W.M.H. Sachtler, Faraday Discuss. 1978, 7.

CHAPTER 8
PERFORMANCE OF MOLYBDENA MODIFIED RHODIUM/ALUMINA CATALYSTS

The effect of addition of molybdena on the performance of Rh/Al_2O_3 catalysts is investigated. First catalysts containing different loading of Mo were investigated. Then, the products are separated according to their rank. The activation energies and the power law indices for the rate expressions were also calculated.

8.1 Catalyst Preparation

The catalysts support used was CATAPAL alumina extrudate. The alumina extrudate was first ground to a particle size of 60-100 mesh. The support was then calcined at 500C under following air (> 99.999% purity) for two hours. The surface area of the support is about 200 m^2/gm. The details of preparation of Rh/Al_2O_3 catalysts are given in chapter 5. A no-excess impregnation technique was used to support rhodium and molybdenum salts on the support. The rhodium was impregnated from a sulfate-free acidic solution (pH=1) from Engelhard. Molybdenum was impregnated using Puratronic grade ammonium molybdate from Alfa Products. All Rhodium was nominally 3 wt.%.

The molybdena-containing catalysts were prepared in stages. In the first stage, Mo was deposited on the alumina using a molybdena solution at a pH of 1-2. The impregnated sample was kept at room temperature for 30-60 minutes. in an oven at 110C for 12-16 hours. The catalysts was later air calcined at 500C for 2 hours. The 2.8 wt. % Mo catalyst was prepared by coimpregnation. All

% Mo numbers quoted are for Mo metal by weight although the Mo is present in an oxide form. In the preparation of 2.8 % Mo catalyst, a white precipitate was formed when Mo solution was added to the rhodium nitrate solution. This precipitate dissolved immediately on shaking. So the addition of ammonium molybdate solution to rhodium nitrate solution was continued drop-wise with vigorous shaking. After addition of three-fourths of the molybdenum solution, further addition of molybdate solution formed a precipitate that did not dissolve on shaking. So, small amounts of concentrated nitric acid was added. Addition of nitric acid dissolved the precipitate and the solution was once again clear. The 7.5 wt. % and 15 wt. % Mo catalyst were prepared by sequential impregnation. First the molybdenum salts were impregnated, followed by drying in air at 110C and air calcination at 500C. Then the rhodium salt was impregnated using rhodium nitrate solution using a no-excess solution impregnation technique. The color of the catalysts on Mo impregnation and after calcination was white. In contrast, the color of catalysts after rhodium impregnation was bright yellow and reddish brown after calcination.

The theory of impregnation of salts from aqueous solution and its relevance to catalysts preparation is discussed in chapter 2. However some results from this theory will be discussed here. Since molybdenum forms anions in solution, molybdenum was impregnated first. In contrast, rhodium exist as hydrated cations in the solution, and hence adsorption of rhodium cation on alumina surface in an acidic solution is not thermodynamically facilitated. In the case of 15 wt. % Mo catalysts, because of the limited solubility of the ammonium molybdate, two successive impregnations were made with a 500C air calcination in between them. Before testing, all catalysts were prereduced with flowing hydrogen with the following schedule, 200C (1/2 hour), 350C (1/2 hour) and at 500C (1 hour).

Catalyst (0.5-1gm) was tested in a flow reactor system. The flow reactor is described in detail in chapter 4 and the procedure for catalysts testing is described

in chapter 6. Unless otherwise specified, all data were obtained at hydrogen. CO ratio of two and a pressure of 30 atm. The analytical system is described in detail in chapter 3. To make activity comparisons, space rates were varied at constant temperature to obtain equal; conversions (limited to 6 % CO conversion), then the conversions were obtained by normalizing to 3000 GHSV by multiplying by the factor: GHSV/3000.

8.2 Performance Testing Results

This section shows the effect of molybdena addition on the reactivity and the selectivity of molybdena modified rhodium/alumina catalysts.

8.2.1 Overall Activity and Selectivity

Table 8.1 summarizes the effect of molybdena addition. The % CO conversions given in table 8.1 are the total conversions. However % selectivities to oxygenates and hydrocarbons are % of CO converted to these products on a CO_2 free basis. The % C2− oxyg. is the percentage of all oxygenates C2 and above. The Mo/alumina catalysts has very low activity for CO conversion and does not form any oxygenates. The effect of incorporating increasing amounts of molybdena in the Rh/alumina system is to increase the activity for CO conversion. For example, table 8.1 shows that the catalyst with Mo/Rh atom ratio of 2.7 (Rh/7.5Mo) is 12 times as active as Rh/Al_2O_3 , when compared at 3000GHSV and at 250C. The water gas shift reaction is greatly enhanced as seen by the appearance of CO_2. Also, the % CO converted to oxygenates(particularly methanol) increases sharply with increasing Mo content, rising from 29 % for Rh/Al_2O_3 ti 65 % for $Rh/7.5Mo/Al_2O_3$ both at 250C. Oxygenates are 89 % for the $Rh/15Mo/Al_2O_3$ catalyst at 200C.

Table 8.1: Effect of addition of Mo on the reactivity of Rh alumina

Catalyst	T(C)	GHSV hr^{-1}	%CO Conv.	% CO conv. to CO_2	% CO conv. to Oxyg. (CO_2 free)	C2− Oxyg. % of Oxyg.
Rh/Al_2O_3	250	3000	5.7	1	29	82
	275	3000	12.5	1	19	87
Rh/2.8Mo/ Al_2O_3	225	3000	9.0	21	59	42
3Rh/7.5Mo Al_2O_3	200	3000	7.3	24	86	17
	250	36000	5.3	25	65	27
Rh/15Mo Al_2O_3	200	3000	6.0	27	89	12
	225	3000	27	37	83	14
$15Mo/Al_2O_3$	225	3000	<1	61	0	
	250	3000	2	50	0	
	275	3000	5	51	0	

The results for Rh-Mo/Al_2O_3 with low loading of Mo are consistent with other investigations[1-8]. The Rh-Mo/Al_2O_3 catalysts derived from monometallic catalysts were less reactive than the conventional catalysts[5]. In contrast, the catalysts derived from bimetallic cluster $RhMo_2Cp_3(CO)_6$ was more reactive than the conventional catalysts[8].

8.2.2 Product Distribution

Table 8.2 shows the detailed product distribution for Rh/Al_2O_3, Mo/Al_2O_3 and Rh-Mo/Al_2O_3 catalysts. There are significant changes in the product distribution on Mo addition to Rh/Al_2O_3 catalysts. For example, there is a steep increase in the CO_2 formed from the water gas shift reaction. Also, there is a decrease in the C2+ oxygenate fraction of the total oxygenates The water gas shift reaction is helpful since this permits use of syngas with lower hydrogen/CO ratios and simplifies the product separation. The complete lack of aldehydes in the product the good hydrogenation capability. The increase in the ethers may be because of the increase in surface acidity due to molybdena addition. Decreased ester formation may be due to decreased acetic acid formation because of increased hydrogenation activity. The most important observations are the drastic reduction in formation of methane, accompanied by a substantial increase in the oxygenates, especially methanol and dimethyl ether.

Further insight can be deduced from the product distribution. The addition of Mo results in oxygenates with much higher percentage of methanol. However, it is important to note that while C2− oxyg. has decreased the %C2− oxyg as a percentage of CO conversion remains nearly at the same level, even though catalyst activity has increased by greater than 10-fold by Mo addition.

In comparison the product distribution for 15 % Mo/Al_2O_3 gives 50 % CO converted to CO_2 and rest to hydrocarbons at 250C with a GHSV of 3000 hr^{-1}.

Table 8.2: Product distribution on CO hydrogenation on Rh-Mo Al_2O_3 catalysts

Catalyst	Rh/Al_2O_3	$Rh\ 2.8Mo/Al_2O_3$	$Rh\ 15Mo/Al_2O_3$	
Temp(C)	250	225	200	250
GHSV	3000	3000	3000	36000
%CO Conv.	6	9	7	5
% CO to CO_2	1	22	24	25
of CO converted, % converted to:(CO_2 free basis)				
Hydrocarbons	72	41.5	13	34
Methane	61	35	9	26
Ethane	4	4.5	3	6
Propane	5	1.5	1	2
Butane	2	0.5	0	0
Oxygenates	28	58.5	87	66
MeOH	2	13	38	16
MeOMe	1	16	30	26
MeCHO	2	0	0	0
EtOH	11	12	6	7
MeOAc	3	2.5	1	1
HOAc	0	0	0	0
EtCHO	0.4	0	0	0
n-PrOH	2.7	2.4	2	1
MeOEt	3	12.6	10	15
EtOAc	3	0	0	0
%of C2+ Oxygenates	82	42	17	27

The overall carbon monoxide conversion under these condition was 1.8%. The carbon percentage in hydrocarbons is as follows: Methane 61%, ethane 29% and propane 10%.

The effect of the amount of molybdena addition on the selectivity to oxygenates is clearly seen from figure 8.1. In this figure the overall oxygenate selectivity on a carbon dioxide free basis is plotted against the overall conversion(including carbon dioxide). For a given catalyst the selectivity to oxygenates decreases with increasing conversion. e.g., for Rh/Al_2O_3 the selectivity to oxygenates decreases from 35 % to 20 % when the CO conversion was increased from 2% to 18%. The x-axis is the selectivity versus conversion curve for Mo/Al_2O_3 since no oxygenates are formed on this catalysts. As seen in figure 8.1 the addition of Mo to Rh/Al_2O_3 shift the selectivity versus conversion curves to higher selectivity. However the slopes of these curves do not change. Also there is an effect of temperature since the selectivity versus conversion curves are shown for different reaction temperature. The effect of reaction temperature on the selectivity to oxygenates will be discussed in detail while calculating the activation energies.

Table 8.3: Effect of Mo addition on Methane/Methanol product distribution

Catalyst	%CO to CH_4	%total oxygen	%C2+ oxygen	Oxygenates Dist. C1	C2	C3	$\%CH_4$ – MeOH
Rh. Al_2O_3	60	30	82	5	21	3	65
Rh/7.5Mo/ Al_2O_3	24	65	27	47	17	1	74

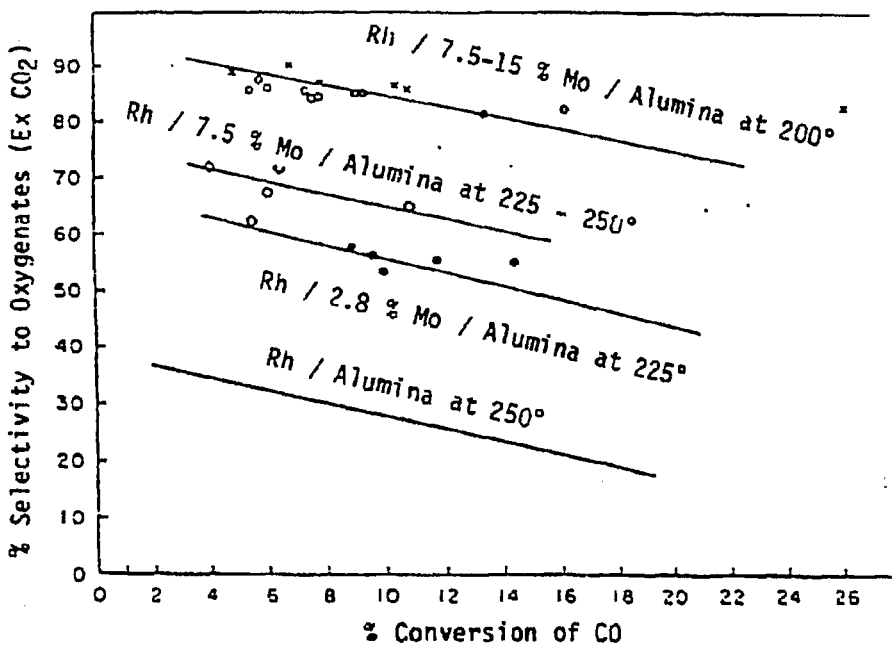

Figure 8.1: Effect of Mo addition and temperature on the selectivity to oxygenates

8.2.3 Approach to Steady State

The initial transient properties of these catalysts show interesting trends. Figure 8.2 shows the approach towards steady state of overall conversion, methane selectivity and oxygenate selectivity. The data in the figure are reported for CO hydrogenation on 3%Rh 7.5%Mo/Al_2O_3 at 200C, 30atm and hydrogen/CO=2. The initial activity of these catalysts is high as seen by the high conversion. However, these data should be interpreted with caution, since the gas phase environment at zero time is only hydrogen and at time zero, carbon monoxide feed is started. Thus the gas phase may contain a different hydrogen/CO ratio than at steady state. However, this transient in gas phase should approach the steady state feed gas composition in an hour. The overall conversion approaches a steady state within 12 hours. Subsequent steady states by changing conditions are approached within 1-2 hours. The methane selectivity also decreases with time and reaches steady state within 12 hours. However, in contrast the percent decrease in methane selectivity is much lower than the percent decrease in the overall conversion. In comparison, the total selectivity to oxygenates increases with time on stream, but the increase is very small compared to the decrease in the overall conversion. This decrease in activity is similar to those reported by Van der Berg[9].

The effect of hydrogen/CO is shown in figure 8.3 on CO hydrogenation on 3%Rh 7.5%Mo/Al_2O_3 is shown in figure 8.3. This set of data was collected at 200C, 30atm and GHSV of 3000hr^{-1}. The conversion increases with increasing hydrogen/CO ratio. this is true with many CO hydrogenation catalysts. Many of the known catalysts do not work below a Hydrogen/CO ratio of 1.

Another way to see the initial transients is to plot the log(1-CO conv.) versus space-time, as given in figure 8.4. The transients in the figure are marked by an arrow. Also, the points at space time 2.4 show the initial transients. For example

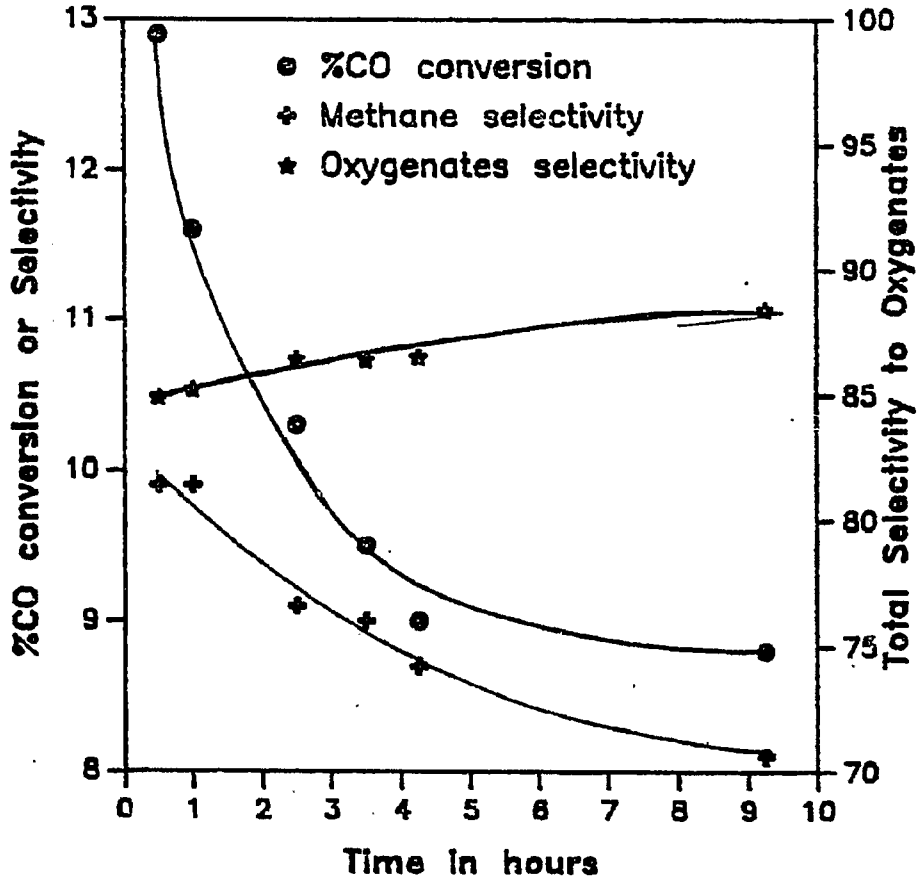

Figure 8.2: Initial transients of CO hydrogenation on 3%Rh 7.5%Mo/Al_2O_3 catalysts at 200C, 30atm and hydrogen/CO=2.

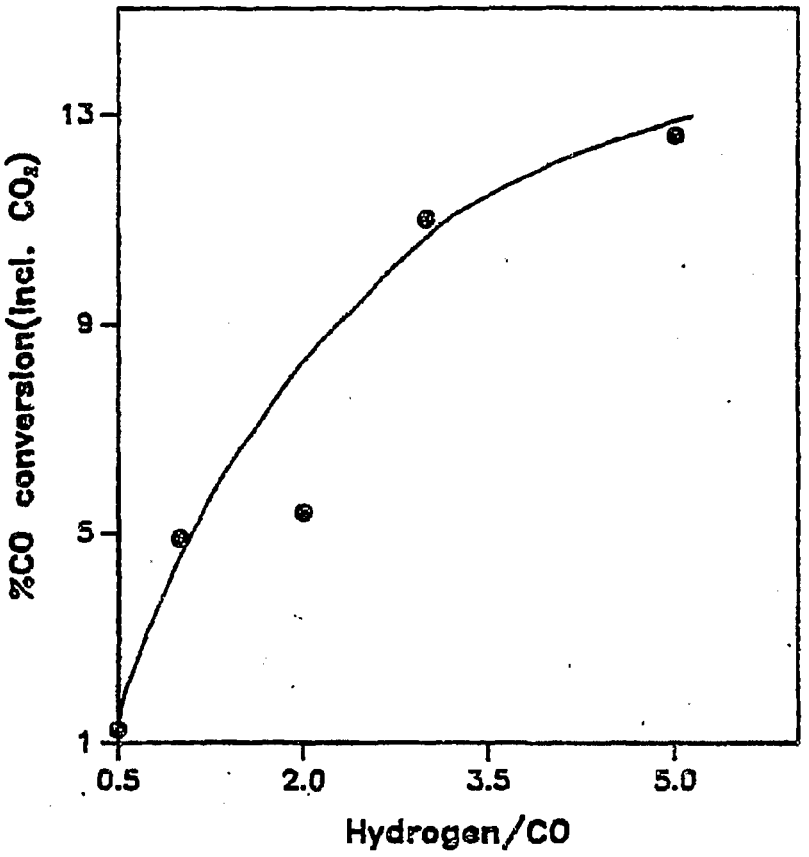

Figure 8.3: Effect of hydrogen/CO ratio on the overall conversion of 3%Rh 7.5%Mo/Al_2O_3 catalysts at 200C, 30 atm and 3000GHSV.

the point at the lowest ordinate or the highest conversion is the point at zero time. and the point move towards the steady state line.

8.3 Transport Limitations

From the calculations in appendix 1, the mass and heat transport limitations for CO hydrogenation on Rh-Na/Al_2O_3 catalysts were shown to be insignificant. Since the process parameters used in the Rh-Na/Al_2O_3 catalysts and the Rh-Mo/Al_2O_3 catalysts are nearly same, the calculations in appendix 1 are valid for the reaction study conducted in this chapter as long as the temperature is lowered to give differential conversions.. Hence the transport limitations are insignificant on CO hydrogenation on Rh-Mo/Al_2O_3 catalysts under the conditions investigated in this chapter.

8.4 Delplot Analysis

The next stage in kinetic analysis of product is to separate products according to their rank, i.e., to separate the primary, secondary and tertiary products. A new method for separation of products according to their rank was developed in chapter 4. In this section this method is applied to the kinetic analysis of carbon monoxide hydrogenation on Rh-Mo/Al_2O_3 catalysts. The basis set has only carbon monoxide since carbon monoxide is the only reactant monitored. From delplot analysis most of the products are kinetic primary products. Sometimes, it is difficult to assign rank to the product because the intercept may be small and finite. In this section first the basic delplot method will be developed, then the extended delplot will be applied to higher rank products. In the last subsection the concept of separation of regimes of product rank will be discussed.

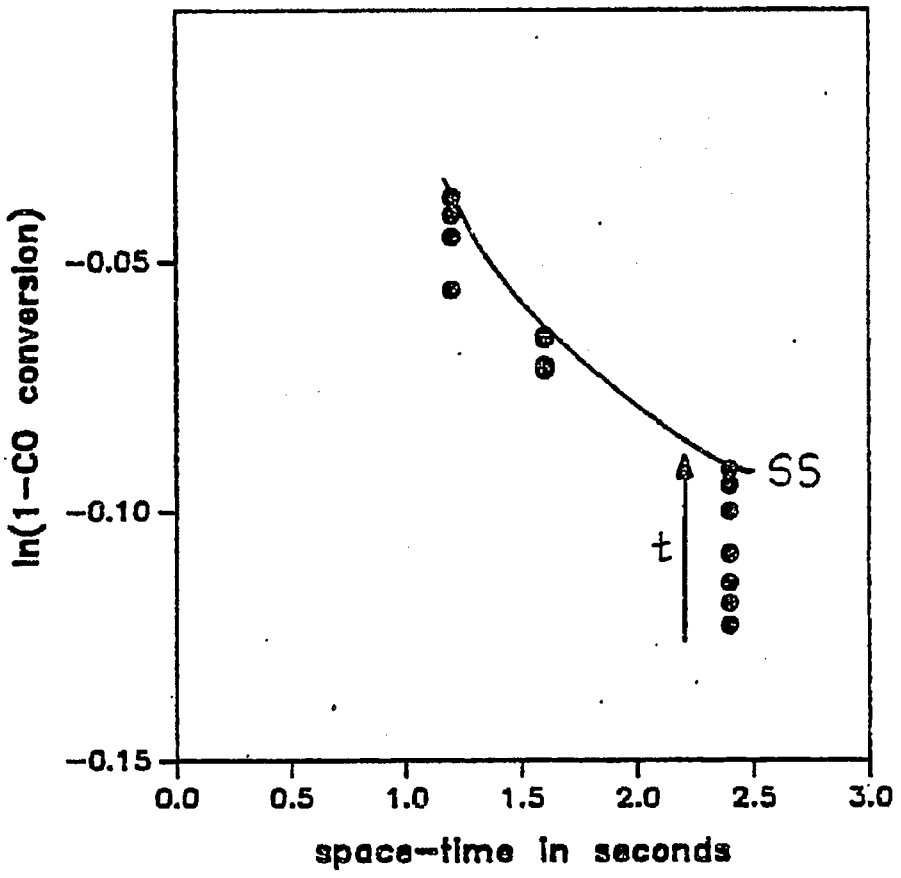

Figure 8.4: Log(1-CO conversion) versus space-time for CO hydrogenation on 3%Rh 7.5%Mo/Al_2O_3 catalysts at 200C. 30atm and hydrogen-CO = 2.

8.4.1 Basic Delplot Analysis

The basic delplot method consists of plotting mole fraction conversion against conversion. A finite intercept denotes a primary product while a zero intercept denotes a secondary product. Figure 8.5 shows the basic delplot for methane. This data was collected for CO hydrogenation on 3%Rh 7.5%Mo/Al_2O_3 catalysts at 30 atm total pressure and 200C reaction temperature. The hydrogen/CO was fixed at 5. The space velocity was varied from 1500 to 6000 hr^{-1}. The basic delplot of methane clearly shows that methane is a primary product. The delplot intercept for methane under the above conditions is 0.1. This is the ratio of the initial rate of formation of methane to the initial rate of consumption of carbon monoxide. Thus there is only one slow step in the methane formation reaction under the above mentioned conditions. The basic delplot of carbon dioxide also shows a finite intercept, this implies that carbon dioxide is a kinetic primary product. This should be compared with the results from the sodium modified catalysts, where carbon dioxide had a small intercept. The carbon dioxide is formed from the water gas shift reaction given by equation (8.1).

$$CO + H_2O = CO_2 + H_2 \qquad (8.1)$$

The reactant water is formed in methane formation, ethanol formation, ethane formation, and dimethyl ether formation. Carbon dioxide is thus formed sequentially: first water is formed then carbon dioxide is formed by the water gas shift reaction. Thus carbon dioxide can be primary product if the water gas shift reaction is fast on the process time scale. Thus the water gas shift reaction is fast on the process time scale on the molybdena modified rhodium/alumina catalysts but is slow on the process time scale on the sodium modified rhodium/alumina catalysts. The delplot intercept for carbon dioxide is 0.09.

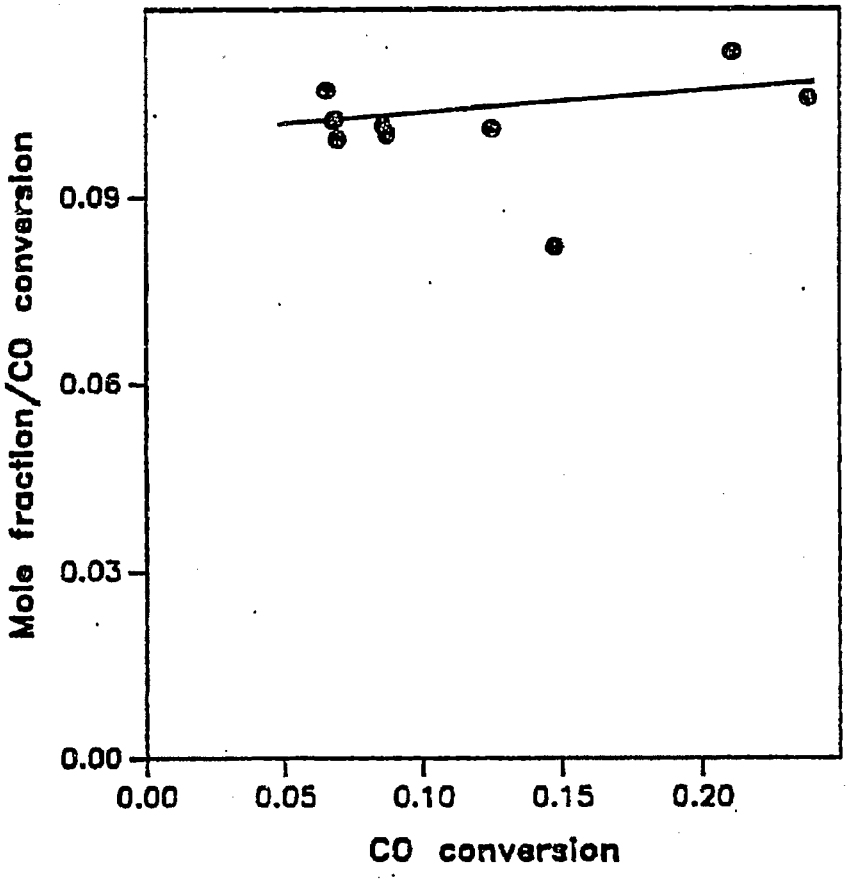

Figure 8.5: Basic delplot of methane formed on carbon monoxide hydrogenation on 3% Rh 7.5% Mo : Al_2O_3 catalysts at 200C, 30 atm. and hydrogen/CO=5

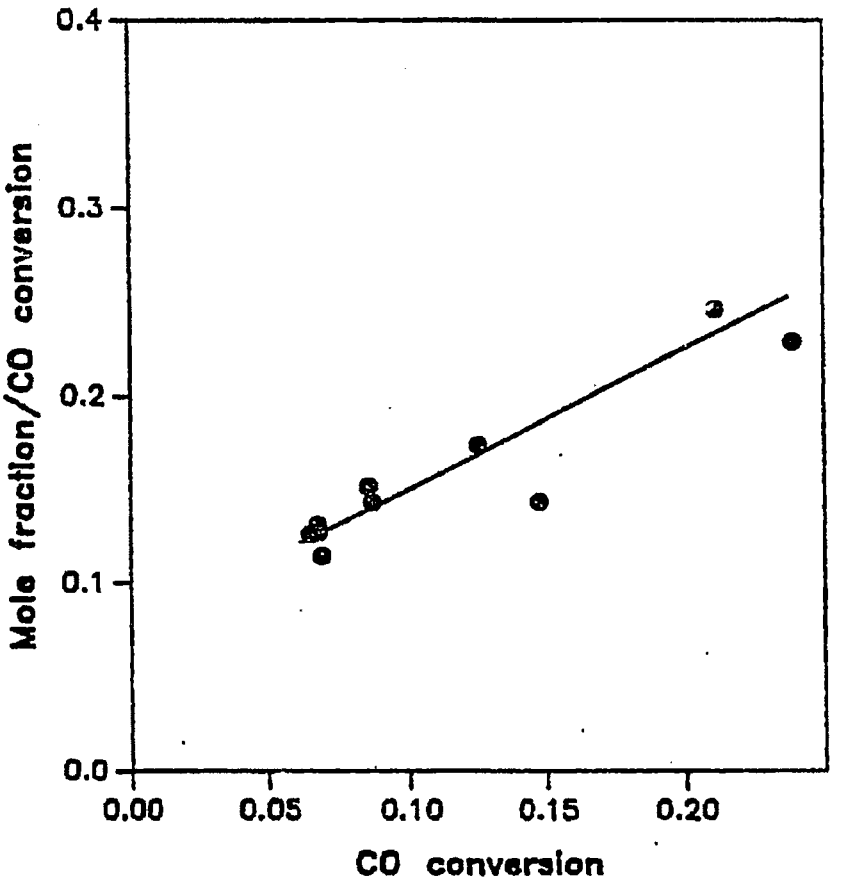

Figure 8.6: Basic delplot of carbon dioxide formed on carbon monoxide hydrogenation on 3% Rh 7.5% Mo / Al_2O_3 catalysts at 200C, 30 atm. and hydrogen/CO=5

Figure 8.7 shows the basic delplot for methanol and dimethyl ether on carbon monoxide hydrogenation with hydrogen/CO of 5. The plot shows finite intercept for both methanol and dimethyl ether, hence both methanol and dimethyl ether are primary products. Thus the formation on ethers is fast on these catalysts because of their higher acidity. In contrast, small amounts of ethers are formed on sodium modified catalysts. The large amount of methanol formed compared to dimethyl ether is reflected in the higher intercept for methanol as compared to dimethyl ether(0.45 versus 0.15). The high hydrogen/CO ratio (5) leads to higher hydrogenation of surface species and less products from recombination. This leads to a high methanol/dimethyl ether ratio. Figure 8.8 shows the basic delplot for ethanol and ethane under the above mentioned conditions. Since ethanol and ethane are formed in small amounts, their intercepts, if any are small, this makes discrimination between finite but low and zero intercepts difficult. However, figure 8.8 clearly shows that ethanol has a finite intercept. The low signal to noise in the analytical data at low conversions for some C2 and higher products prevents the discrimination between zero and small but finite intercept.

The delplot analysis can be checked for internal consistency by checking the sum of product of stoichiometric coefficients and the delplot intercepts. Table 8.4 list the delplot intercepts and the stoichiometric coefficients of each product. For example, the delplot intercept of dimethyl ether is 0.15 and its stoichiometric coefficient is 2. The stoichiometric coefficient here is easily found from the carbon balance.

Thus the sum of stoichiometrically accounted delplot intercepts, given in

$$\sum_{P} \nu_P \, {}^{1}P_{CO} = 1.00 \qquad (8.2)$$

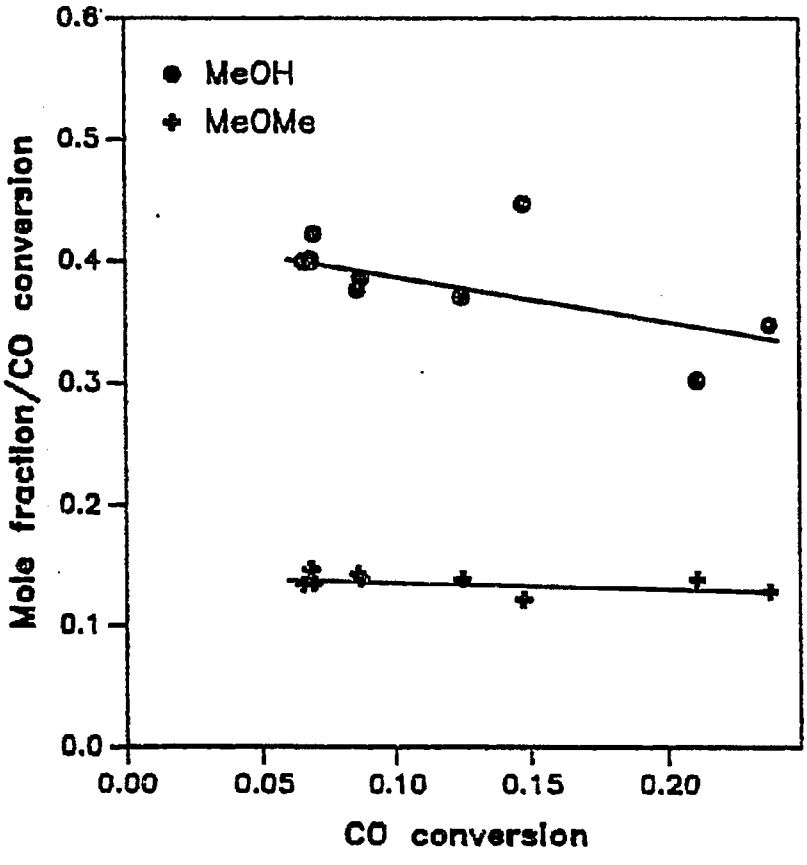

Figure 8.7: Basic delplot of methanol and dimethyl ether formed on carbon monoxide hydrogenation on 3% Rh 7.5% Mo Al_2O_3 catalysts at 200C, 30 atm, and hydrogen/CO=5

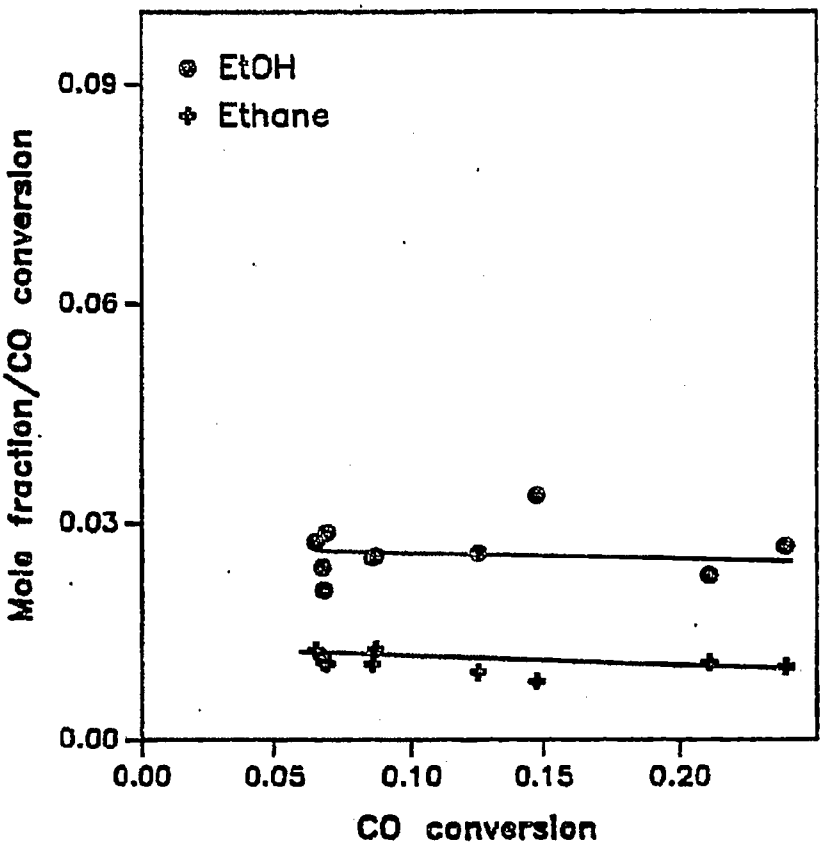

Figure 8.8: Basic delplot of ethanol and ethane formed on carbon monoxide hydrogenation on 3% Rh 7.5% Mo /Al_2O_3 catalysts at 200C. 30 atm. and hydrogen/CO=5

Table 8.4: Delplot intercepts and stoichiometric coefficients of products formed on CO hydrogenation on 3% Rh 7.5% Mo/Al_2O_3 catalysts at 200C. 30 atm and hydrogen/CO=5.

Product(P)	Delplot Int.($^1P_{CO}$)	Type	Sto. Coeff.(ν_i)
Methane	0.1	Primary	1
CO_2	0.08	Primary	1
Methanol	0.45	Primary	1
Ethanol	0.025	Primary	2
Dimethyl ether	0.15	Primary	2
Ethane	0.01	Primary	2

equation (8.2) is close to unity within experimental limits. Hence rule 3 of basic delplot analysis given in chapter 4 is satisfied.

8.4.2 Separation of Regimes

In the last section of chapter 4, the concept of separation of regimes was developed and quantified. A primary product is a product that has only one slow step between the the reactant and itself, while a secondary product is a product which has two slow steps between reactant and itself. A reaction is slow or fast on the process time scale and not on a relative scale. Now, if the process time scale changes, then a reaction step can change from a slow step to a fast step or vice versa. The process time scale can be changed by looking at two different conversion regions.

However, this phenomenon is not seen in many products because, in a reaction network, one step is often much slower than the remaining steps. Thus to make one of the fast steps as a slow step, we have to use extremely small process time. At these low process time, the conversions are low and this causes analytical problems. However, an example of a product which changes regimes will be shown here.

The basic delplot of MeOEt is shown in figure 8.9 The figure shows two distinct regimes. The first regime is above 1.5% CO conversion where the basic delplot gives a finite intercept. In contrast, the second regime below 1.5% conversions shows a zero basic delplot intercept. Hence MeOEt is a secondary product below 1.5%CO conversion and a primary product above 1.5% conversion. Regime 1(above 1.5% CO conversion) consists of high conversion or low space time runs, while regime 2 consists of low conversion or high space time runs. The above behavior is qualitatively and quantitatively explained using order of magnitude analysis and singular perturbation analysis in chapter 4.